THE UNIVERSITY OF CHICAGO

MORPHOLOGICAL DIVERSITY AND BIOMECHANICAL DETERMINANTS OF TRABECULAR BONE IN AMNIOTES

A DISSERTATION SUBMITTED TO

THE FACULTY OF THE DIVISION OF THE BIOLOGICAL SCIENCES

AND THE PRITZKER SCHOOL OF MEDICINE

IN CANDIDACY FOR THE DEGREE OF

DOCTOR OF PHILOSOPHY

COMMITTEE ON EVOLUTIONARY BIOLOGY

BY

TRISTAN REINECKE

CHICAGO, ILLINOIS

JUNE 2025

Table of Contents

Supplementary files are available online

List of Figures

List of Tables

Acknowledgements

I would like to thank my advisor, Dr. Kenneth Angielczyk whose guidance, considerable experience and knowledge made this project possible. Thanks also to my committee, Dr. Mark Webster, Dr. Mark Westneat, and Dr. Zhe-Xi Luo who provided additional support and knowledge on areas related to statistical analysis, biomechanics, and phylogenetic analysis. I would also like to thank Dr. Stephanie Smith who acted as an unofficial mentor in troubleshooting various issues with CT processing programs. Thanks also to April Neander for assistance with the PaleoCT. I also want to thank Adam Ferguson and John Phelps Jr. (Field Museum of Natural History), Meredith Mahoney (Illinois State Museum), David Blackburn and Coleman Sheehy III (University of Florida), Lauren Caspers (American Museum of Natural History), and Megan Viera (Smithsonian Natural History Museum) for access to museum collections and assistance in selecting the specimens used in this study. I also thank Gregory Schneider (University of Michigan Museum of Zoology) who approved for the use of a μCT scan hosted through Morphosource.

Abstract

Trabecular bone, a lattice-like network of bony struts within the cortical shell of many skeletal elements, provides critical internal support against mechanical strain while minimizing weight. Although studied for over a century, its intricate microscopic architecture long hindered comprehensive analysis. Advances in high-resolution micro-CT imaging and computational tools have now enabled researchers to decode its complexity, though most work has focused on human anatomy and biomedical applications. In contrast, research on non-primate species remains comparatively limited, often restricted to isolated elements, narrow taxonomic groups, or domesticated species that have been found to exhibit modified trabeculae. This study expands upon existing methodologies to investigate trabecular bone diversity across amniotes and identify key drivers of its variation among species and limb elements. First, ontogenetic changes in raccoon trabecular structure were analyzed. Several trabecular characteristics were found to

peak during puberty, indicating a rapid shift in bone remodeling to accommodate changes in behavior and body mass before settling on a more optimized adult plateau. Second, a broad comparative analysis of amniotes showed that while mammals exhibit pronounced differences between forelimb and hindlimb trabeculae, reptilian limbs display greater uniformity. Ecological niche and posture poorly predicted traditional trabecular metrics, but primary trabecular orientation clustered by major clades. The third portion of this thesis compared lower limb elements and found that despite the higher magnitude of stresses exerted on these bones during locomotion, trabecular characteristics were more uniform than more proximal limb bones. Trabecular orientations for these features generally aligned in the direction of joints and tendons, indicating these distal bones' more limited range of motion is reflected in the trabeculae as well. Collectively, these findings underscore the functional and phylogenetic complexity of trabecular bone, challenging generalized assumptions about its uniformity across the skeleton. Instead, each element's trabecular architecture appears uniquely tuned to its biomechanical context. The methodological framework developed here, particularly for standardizing orientation in morphologically diverse bones, provides a foundation for future comparative studies of trabecular organization across taxa.

Chapter 1: Introduction and Literature Review

The tetrapod body is a remarkable example of a living system; a complex network of interconnected components that work in harmony to maintain life. Unlike static structures, living systems are dynamic, adaptive, and self-regulating, capable of responding to internal and external changes to sustain homeostasis. The dynamic nature of some of these systems is well known even by a layperson; the immune system will actively defend against pathogens, the nervous system will react to outside stimuli, and the circulatory system will increase blood flow to fuel the body with oxygen and nutrients during high stress activity. The reactive nature of the body extends beyond these well-known anatomical systems and can be found in some unexpected places. The skeletal system is typically assumed to be a fairly static system. Outside of growth during ontogeny and repairing from injury, the skeleton is often considered to be an unchanging framework to which the other bodily systems attach.

Despite its primary function as the body's framework, the skeletal system is both active and reactive and has the capacity for significant changes in its morphology. This modification is driven by a series of bone cells that function to regulate bone remodeling. In the event of mechanical stress or micro-damage, osteocytes embedded within bone matrix act as mechanosensors that detect injuries and signal to other bone cells (Noble 2008). The first of these cells to act are osteoclasts, which work to seal off the damaged area in a compartment known as a resorption bay. Acidic H^+ ions and collagenase are released to dissolve the mineralized bone matrix, releasing calcium and phosphate into the bloodstream (Teitelbaum 2000; Siddiqui 2019). Following reabsorption, osteoclasts undergo a programmed cell death known as apoptosis as the osteocytes signal for new cells to take their place (Boyle et al. 2003). These new cells, known as osteoblasts, use the collagen within their cell bodies to deposit

calcium and phosphate within the resorption bay in a new, stronger structure (Blair et al. 2007). As mineralization occurs, some osteoblasts are embedded into the new bone matrix and differentiate into osteocytes which work to monitor this new bone (Anderson 2003; Bonewald 2011).

Along with incorrect assumptions regarding the static nature of bony structures, there is also a lack of understanding among the general public with respect to the diversity of bones themselves. When looking at the skeleton one can observe a hard, rigid bony tissue arranged into a number of different sizes and shapes, totaling 206 individual pieces in the adult human skeleton. This hard outer shell, referred to as cortical or compact bone, serves as the support for muscle tendons, storage for calcium, and as protection for organs. Within this shell is semi-solid soft tissue known as bone marrow from which the bone modifying cells are formed (Farhi 2009; Arkin 2014). Finally, nestled alongside the marrow is cancellous bone, otherwise known as a trabecular bone. Unlike cortical bone which creates thick walls for support, trabecular bone instead forms numerous small struts that form a complex interwoven honeycomb-like structure of bone. Trabeculae can be found in a number of distinct bony elements but are typically associated with the epiphyses of long bones, vertebrae, and the skull.

History of Trabecular Bone Research

Given the complex morphology of regions of trabecular bone, understanding the specific nature of their shape and structure has proven difficult. Analysis of trabecular bone has a long history however, dating back to 1892, when the forces impacting trabecular bones were first described. German anatomist and surgeon Julius Wolff was the first to catalogue the alignment of trabecular struts within the proximal femur, and noticed they had a striking similarity to the internal stress lines of a Fairbairn crane, whose rounded curved structure was similar in shape to the femoral

articular head. Building on principles described by Culmann and von Meyer, Wolff stated that bone, including trabecular bone, reacts to loading and will remodel itself over time to resist against this strain (Culmann 1865; von Meyer 1867; Wolff 1892; O'Conner 2010). Higher magnitudes of strain would drive more changes to skeletal architecture, while diminished strain could see bone loss occur. In the case of trabecular bone, struts could orient themselves parallel to the direction of strain in order to maximize strength while minimizing the overall weight of the bony structures. Future work would identify that trabecular bone, due to its small size and proximity to bone marrow, could rearrange its structure much faster than cortical bone. Adjustments in trabecular bone due to injury can occur in a timespan of weeks to months, whereas cortical structures would take roughly 10 times as long to see similar changes (Parfit 1988; Morgan 2013). These findings were hidden from Wolff and other contemporary osteologists as the cross sections of bones used for trabecular analysis could capture neither growth rates, nor the median values of trabecular characteristics spread throughout a cancellous region.

The first half of the 20th century saw minimal progression in our understanding of trabecular structures, even as new biomedical technologies allowing more intimate analysis of bony structures were developed. X-ray devices, able to peer past the cortical structures of bones, became an increasingly common sight in hospitals and research laboratories through the first decades of the century, but their relative unreliability and low resolution made them impractical for trabecular analysis (van der Plaats 2012). In 1966 Albert Crewe the University of Chicago developed the scanning transmission electron microscope, allowing for microscopes to process scans at a much higher resolution (Crewe 1966). Although this technology did allow for better analysis of trabeculae, their complex arrangement still made meaningful analysis difficult, and

biomedical analysis remained focused on cortical bone. These studies did provide some results that were applicable to trabeculae, such as Frost's development of the "mechanostat theory", in which bone adapts to overload through the removal, replacement, and remodeling of bone near the marrow (Frost 1979, 1987; Tyrovola et al. 2015). The cellular processes leading to these changes were unknown to Frost at the time, but this concept would be reaffirmed by him through later studies identifying the process of osteoblast and osteoclast activation (Frost 1990).

The 1980s would prove to be a pivotal decade for trabecular research. Nineteen eighty-two saw the development of the first X-ray microtomography system, in which an object was scanned and separated into a series of slices that could be reconstructed into a 3D model while retaining incredibly small details. These first scans exhibited a pixel size of only 50 micrometers, a resolution that would finally make practical scans of trabecular features (Elliott & Dover 1982). In 1987, Parfitt and colleagues would be the first to define and standardize several trabecular characteristics still used in analyses today. These were trabecular thickness (Tb.Th) and trabecular spacing (Tb.Sp) which, when measured against the overall volume of a sampled region of bone, could provide the bone volume fraction (BV/TV). These values were collected from indirect calculations of area and perimeter due to the difficulty in measuring all struts collectively. The methods proved less accurate than comparable measurements taken of cortical structures but still provided a framework for future research to utilize (Parfitt et al. 1987). Finally, in 1989 Feldkamp and colleagues would publish the first paper utilizing micro-CT imaging to measure several trabecular characteristics and identify the ways in which disease would have an impact on trabecular microstructure (Feldkamp et al. 1989).

Although scientists now had the tools to identify and describe trabecular architecture, the methods of analysis still proved problematic. Studies of trabeculae in the late 1980s and 1990s,

primarily centered around determining the bone's tensile strength and Young's modulus, typically focused on singular struts that were then applied broadly across a larger region of bone (Kuhn et al. 1989; Ryan & Williams 1989; Choi et al. 1990; Choi & Goldstein 1992). These tests assumed homogeneity in trabecular structure, which we now know to be incorrect given the large difference in strain magnitude and direction that can be exerted across a single skeletal element. As a result, their results were highly disparate, with overall results across publications ranging from 0.4 to 14.8 GPa, although each individual paper found values to only range a few gigapascals. Van Rietbergen and colleagues looked to address this issue, and in 1995 built upon 2D finite element models (Williams & Lewis 1982) to develop a new FE system for identifying the elastic and loading properties of trabecular bone. Using novel three-dimensional reconstruction techniques, van Rietbergen's team could convert micro-CT voxels into elements and construct a large-scale FE-model that preserved the greater diversity of trabecular size and shape across a wide sampling of bone.

By the 2000's, advancements in both high-resolution imaging and computational programs allowed researchers to measure trabecular architecture at a level of precision for viable and meaningful biomedical application. As is often the case with advancements in anatomical research, human trabecular morphology has been the focus for this new, modern era of bone analysis. Human-related trabecular research can generally be organized into two groups: studies focused on understanding how age and disease affect bone growth, and studies seeking to compare trabeculae in primates to understand how its architecture changes with the evolution of bipedal locomotion.

Human Trabecular Research: Aging

During fetal development, the primarily cartilaginous skeleton is surrounded by perichondrium, a dense layer of connective tissue (Pawlina & Ross 2018). This layer is gradually transformed into the periosteum as chondrocyte cartilage cells of the diaphysis mature into osteoblasts which in turn form the initial intramembranous bone (Fig. 1.1).

Figure 1.1

A figure modified from Pawlina & Ross 2018 illustrating the presence and removal of perichondrium in bone during early stages of ontogeny

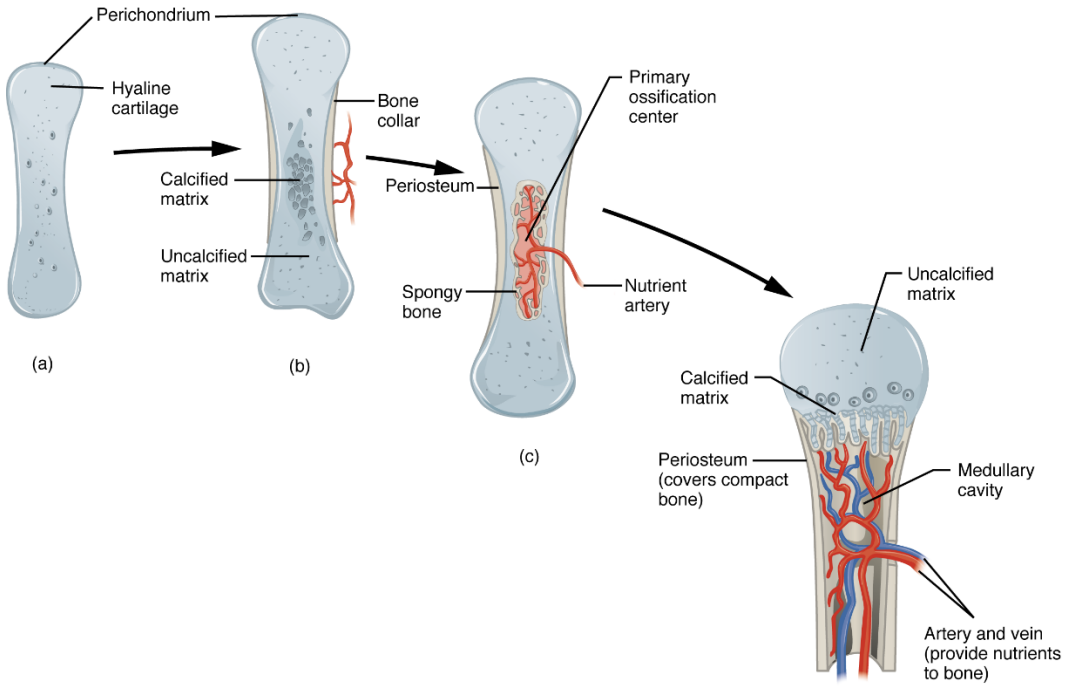

Chondrocytes remaining near the periosteum begin to undergo hypertrophy and secrete collagen type X, matrix metalloproteinases, and alkaline phosphatase (Šromová et al. 2023). These chemicals act to further kill chondrocytes and expand the physical space between chondrocyte housing lacunae (Mescher 2023). Blood vessels invade these open spaces bringing mesenchymal stem cells that mature into new osteoblasts that deposit more permanent bony structures such as

trabeculae (Chagin & Chu 2023). After birth, a secondary ossification center forms at the epiphysis of long bones, undergoing a similar process as the primary ossification centers in the midshaft. A major distinction is the presence of an epiphyseal growth plate comprised of chondrocytes that stimulate longitudinal bone growth (Pawlina & Ross 2018). This growth plate is retained through adolescence and acts as a "mount" for trabecular struts to brace against orthogonally that is lost in adulthood (Carter & Beaupré 2000).

In comparing the trabecular architecture of humans and primates across these early ontogenetic stages, scientists have identified three major phases of development. The pre-locomotor phase is marked by a rapid deposition of trabeculae broadly throughout the diaphysis and epiphysis during fetal and immediate postnatal development. After this initial deposition, underloaded regions of bone are reabsorbed and removed, resulting in a rapid drop in BV/TV (Carter & Beaupré 2000). In the neuromaturation phase, an individual begins to develop locomotory behaviors alongside an increasing body mass, adding strain to specific areas of bone that see a deposition of trabeculae and a sharp increase in BV/TV and Tb.Th, and a decrease in Tb.N. As an individual ages into the mature locomotor phase, the rate of positive allometric bone growth slows and approaches an adult plateau (Saers et al. 2022). By this phase, the body has completed both primary and secondary ossification, and additional modifications to trabecular architecture are primarily driven by changes in strain due to behavior. This pattern of growth has been observed in several limb bones in both humans (Ryan & Krovitz 2006; Saers et al. 2022; Reid et al. 2025) and other primates (Tsegai et al. 2018; Ragni 2020; Nadel et al. 2020).

As humans continue to age bone mass and density steadily decrease. This loss of bone mass has been defined by the World Health Organization to fall into one of two categories. If bone mineral density (BMD) falls below one standard deviation of the average seen in young adults, a person

is diagnosed with osteopenia. If BMD levels continue to decrease down to 2.5 standard deviations below the mean the diagnosis is changed to osteoporosis (World Health Organization). Both osteopenia and osteoporosis can significantly increase the risk of a stress fracture, primarily within the femur, vertebrae, or wrist (Wehrli 2009). Osteoporosis impacts trabeculae through the thinning and eventual reabsorption of individual struts, leading to a decreased ability for bone to resist loading strain. These changes are also gender specific, with women exhibiting more frequent instances of osteoporosis during menopause (Kanis 1996; Parkinson & Fazzalari 2012; Svejme et al. 2012). Similar postmenopausal osteoporosis has been observed in other primate species, though it is still unclear how comparable these processes are to humans (Brommage 2001; Smith et al. 2009)

Human Trabecular Research: Postural Evolution

The ways in which humans bipedally navigate are unique among extant taxa, with only our extinct relatives sharing strong similarities to our posture and gait. As such, understanding how humans evolved this novel postural grade requires paleontologists to analyze fossilized skeletal remains of ancient hominids in lieu of living organisms to monitor and compare with. Analysis of the cortical morphologies of upper limb and foot bones provide key insights into the posture of these extinct taxa. For instance, the lengthening of the femur and the presence of a longitudinal arch in the foot are indicative of habitual upright walking (Lovejoy 1988; Harcourt-Smith & Aiello 2004). Determining the maximum range of motion through evaluation of joint shapes and muscle attachment scars can further highlight the locomotor behaviors an individual's skeleton is capable of (Skoyles 2006). However, the possibility of a behavior does not indicate the presence or absence of said behavior. For instance, many humans have the capacity for the flexibility and balance seen in gymnasts, yet there are few who regularly utilize these exercises.

Additionally, these atypical behaviors are not a key component of our standard walk cycle, and do not reflect how most individuals move through space day to day. Although range of motion can highlight the possibility of both standard and extreme behaviors, it is often ill-equipped to distinguish between the two. Trabeculae, by contrast, reflect habitual loading strains caused by consistent behavior, and are much better indicators of morphological adaptation to a standard gait. Studies of *Australopithecus afarensis,* one of the earliest hominids to develop a bipedal posture, have revealed trabecular patterns consistent with bipedal locomotion that also retain adaptations for arboreal climbing more in line with other primate species (DeSilva & Devlin 2012; Ryan & Shaw 2015; Georgiou et al. 2020). Other projects have been able to determine differences in neolithic and modern human trabeculae, likely stemming from differences in physical activity and subsistence techniques (Scherf et al. 2016). Comparisons between humans and extant hominids have further underscored the potential for trabecular bone to highlight differences in skeletal anatomy driven by behavior (Griffin et al. 2010). Despite the novelty of this field of inquiry, the already promising results suggest avenues for future research to explore the mechanisms driving bipedal evolution through the lens of trabecular bone diversity (Kivell 2016).

Non-Primate Trabecular Bone Studies

Although biomedical and evolutionary research has highlighted a number of key factors that influence trabecular growth, structure and evolution in primates, there is comparatively far less work done on non-primate clades. This is unfortunate as the unique adaptations towards brachiation in primates has resulted in a hindlimb dominated morphology that is distinct within Mammalia and other terrestrial vertebrates (Larson et al. 2000; Young 2012). By contrast, the majority of mammalian taxa are forelimb dominated, where the forelimb acts as the primary

bracer during locomotion, and in turn endures a strong substrate reactive force (Demes et al. 1994; Schmitt and Hanna 2004). Additionally, given the bipedal stance that defines human locomotion, trabecular analysis has further focused on the hindlimb and vertebral column (Nottestad et al. 1987; Lotz et al. 1990; Rafferty 1998; Fajardo & Müller 2001; Baum et al. 2010; Georgiou et al. 2019; Sukhdeo et al. 2020; Wang et al. 2023). This focus has resulted in a limited understanding of trabecular bone structure in other skeletal elements across both primate and non-primate taxa. By neglecting the broader sample of mammalian taxa, critical opportunities to explore how trabecular bone adapts to different functional demands and ecological niches have not been exploited. For example, the forelimbs of digging species like moles or armadillos likely exhibit unique trabecular patterns that reflect their specialized burrowing behaviors, yet these taxa remain understudied (Kley & Kearney, 2007). Similarly, the trabecular structure of arboreal mammals like squirrels or marsupials, which rely on both the fore- and hindlimbs for climbing and grasping, could provide insights into the evolution of arboreal locomotion that are not captured by primate-centric studies. Expanding the scope of trabecular analysis allows researchers to better identify universal principles of trabecular bone adaptation and evolution, as well as address the diversity in structures between species and distinct skeletal elements alike.

That is not to say there has been no work done to measure trabecular structures in non-primate taxa; a number of these studies have served as a foundational basis for this dissertation. Some of the initial trabecular analysis of non-primate taxa involved controlled experiments where limb orientations and joint loading conditions were manually modified through various artificial constraints and specific repeated exercise. This enabled researchers to directly evaluate how trabecular bone adapts in response to changes in mechanical stress. The majority of these studies sampled domesticated species, such as horses (Vander Sloten & Van der Perre 1989); sheep

(Barak et al. 2011; Polk et al. 2008), pigs (Metzger et al. 2015), cattle (Yamada et al. 2022) and rabbits (van der Meulen et al. 2006). In assessing the growth patterns of trabeculae across several species, researchers could confirm that the microstructural adaptations in response to injury or changes to stress orientation were present and consistent across Mammalia.

Although these studies sampled exclusively adult individuals, work by Tanck and colleagues sought to measure the effects of ontogenetic growth on trabecular density in quadrupedal species using the domesticated pig (*Sus scrufa*) as a model (Tanck et al. 2001). The team found an almost inverted trend compared with that seen in primates, in which there is significant positive allometric growth in BV/TV and anisotropy values after birth that decreased down to a steady asymptote around 60 weeks of age. This immediate increase in trabecular density is likely driven by the speed at which pigs are able to freely walk unassisted compared to chimpanzees and humans. The former is not sedentary for long enough to drive osteoclasts to remove redundant bone material before an increase in BV/TV is needed to support against locomotory driven loading strain. As of writing, there are no other ontogenetic analyses of trabecular growth in other taxa due to the difficulty in accurately aging the majority of mammalian species, restricting viable candidates for study down to raccoons (Grau et al. 1970; Junge & Hoffmeister 1980; Fiero & Berts 1986) and coyotes (Linhart & Knowlton 1967; Maher 2002).

Other studies have sought to explore the impact of body mass on trabecular architecture across several higher clades of amniote. Metanalysis of the proximal femur in several mammalian species ranging in size from the Asian elephant (*Elephas maximus*) to the house mouse (*Mus musculus*) found Tb.Th and Tb.Sp to demonstrate positive allometric growth with respect to body size, whereas Tb.N exhibits negative growth (Barak et al. 2013). Comparable trends have also been observed in Aves (Doube et al. 2011) and non-avian reptiles (Plasse et al. 2019)

suggesting these trends are consistent across the amniote femur. BV/TV was largely unaffected by body mass, suggesting other ecomorphological factors may be driving the variation seen across Mammalia. Aquatic species have been demonstrated to exhibit less dense trabecular regions than semi-aquatic and terrestrial species; whether this pattern is driven by buoyancy diminishing limb strain or the shape of flippers limiting trabecular growth is unclear (Houssaye et al. 2016).

Looking beyond higher-order clades, several studies have focused on specific families of mammals to identify if ecological niche or phylogeny may play a role in determining trabecular architecture. These studies have found mixed results, with some identifying a clear distinction with respect to ecological niche (Amson et al. 2017; Mielke et al. 2018), whereas others have highlighted the difficulty in decoupling body mass from ecology (Zack et al. 2023). Work by Smith and colleagues on earthworm mice found that in smaller taxa, differences in morphology and ecosystem must be extreme to produce statistically significant differences in trabecular structure (Smith et al. 2023).

Identifying Research Gaps

Although these studies have served as solid foundational work in exploring trabecular architecture across Amniota, there is still more to be done to understand intra- and interspecific trabecular diversity, and what factors drive that diversity. It is also important to note that in recent years, several studies have identified that the sedentary lifestyle of captive zoo and domesticated farm animals has a significant impact to trabecular growth and structure (Chirchir et al. 2022; Zack et al. 2022). Many of the previously mentioned studies have sampled animals that fall under these categories due to their prevalence in museum collections and the ease of

access for living samples, so our understanding of the broad trabecular structures of wild individuals is far more limited than the breadth of research would suggest.

This dissertation seeks to address this gap in knowledge and investigate trabecular architecture in wild non-primate taxa through three lenses. In chapter one, I will measure trabecular development across ontogeny in raccoons (*Procyon lotor*). This species was selected for its abundance in local collections, its generalist nature utilizing a wide range of behaviors, and the accurate methods of aging skeletal remains. For chapter two, I will measure trabecular structures across Mammalia and Reptilia to identify the extent to which phylogeny, ecomorphotype, and general postural grade impact key trabecular characteristics. Finally, chapter three seeks to sample several species of Didelphidae to explore the variation present within both upper and lower limb elements. In all three chapters, I will compare at least two distinct bony elements to highlight the potential diversity in trabeculae across the skeleton rather than assume uniformity as many papers have done in focusing exclusively on the proximal femur.

Additionally, several recent works have highlighted the potential for primary trabecular orientation to be a diagnostic characteristic for postural grade and ecology (Amson et al. 2017; Mielke et al. 2018; Lukova et al. 2024; Alfieri et al. 2025). These studies have all measured trabecular orientation in species with relatively homogeneous cortical morphologies, making a standardized orientation of the bones themselves relatively simple. For measuring species with widely disparate gross morphologies, such as the mammalian and reptilian femur, I have developed an orientation methodology that moves away from *in vivo* orientations to allow for more meaningful comparisons of the trabeculae within. To visualize these orientations, I will utilize modified stereomorphic projections, commonly used in geology to map planar structures,

to represent these directions in 2D space. A similar methodology has already been successfully utilized to illustrate trabecular directionality (Amson et al. 2017; Mielke et al. 2018).

My goal with this dissertation is to establish a foundational understanding of trabecular diversity that highlights the complexity of these structures while shining a light on the factors that influence their architecture. These results may provide potential applications for more optimal use of endosseous devices by highlighting more efficient orientations and loading regimes for stimulated trabecular remodeling. Additionally, if it is found that trabecular characteristics can serve as a proxy for postural grade or ecomorphotype, there are opportunities to utilize these techniques to analyze fossil specimens. Although traditional range of motion (ROM) analysis has provided paleontologists the means to understand an extinct species' capacity for movement (Hutson & Hutson 2012; White et al. 2015; Senter & Sullivan 2019; Gatesy et al. 2022; Brocklehurst & Pierce 2023), the reactive nature of trabeculae suggests they may be a more diagnostic metric of specific loading strains caused by frequent locomotor behavior.

Chapter 2: Raccoons Reveal Hidden Diversity in Trabecular Bone Development

Abstract:

Trabecular bone, and its ability to rapidly modify its structure in response to strain exerted on skeletal elements, has garnered increased attention from researchers with the advancement of CT technology that allows for the analysis of its complex lattice-like framework. Much of this research has focused on adults of select taxa, but analysis into trabecular development across ontogeny remains limited. In this paper, we explore the shift in several trabecular characteristics in the articular head of the humerus and femur in Procyon lotor across the entirely of the species' lifespan. Our results show that while body mass plays a role in determining trabecular structure, other elements such as bone growth, increased activity, and puberty result in trends not observed in the interspecific analysis of adults. Furthermore, differences in the trabeculae of the humerus and femur suggest combining distinct boney elements in metanalyses may obfuscate the variety in the structures. Finally, rates at which fore and hindlimb trabeculae orient themselves early in life differ enough to warrant further exploration to identify the currently unknown causes for their variation.

Introduction:

The bony portion of the skeletal system that comprises the internal framework for most vertebrate species is comprised of two types of tissue: cortical and cancellous bone. The cortex forms the rigid and smooth dense outer layer of bone, whereas cancellous bone is internally arranged as a complex web of bony struts surrounded by bone marrow. These struts, commonly

known as trabeculae, typically orient in the direction of primary strain to increase the overall strength of the bone with a diminished weight when compared to cortical structures (Wolff 1892; Koch 1917; Fyhrie & Carter 1986). The direction and magnitude of strain exerted on bone can vary widely throughout an individual's life, and trabeculae have evolved to rapidly adapt to these changes. As these struts are individually small and are surrounded by red marrow rich in osteoblasts and osteoclasts responsible for bone modification, trabeculae have been demonstrated to reorient and change shape in a period of weeks to months, a process that would take cortical bone up to ten times as long **(**Parfitt 1988; Morgan et al. 2013). Due to its ability to rapidly adjust its structure, trabecular bone has become an important model for understanding the ways in which bones remodel in response to changes in loading strain.

Advancements in high resolution computed tomography scans and computational analysis over the last few decades have allowed researchers to better describe and interpret complex trabecular structures, and numerous studies of cancellous bone in humans and our primate relatives have been undertaken. These studies have explored variation across trabecular characteristics in several load-bearing bones (e.g., vertebrae, femur, tibia) and the ways in which cancellous bone scales with body size (Rafferty 1998; MacLatchy & Müller 2002; Doube et al. 2010; Ryan & Walker 2010; Barak et al. 2017; Tsegai,et al. 2018). Studies that have focused on the effects of ontogeny in primates have identified a trend towards increasing bone volume fraction and thickness as juveniles develop the locomotor mechanics they will utilize as adults (Ryan et al. 2017; Tsegai et al. 2018; Saers et al. 2022A). Humans demonstrate a sharp decrease in these values during their first year, likely caused by the delay in locomotor transitions compared to our closest relatives (Ryan & Krovitz 2006).

Although research on humans and primates has highlighted applications for biomedical work and models for understanding the evolution of bipedality (Ryan & Krovitz 2006; Ryan & Raichlen 2017; Saers et al. 2017; Tsegai et al. 2018; Saers et al. 2022A), there have been far fewer publications released focused on other mammalian clades. Primates are a less-than-optimal clade to use as a basis for extrapolating trends in other mammals as their adaptations towards specialized grasping arboreal behaviors have resulted in limb structures and hindlimb dominance that stand out as distinct to many other mammals (Larson et al. 2000; 2011, Young 2012). Humans are an even poorer model as our unique bipedal stance limits the use of our forelimbs in regular locomotory behavior. It should come as little surprise, then, that analysis of trabecular bone in humans and primates focuses primarily on the hindlimb and vertebral column (Nottestad et al. 1987; Rafferty 1998; Fajardo & Müller 2001; Morgan & Keaveny 2001; MacLatchy & Müller 2002; Ryan & Krovitz 2006; Fields et al. 2011; Wang et al. 2015). Additionally, advancements in medicine and quality of life have extended human lifespans far beyond the average range seen in pre-civilization individuals, resulting in trabecular changes in later stages of life that are frequently driven by diseases such as osteoporosis, rather than the standard effects induced solely by aging (McDonnel et al. 2007; Chen et al. 2013). Although studies of non-primate taxa have been conducted (Tanck et al. 2001; Amson et al. 2017; Mielke 2018; Smith 2020; Zack et al. 2023), these analyses often sample small and/or autapomorphic clades or do not consider the potential effects of ontogenetic variation. Our understanding of trabecular development primarily stems from primate clades with a distinct brachial locomotor system and limb pair dominance compared to other mammals (Demes et al. 1994; Schmitt & Hanna 2004; Young 2012), but it is possible the trabeculae of other species differ in their development, especially given differences in which pair of limbs endures more strain during locomotion.

Recent research has sought to investigate ontogenetic trabecular development in Japanese macaques as a model for a terrestrial quadrupedal ecomorphotype (Saers et al. 2022A), but more work will be necessary to analyze differences present in long limb elements, and to identify trabecular growth trends unique to primates. As trabecular research continues to expand in scope, identifying sources of potential trabecular variability will become integral in better understanding its diversity across a wide spectrum of taxa.

This study seeks to explore the development of trabecular structures in the articular heads of both the humerus and femur across the ontogeny of a less derived mammal species: *Procyon lotor* (raccoon). Raccoons were selected for two key reasons. First, they are one of the few species with a robust, non-destructive age-determination system that facilitates precision sampling of individuals across a full range of ages and ontogenetic stages (Grau et al. 1970). Second, as a prevalent mid-sized mammal present throughout much of North America, the high number of raccoon specimens housed within collections ensures that a large and diverse assemblage of individuals from a specific region can be sampled.

Based on observations in primates and *Sus domesticus*, I predict a significant difference in the trabecular characteristics between the humerus and femur of raccoons over the course of ontogeny (Tanck et al. 2001; Tsegai et al. 2018; Saers et al. 2022B). I also predict a significant difference in the trabecular architecture of the femur and humerus of adult raccoons due to several behaviors that exert higher strain on the hindlimbs. Adult raccoons often engage in vertical climbing that utilizes the hindlimbs as both a bracer and propeller which in turn places a greater strain on the femur (Hanna et al. 2017). Raccoons also regularly utilize a bipedal posture to both forage for and carry food (MacClintok & Thomas 1981; McClearn 1992). Juvenile raccoons younger than 12 weeks of age that have yet to leave the den and practice these more

strenuous hindlimb-dominated behaviors will likely feature a diminished difference in fore- and hindlimb trabeculae as all four limbs are utilized more consistently. Additionally, a lack of specific high-strain locomotor behaviors will likely result in more variable trabecular primary orientations in these pre-pubescent raccoons. Finally, following trends seen in other taxa, I predict trabecular bone volume fraction and anisotropy to increase with age as individuals grow and develop (Tanck et al 2001; Saers et al. 2022A).

Methods

Fifty-five wild specimens of raccoon (*Procyon lotor)* native to the Great Lakes region were sampled. The skeletal remains of all specimens were housed at the Field Museum of Natural History and the Illinois State Museum. Only wild specimens were selected as limited mobility, behavioral variance, and other factors have been demonstrated to have a measurable effect on trabecular structures of captive specimens (Chirchir et al. 2022; Zack et al. 2022). Individuals were aged based on the presence or absence of several skull sutures following Junge and Hoffmeister (1980), an approach that has been demonstrated to have a high level of accuracy for both sexes compared to other non-destructive methods (Grau et al. 1970; Fiero & Berts 1986) (specimen ages along with trabecular characteristics have been provided in Supplemental Dataset S2.1). Each specimen was assigned to one of five age groups: 2 months (n=13), 4-12 months (n=11), 14-24 months (n=10), 26-38 months (n=7), and 46+ months (n=14). The gaps between age groups are a part of Junge and Hoffmeister's (1980) approach and are retained here. These age groups separate several stages in raccoon ontogeny, with juveniles beginning to walk around their nests by two months, and individuals reaching sexual maturity around 12-13 months of age (MacClintock & Thomas 1981). The exact timing of the loss of the cartilaginous growth plates and the fusion of the epiphyses, signaling the end of elongation of the limb bones, varies among

individuals, but typically occurs between the first and second years of life (Johnson III 1969). Age groups past two years were segregated to determine the effect increasing body mass and age-related wear might have on trabecular structures.

The right humerus and femur of each specimen were selected for analysis. Any bones that featured damage to the proximal articular head or morphological features affected by disease were excluded. If a specimen lacked a viable element from the right side, the corresponding left element was mirrored to replace it. This mirroring was only necessary in a small number of cases: four of the humeri and seven of the femora.

Specimens were scanned using a GE phoenix v | tome | x µCT (micro-computed tomography) scanner with a 240 kV micro-focus X-ray tube at the University of Chicago's PaleoCT facility (RRID:SCR_024763). Each scan was conducted to capture the entire morphology of upper limb elements, with multi-scans conducted for larger specimens. Scan resolution ranged from 24.0375 to 46.937 µm, with smaller specimens requiring a higher resolution to preserve all material (see S1.1). Within each age group, resolutions varied by no more than 10 µm. Scans were reconstructed in GE phoenix datos | x, and image stacks were aligned and cropped in VGStudioMAX 3.3.

Scans were modified in the image processing program Dragonfly 2022.2 (Dragonfly 2022) so that each bone was uniformly oriented. First, the midpoint of the distal and proximal metaphyses were aligned along the Z-axis. Second, the lateralmost points where the proximal articular head contacted the anatomical neck were aligned along the Y-axis such that the articular surface pointed in the -X direction, and the tubercles point in the +X direction (Fig. 2.1. This orientation does not reflect how an animal would hold their proximal limb elements in life but rather reflects

a uniform orientation for comparison between individuals that can be replicated for other species as well.

Figure 2.1
Standardized orientations for the Humerus (A) and Femur (B) at various ages. The blue spheres represent the ROI sampled from each bone. Cross-sectional views along the X-Z plane are also provided.

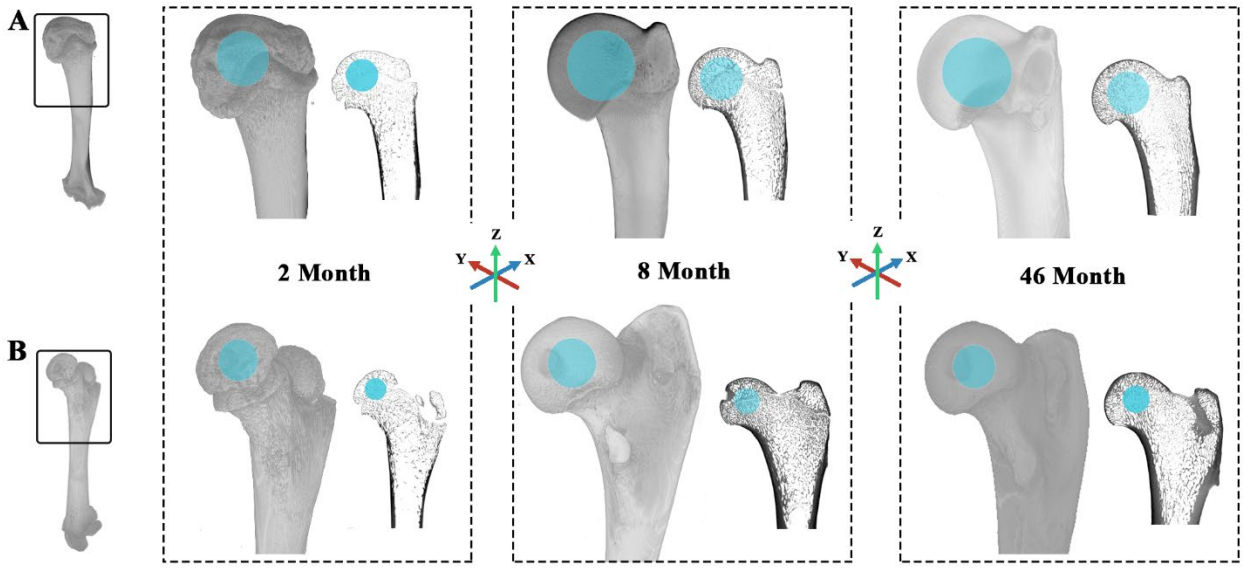

Previous studies have largely ignored the need for a standard orientation of the entire element due to the exclusion of trabecular orientation measurements and have instead used landmarks of a specific element (Barak et al. 2011) or the midsection of anatomical planes relative to the articular head (Ryan & Ketcham 2005) to determine a region of interest (ROI). Those that have included specific orientations for long limb elements have used similar methods to orient the bones vertically but rely on taxon-specific features for its rotation (Amson et al. 2017; Mielke et al. 2018). My approach in this study has been designed to facilitate comparative analysis of disparate limb elements. Additionally, because these methods utilize the overall shape of the bone, rather than relying on taxonomic-specific landmarks, this methodology can be used for comparisons between taxa in an interspecific analysis.

Once bones were oriented, the articular head was isolated within a box whose sides contacted the innermost edges of the cortical bone. A spherical ROI was expanded out from the center of this box to include the maximum number of trabeculae while excluding any cortical bone (see Appendix A2.1A-E for a visual representation of the orienting and ROI selection process). This ROI was segmented using an Otsu sorting algorithm (Otsu 1979), which has been shown to preserve small trabecular structures and remove free-floating particles while avoiding the overestimation of bone volume fraction (Smith & Angielczyk 2020).

The volume of the segmented trabeculae was compared in Dragonfly to the volume of the spherical ROI to determine bone volume fraction (BV/TV). Two binarized TIFF-stacks, one of the trabeculae and one of the non-trabecular spaces, were imported into ImageJ for further analysis (Rasband 1997). Using the plugin BoneJ (Doube et al. 2010) each TIFF-stack was purified (i.e., small floater particles are removed) before being processed to determine anisotropy (DA), trabecular thickness (Tb.Th) and trabecular spacing (Tb.Sp). These stacks were then imported into Quant3D (Hoebeke & Trubuil 1999) where trabecular number (Tb.N) was measured, and the primary trabecular eigenvectors were identified; the latter were then converted into azimuth and plunge using code developed by Amson et al. (2017). The mean intercept length (MIL) tensor was selected to determine the fabric tensor as it has been demonstrated to more accurately predict the mechanical properties of trabecular bone compared to other methods tensors (Zysset 2003; Cowin & Doty 2007; Moreno et al. 2014).

Log-transformed body mass estimates for each specimen were calculated using the circumferences of the humerus and femur and the scaling equation of Campione and Evans (2012). As various trabecular structures have been demonstrated to scale with body mass in several mammalian species (Barak, Lieberman & Hublin 2013; Kim et al. 2017; Mazzetti et al.

2017; Saers 2017; Zack et al 2023; Smith et al., 2024), several regression plots were constructed to assess the relationship between trabecular characteristics and body size. K-fold cross validations were utilized to determine which degree featured the lowest mean square error (MSE) for each of the polynomial regressions. The predicted linear regression slopes were also estimated for each characteristic and varied depending on their units. BV/TV and anisotropy are unitless ratios with an isometric slope of 0. Tb.N is measured as individual struts per mm and has an expected isometric slope of -1/3. Tb.Th and Tb.Sp are both linear measurements and have a predicted isometric slope of 0.33 as these features scale at 1/3 relative to volume (Mielke et al. 2018; Plasse et al. 2019; Smith et al 2023).

Pearson's correlation coefficients were calculated between every univariate trabecular characteristic in both the humerus and femur using the pcor function of the ppcor package in R (Kim 2015). The correlation coefficients were used to identify the presence and strength of any potential linear correlation between features. The variability of the trabecular bone metrics was compared using the coefficient of variation. This statistic expresses standard deviation as a proportion of the mean, making it appropriate for comparing metrics with different absolute magnitudes. The coefficient of variation was calculated using the cv function as a part of the raster package in R (Hijmans 2023).

A principal component analysis (PCA) was performed on the estimated body mass, trabecular number, spacing, thickness, density, anisotropy and trabecular orientation for the femur and humerus of each specimen. A PCA plot was calculated with the raw values of all trabecular characteristics save for azimuth, whose values were transformed using the formula $\left||x-180|-90\right|$. This transformation was used to more closely pair nearby angle measurements with differing angle values (e.g., 359° and 1°) and to quantify trabecular azimuth as pointing

somewhere along the spectrum between the anterior/posterior and medial/lateral planes. Each PCA analysis was performed using the prcomp function as part of the stats package in R (R Core Team 2023).

Because several trabecular characteristics featured a non-normal distribution that could not be transformed, nonparametric Kruskal-Wallis (Kruskal & Wallis 1952) and Dunn tests (Dunn 1964) were utilized in R using the kruskal.test (R Core Team 2023) and dunnTest (Dinno et al. 2017) packages respectively. The aims of these tests were to determine if the means for each trabecular characteristic were significantly different over the course of the species' ontogeny. If the results of Kruskal-Wallis test of a characteristic was significant at $\alpha = 0.05$ significance level, a Dunn test was run to determine which age group means were significantly different.

Results

When the raw trabecular characteristics are divided into age bins, I observed a consistent pattern in which all metrics for two-month raccoons except femoral Tb.N are statistically lower than for older age groups (Table 2.1; Fig. 2.2).

Table 2.1
Raw mean values of each trabecular characteristic separated by age groups

		Humerus					Femur				
Age Group	Number of Individuals	Anisotropy	BV/TV	TbTh (cm)	TbSp (cm)	TbN	Anisotropy	BV/TV	TbTh (cm)	TbSp (cm)	TbN
2 Months	13	0.19	0.276	0.0135	0.0311	1.71	0.16	0.358	0.0137	0.0245	2.13
4-12 Months	11	0.342	0.437	0.0185	0.0315	1.87	0.333	0.477	0.0214	0.028	1.86
14-24 Months	10	0.355	0.369	0.0177	0.0354	1.69	0.411	0.468	0.0252	0.0319	1.62
26-38 Months	7	0.351	0.314	0.0174	0.0386	1.51	0.399	0.412	0.0228	0.0358	1.52
46+ Months	14	0.386	0.311	0.0174	0.0419	1.45	0.434	0.404	0.0226	0.0361	1.57

Figure 2.2
Boxplots plots for each trabecular characteristic in the femur and humerus (A-E) and estimated log-body mass (F).

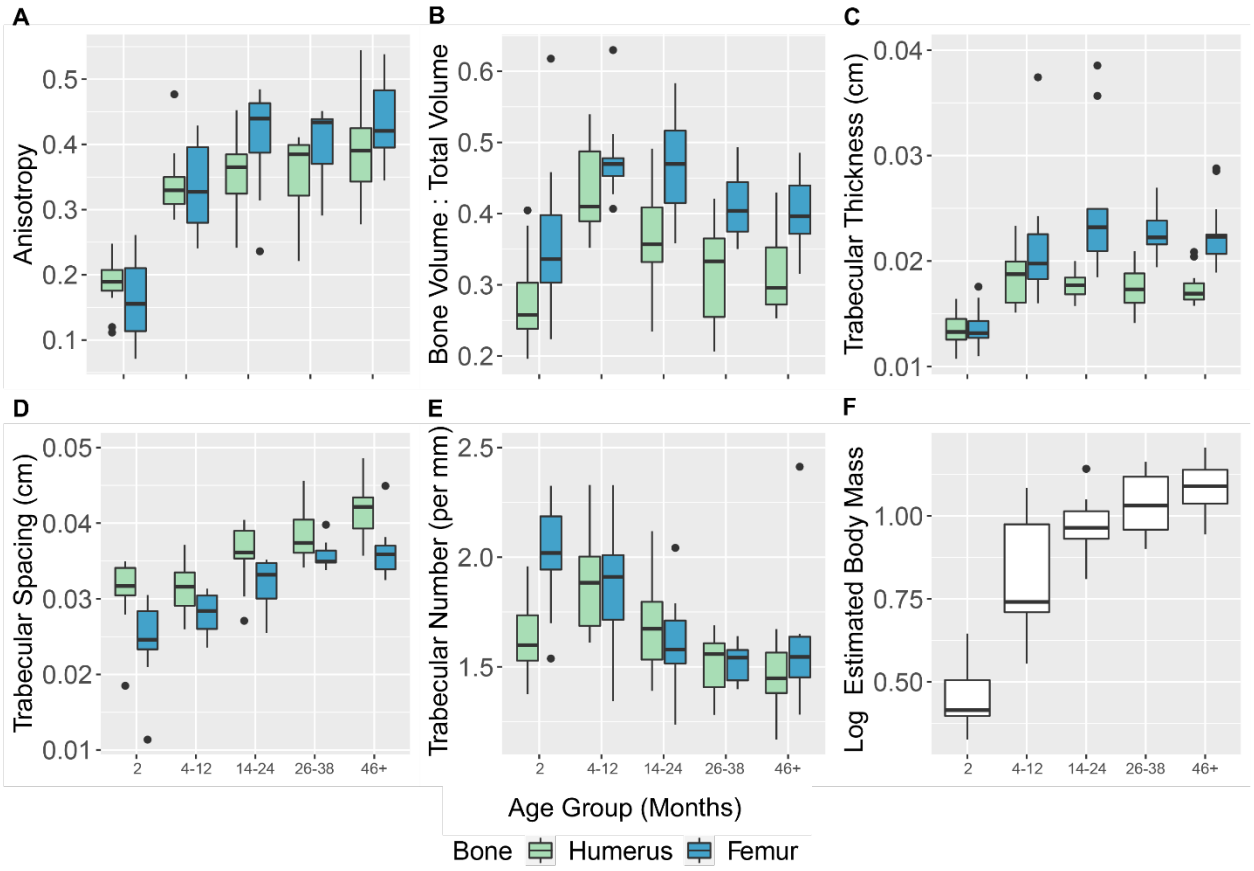

Both bones demonstrate a peak in BV/TV values within the 4-12 month groups, before gradually decreasing for all subsequent age groups. In the case of the 46+ month group, femoral BV/TV values are nearly comparable to those of the 2 month group. Trabecular number is also unique in that it displays the highest difference in values between the humerus and femur in two-month individuals, with the values becoming more comparable between the fore- and hindlimbs by eight months. From four months onward, trabecular values either approximate a plateau or form a gradual logarithmic curve (Figs. 2.3 & 2.4). The coefficients of variation of the age groups indicate that for both the humerus and femur, 2-month raccoons present the highest spread for anisotropy, BV/TV, and Tb.N (Table 2.2).

Figure 2.3

Regression plots of the trabecular characteristics of the humerus v log corrected body mass estimates. The characteristics in order are DA (A), BV/TV (B), Tb.Th (C), Tb.Sp (D), and Tb.N (E).

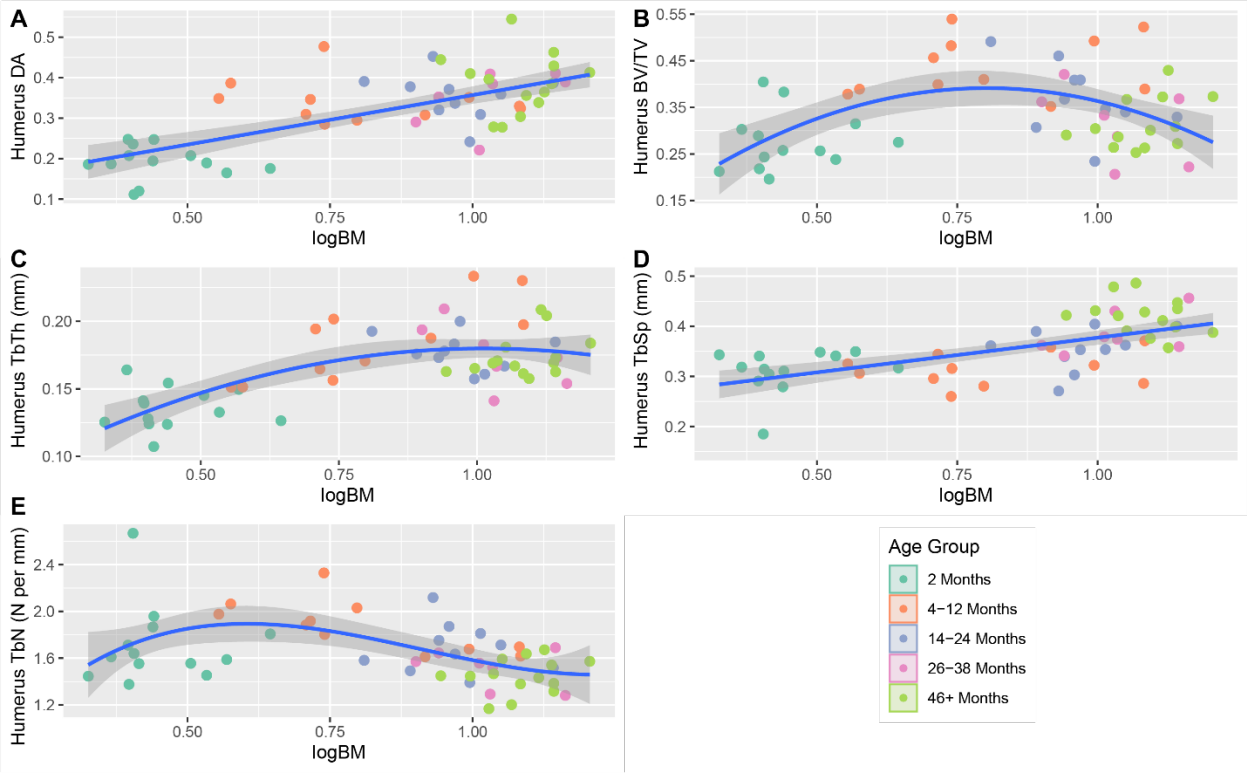

Figure 2.4
Regression plots of the trabecular characteristics of the femur v log corrected body mass estimates. The characteristics in order are DA (A), BV/TV (B), Tb.Th (C), Tb.Sp (D), and Tb.N (E).

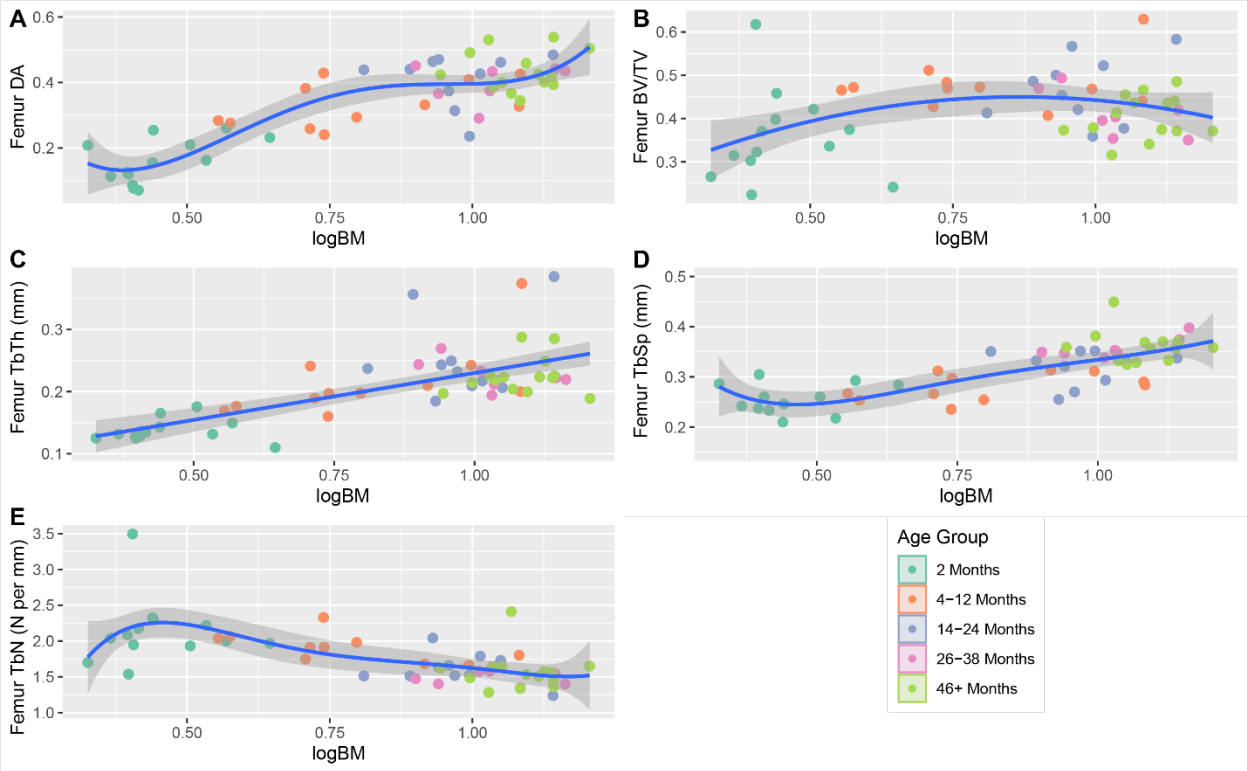

Table 2.2
Coefficients of variation for each trabecular characteristic separated by age groups

		Humerus					Femur				
Age Group	Number of Individuals	Anisotropy	BV/TV	TbTh (cm)	TbSp (cm)	TbN	Anisotropy	BV/TV	TbTh (cm)	TbSp (cm)	TbN
2 Months	13	22.1	22.7	11.3	14.1	19.5	42.1	29.1	12.9	20	21.8
4-12 Months	11	15.6	14.6	15.8	10.8	11.8	20.7	12.2	27.6	9.61	13.9
14-24 Months	10	16	20.5	7.59	11.8	12.6	19.5	16.4	26.1	10.9	13.2
26-38 Months	7	20.2	25.2	13.3	10.8	10.7	14.6	13.1	10.6	5.77	6.14
46+ Months	14	19.2	17.1	8.9	8.7	10.4	14	12.5	13.1	8.6	17.1

Principal component analyses for both the humerus and femur feature a clear separation between the two-month-old specimens and the other age groups, which cluster towards the left of the PCA plots (Fig. 2.5).

Figure 2.5
PCA and biplots plots of all trabecular characteristics and estimated logBM for both the humerus (A) and femur (B). PCA plots include a cross sectional view of the trabeculae of certain individuals taken from the center of the ROI.

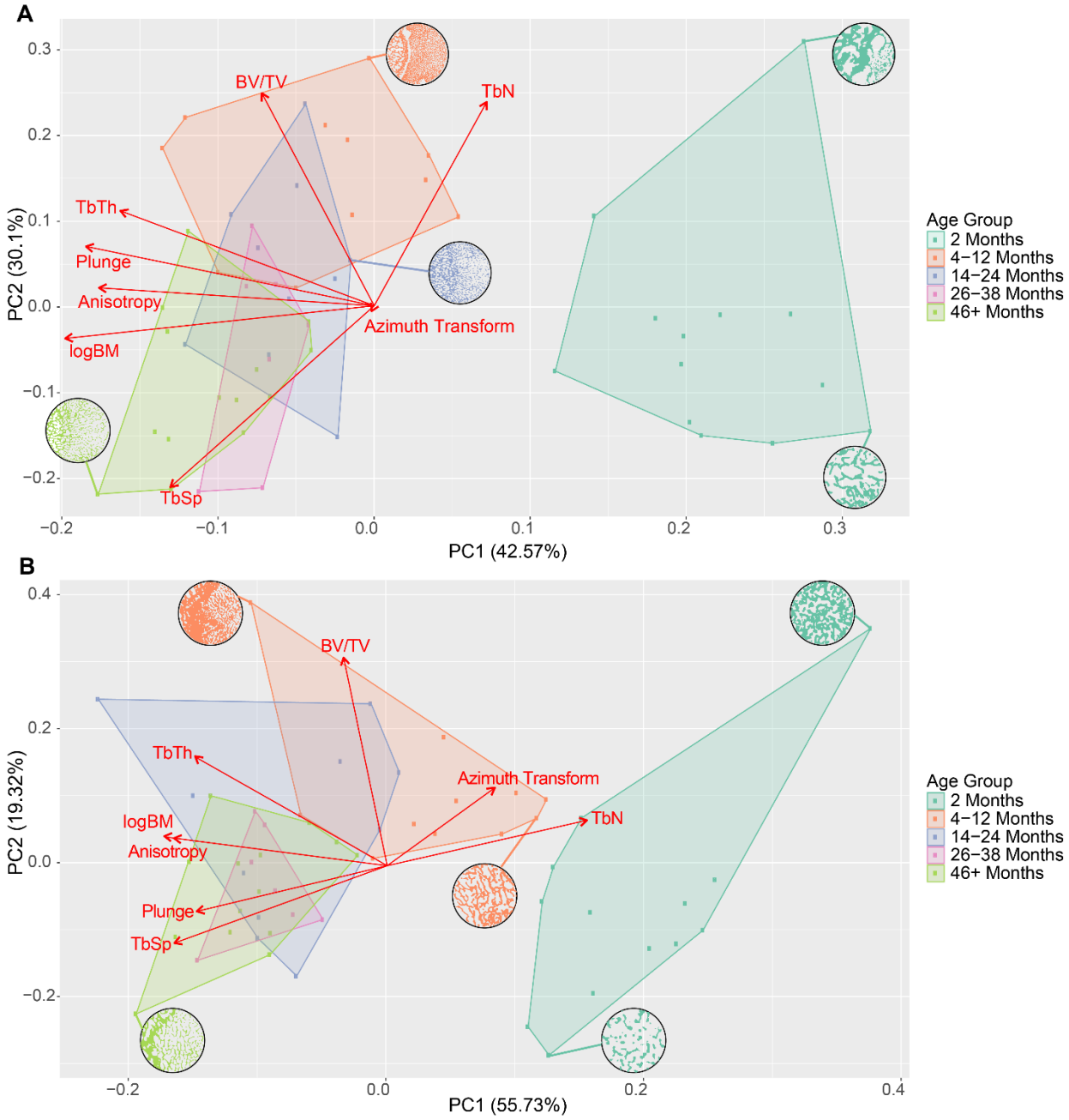

For both limb elements, logBM, DA, and plunge receive strong loadings on the first PC, with all values decreasing as one moves towards higher PC scores. Principal component two features

more diversity in loadings between the humerus and femur, with only BV/TV featuring a strong loading in the positive direction in both cases. For the humerus, Tb.N and Tb.Sp have strong loadings in the positive and negative directions respectively, whereas the femur only exhibits a mild loading for the transformed azimuth on PC two.

Kruskal Wallis tests on each trabecular characteristic determined that there was a statistically significant difference for the means of all femoral and humeral metrics with respect to age (Table 2.3). The Dunn tests (Dunn 1964) demonstrated that among all age groups, the 2-month age group most consistently demonstrated significant differences in trabecular metric means when compared to the older age groups; comparisons between the older age groups more frequently returned non-significant differences (see Appendix A2.2).

Table 2.3
Results of Kruskal-Wallis tests conducted of each trabecular characteristic and logBM for five distinct age groups (2 months, 4-12 months, 14-24 months, 26-38 months, and 46+ months)

	Trabecular Characteristic	Chi-Squared	df	P-Value
Humerus	DA	30.268	4	$4.216e^{-6}$
	BV/TV	23.5	4	0.0001006
	Tb.Th	26.035	4	$3.113e^{-5}$
	Tb.Sp	34.502	4	$5.878e^{-7}$
	Tb.N	21.908	4	0.0002091
	Azimuth Transform	1.9958	4	0.7365
	Plunge	32.604	4	$1.439e^{-6}$
Femur	DA	34.184	4	$6.83e^{-7}$
	BV/TV	18.395	4	0.001033
	Tb.Th	31.692	4	$2.211e^{-6}$
	Tb.Sp	39.847	4	$4.656e^{-8}$
	Tb.N	25.568	4	$3.867e^{-5}$
	Azimuth Transform	7.6264	4	0.1063
	Plunge	23.704	4	$9.154e^{-5}$
	logBM	39.07	4	$6.738e^{-8}$

Although analysis of Pearson's correlation coefficient found nearly all trabecular characteristics to be significantly correlated with one another, only Tb.Th and BV/TV featured a "very strong" correlation in both the humerus and femur (absolute r value between 0.8 and 1; Evans 1996) (Table 2.4). The next highest r value pair in both bones was DA with Tb.Sp, with each bone featuring an *r* value above 0.7. Regression analysis indicated a significant relationship between all trabecular characteristics and body mass. Both the humeral (Fig. 2.3) and femoral (Fig. 2.4) trabeculae show similar trends as body mass increases, with DA, Tb.Th, and Tb.Sp increasing with body mass, and BV/TV and Tb.N represented by convex-upward parabolic arcs. For the humerus, the rate of increase in Tb.Th during the first year of life is only half that of Tb.Sp before leveling out to a relative plateau at the end of puberty. This trend is not present in the femur where Tb.Th and Tb.Sp growth rates remain relatively similar throughout all age groups. Despite this difference, both bones see a peak of BV/TV around 8-12 months, with the subsequent decrease at later ages likely stemming from a steady decline in Tb.N from the age of 4 months onward.

Table 2.4
Pearson's correlation coefficients of each trabecular characteristic in the humerus (A) and femur (B). Any pair that features a "very strong" correlation (absolute r value between 0.8 and 1) are colored in gray, and any correlation with a p-value ≤ 0.05 are marked with a *.

A	DA	BV/TV	Tb.Th	Tb.N	Tb.Sp
DA	~	0.204	-0.00152	0.389*	0.71*
BV/TV	0.204	~	0.911*	0.557*	-0.237
Tb.Th	-0.00152	0.911*	~	-0.579*	0.13
Tb.N	0.389*	0.557*	-0.579*	~	-0.609*
Tb.Sp	0.71*	-0.237	0.13	-0.609*	~
B	DA	BV/TV	Tb.Th	Tb.N	Tb.Sp
DA	~	0.406*	-0.0768	0.00655	0.632*
BV/TV	0.406*	~	0.841*	0.491*	0.478*
Tb.Th	-0.0768	0.841*	~	-0.655*	0.233
Tb.N	0.00655	0.491*	-0.655*	~	-0.364*
Tb.Sp	0.632*	0.478*	0.233	-0.364*	~

Separating the raccoons into three distinct age bins (Figs. 2.6 and 2.7) highlights that a consistent scaling of each trabecular characteristic with body mass is not preserved in individual age groups. Of the three age groups, individuals 14 months and older show the most consistently allometric trends, and often with negative gradients as opposed to the positive slopes seen in younger age bins.

Figure 2.6

Regression plots for each trabecular characteristic of the humerus with regression slopes calculated for three age groups: 2 months, 4-12 months, and 14+ months. Groups were selected to identify trends in trabecular development before, during, and after puberty. The black dotted line represented the estimated regression slope with respect to isometry. The characteristics in order are DA (A), BV/TV (B), Tb.Th (C), Tb.Sp (D), and Tb.N(E).

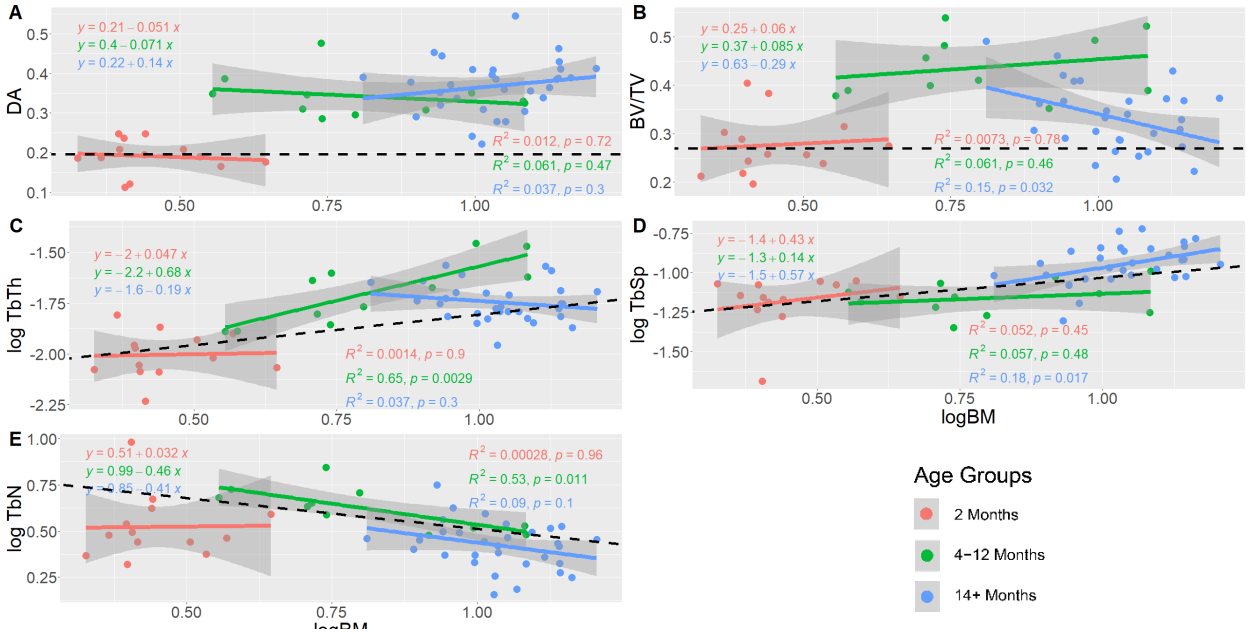

Figure 2.7
Regression plots for each trabecular characteristic of the femur with regression slopes calculated for three age groups: 2 months, 4-12 months, and 14+ months. Groups were selected to identify trends in trabecular development before, during, and after puberty. The black dotted line represented the estimated regression slope with respect to isometry. The characteristics in order are DA (A), BV/TV (B), Tb.Th (C), Tb.Sp (D), and Tb.N(E).

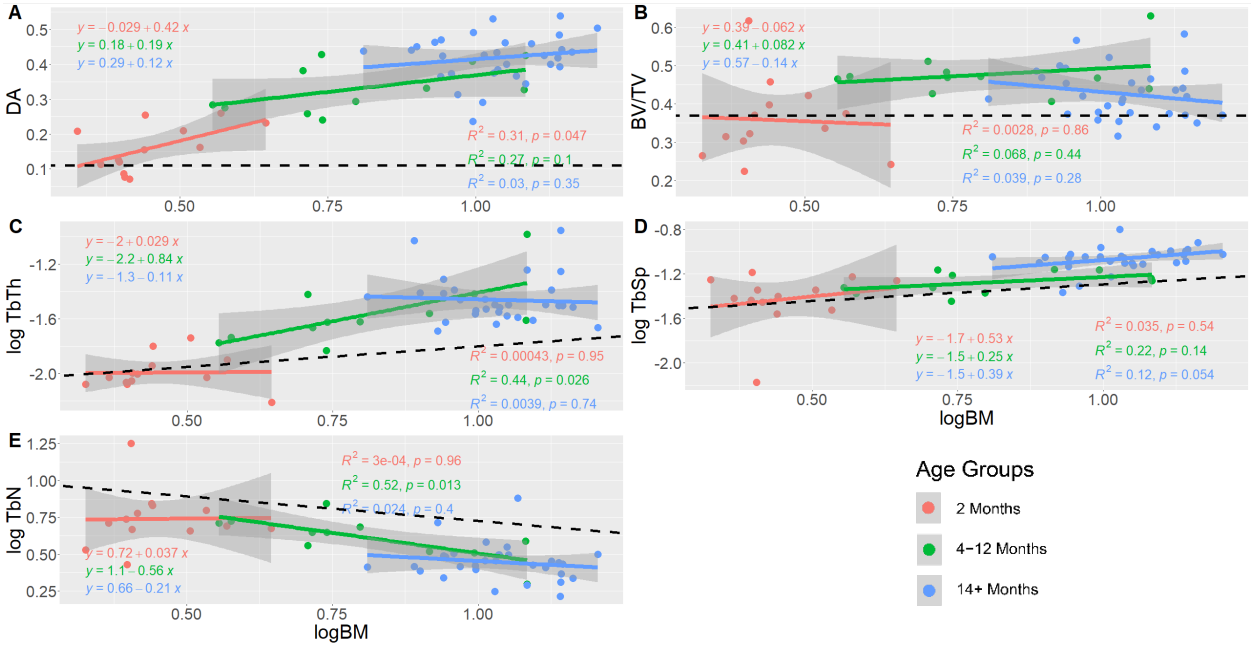

When representing the primary trabecular orientation via stereomorphic projection (Fig. 2.8), two-month individuals again display values that notably deviate from the other age groups. Specifically, the orientations for two-month raccoons trend towards very horizontal directions, with trabeculae in the humerus and femur aligned with the anterior/posterior axis for each bone. Although the trabeculae rapidly converge towards a nearly vertical orientation in the center of the stereomorphic projection as the raccoons age, there seems to be a lag in the femur, with raccoons in the 4-12 month age range still featuring subhorizontal trabecular orientations, albeit more vertical than younger individuals.

Figure 2.8
Primary trabecular orientations of the trabeculae in the humerus and femur for each *Procyon lotor* individual. Points are color coded with regards to age groups, and the size of each point reflects anisotropy, with larger points representing higher anisotropic values (DA). Cross sectional views of both the humeral and femoral articular heads are included to illustrate the orientations of each bone. The X and Y axes are included in the margins to match those presented in figure 2.1. The orientations of each bone do not reflect how the bone is held in life but rather reflect a uniform orientation that makes direct comparison between the two more pronounced.

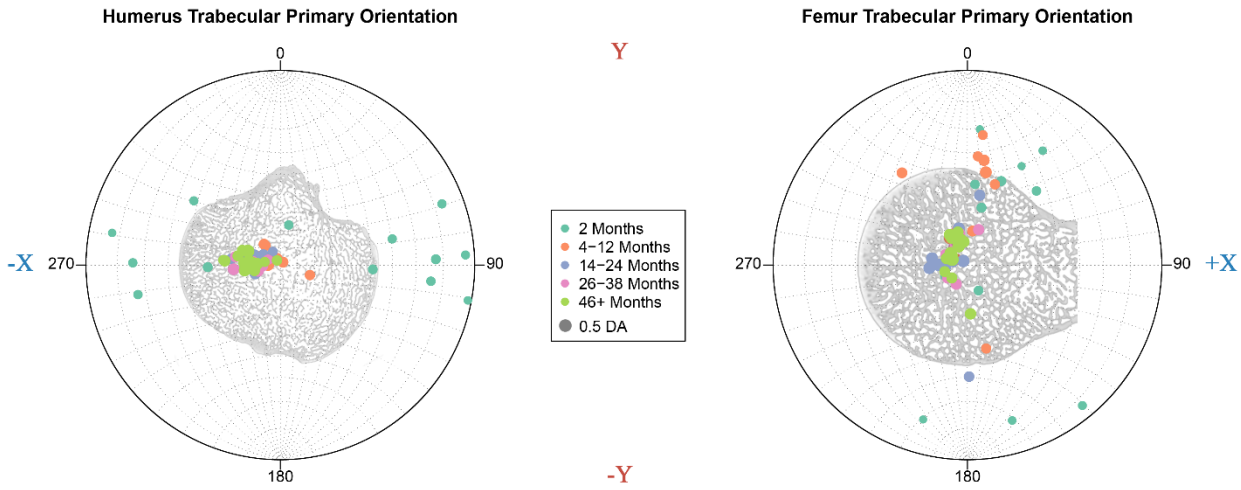

Discussion

Trabecular Characteristics Across Ontogeny

In this analysis I quantified trabecular bone architecture in the proximal articular head of the humerus and femur across an ontogenetic series of raccoons ranging in age from two months to over 46 months. One of the most striking aspects of the results presented here is the consistent difference in most aspects of trabecular bone structure between the two-month-old raccoons and the older individuals in the dataset. At two months of age large portions of the long limb bones are still undergoing endochondral ossification, a process that forms and arranges chondrocytes before activating regional cell death to prepare nearby cartilage to calcify into bony structures (Mackie et al. 2008). By eight months, the ossification process has replaced most of the hyaline

cartilage with bone, resulting in only a thin layer of cartilage surrounding the articular head and an internal epiphyseal growth plate that will fade between the first and second year (Johnson III 1969) (Fig. 2.1). This cartilage, while still operating as a shock absorber and distributor for strain strong enough to influence trabecular development (McKinley 2001), does not deflect the same magnitude of strain on the bony articular head itself as the original cartilaginous growth plate. Although the effect of ontogenetic cartilaginous development on trabecular structures has not been formally tested, it is logical to hypothesize the diminished volume of soft tissue buffer drives the trabeculae towards a larger, denser, and more anisotropic arrangement in response to higher locomotor stresses.

It is also important to note the presence of an epiphyseal growth plate in younger raccoons that is formed during endochondral ossification and is gradually remodeled as the cartilage is replaced by bone (Grau et al. 1970; Wheeler 1975; Reno et al. 2007). In raccoons these plates are present within the articular head of both the humerus and femur, and the ROIs include these structures. Given that the plates act as bracing points for trabecular attachment, I might expect trabeculae for younger individuals to display higher DA and thickness values than adults who have lost this plate. However, these results suggest that these characteristics are significantly lower in younger individuals (Fig. 2.2), with trabeculae becoming thicker and more uniformly oriented as the plate begins to be remodeled. Therefore, I posit that the plate's impact on the trabeculae of the articular head is minimal and does not impact the results of this paper. The specific impact of the epiphyseal plates on trabecular growth is important to quantify, and I am hopeful that future research examining ontogenetic development in other mammal clades will delve more deeply into this topic.

Although two-month-old raccoon cubs have developed enough muscularity to allow small excursions around their den, it has only been a week or two since these exploratory outings began (MacClintock & Thomans 1981). Trabeculae have been demonstrated to undergo rapid remodeling in response to stress (Barak, Lieberman & Hublin 2013), but a period of only one to two weeks is not long enough to have facilitated the shift in trabeculae to match the structures present in older individuals, consistent with observations over ontogeny in other species (Tanck et al. 2001). More than just time, the sporadic low stress behaviors of which these juveniles are capable at such a young age would have a weaker effect on trabecular development when compared to behaviors with high magnitudes of loading in which adults engage, such as climbing, carrying food, and rearing up on hind legs (McClearn 1992; Ruff et al. 2006).

After several more weeks of increasingly long trips from the den, raccoon pups are fully weaned and left to explore the world on their own. It is possible that their increased reliance on high stress foraging behavior may lead to a rapid development of trabecular architecture more in line with structures present in older adults. Additionally, the loss of substantial hyaline cartilage may ensure that the direction and intensity of loading strain on the bone itself is more in line with that seen in sexually mature adults.

When looking broadly at trabecular trends across the entire range of ontogeny (Fig. 2.2) nearly all follow a similar trajectory to body mass: a rapid increase from the 2 month age group to the 4-12 month bin before gradually settling along a horizontal trend. Among this clustering of trabecular characteristics only DA features values that consistently increase with age for both the humerus and femur. Trabecular spacing is the sole characteristic that appears to steadily increase at a relatively consistent rate for both the humerus and femur over the course of a raccoon's life. The reason for this increase, especially in relation to other characteristics, is unclear, but this

steady trend of increasing porosity within the bone appears to drive struts to reach a maximum thickness before decreasing the number of struts found within a sampled volume. This decrease in strut number, paired with increased strain exerted on the long limb elements and a decline in bone's ultimate stress with age (Keaveny et al. 2001), appears to drive struts towards a more uniform directionality. However, despite the linear increase of Tb.Sp the asymptotic DA graph suggests there is a maximum uniformity in the direction of trabecular struts that still allows for enough diversity to support the range of loading strains exerted on the long limb elements. Future research is needed to assess if a DA asymptote of 0.5 is present in other species and niches, or if this maximum varies across a wide spectrum of taxa and ecomorphotypes.

The development of BV/TV and DA across ontogeny in raccoons compared with previously tested species shows a progression more in line with *Sus* than primates. BV/TV in both quadrupedal species peaks during puberty before gradually decreasing through adulthood, whereas primates display a sharp decline in BV/TV during their pre-locomotor ages before steadily increasing towards a plateau in adulthood. Trabecular anisotropy in *Procyon* and *Sus* also increases rapidly during puberty and tapers off into adulthood, whereas chimpanzee trabeculae display a concave pattern across ontogeny that reaches a low around 6 years before returning to comparable levels as newborns (Tanck et al. 2001; Tsegai et al. 2018; Saers et al. 2022). This difference in trabecular growth can be attributed to a variety of potential factors. These include differences in posture between quadrupedal and brachial species, variations in maturation rates, and phylogenetic position. Further analysis will need to independently explore each of these factors to identify which have the most notable impact.

Correlations Between Trabecular Characteristics

A previous meta-analysis of correlations between trabecular characteristics identified relationships between Tb.Th and BV/TV, and Tb.N and BV/TV, with both featuring positive regression slopes in humans, mice, and rats (Barak, Lieberman & Hublin 2013). Other research by Ryan and Shaw (2012) further highlighted the interrelated nature of many trabecular characteristics and suggests that these features should be analyzed as a suite of traits that directly influence one another. My analysis of the humerus and femur identified a strong correlation between Tb.Th and BV/TV in each bone independently, but only a moderate correlation between Tb.N and BV/TV. Much of this distinction may be attributed to changes that occur over ontogeny, with both Tb.Th and BV/TV reaching a maximum within the 4-12 month age range, whereas Tb.N steadily decreases with age.

The positive linear regression slope between Tb.Th and BV/TV within the humerus was congruent with values found in rats and mice, and higher than the values seen in humans (Barak, Lieberman & Hublin 2013). However, the same analysis conducted on femoral trabeculae resulted in a slope less than half that seen in the humerus, and significantly lower than the aggregate slopes of rats, mice, or humans. Given the wide difference in correlations between Tb.Th and BV/TV within different bones, future research should be conducted to fully assess the diversity in trabecular architecture within commonly sampled bones (vertebrae, femur, humerus, tibia, ulna) and regions of said bones (vertebral body, articular head, midshaft, condyles). Additionally, meta-analyses of trabecular properties should prioritize isolating different bones from one another because signals may not be consistent across elements.

Trabecular Characteristics and Body Mass

Numerous studies have shown a correlation between trabecular architecture and body mass, especially for trabecular thickness and number (Doube et al. 2011; Barak, Lieberman & Hublin

2013; Kim et al. 2017; Shin et al. 2019). My findings corroborate this relationship, with regressions indicating that every trabecular characteristic in both the humerus and femur is impacted by overall body mass (Mielke et al. 2018; Plasse et al. 2019; Smith et al 2023). However, previous studies have indicated linear trends between trabecular structure and body mass, with the majority of these investigations focusing exclusively on adult individuals. The few that have sampled other age groups have focused exclusively on Hominini and have relied on small sample sizes due to difficulty in acquiring juvenile specimens (Ryan & Krovitz 2006; Tsegai et al. 2018).

A few notable characteristics display a positive trend with regards to body mass in the dataset: DA and Tb.Sp in the humerus, and DA, Tb.Th, and Tb.Sp in the femur. By contrast, the remaining characteristics see a peak at a relatively young age, typically 4-12 months, before gradually decreasing for the remaining older individuals. The parabolic nature of these regression slopes can be explained by the interplay of other trabecular characteristics. BV/TV in both the humerus and femur sees a rapid increase in tandem with trabecular struts increasing in thickness through the first year of life. Starting at a logBM value of 0.75 (~5.62 kg), a mass primarily presented by individuals within the 4-12 month age group, the change in strut thickness plateaus whereas space between struts continues to increase and trabecular number steadily declines. Eventually, this widening of space between struts results in an overall BV/TV value by 3 to 4 years of age that is comparable to that seen in 2-month-old individuals.

Despite the allometric trends in trabecular characteristics across ontogeny, individual age bins are primarily in line with estimated isometric growth rates (Figs. 6 and 7). In both the humerus and femur, individuals in the 4-12 month age group who are old enough to have left the den retain a higher number of trabecular struts than predicted. Given that raccoons are generalist

species who engage in a wide range of behaviors, the preservation of a higher number of struts may serve to act as a buffer against variable strains. Comparisons with other analyses places the slope for raccoon Tb.N with respect to body mass as lower than other species (ranging from -0.21 to -0.56 compared to -0.146 respectively) (Barak, Lieberman & Hublin 2013), although the interspecific slope was measured using adults only, rather than multiple age groups within a single species. Further analysis of the ontogenetic development of other species is needed to determine if there are measurable differences in rate of strut loss between species with respect to body mass when compared to intraspecific analyses.

Beyond Tb.N, the humeri of 4+ month old raccoons also display a significantly different rate of change in Tb.Th with isometry. Unlike Tb.N, which retained a negative allometric rate of change during and after puberty, the thickness of humeral struts appears to reach a peak around 1 logBM and 12 months of age, before decreasing throughout the remainder of an animal's life. This trend is once again at odds with interspecific trends, which show a steady positive correlation with body mass (Barak, Lieberman & Hublin 2013). My results suggest that raccoons undergo a process of significant trabecular thickening through puberty. Once individuals have reached sexual maturity and the need for rapid bodily growth is diminished, the body begins to gradually reduce the thickness of struts to reduce density and maximize strut efficiency.

It is once again important to note that in comparing the slope of these raccoon age bins to interspecific trends presented by Barak, Lieberman & Hublin (2013), the latter values are based on a meta-analysis encompasses a variety of skeletal elements. The present scope of trabecular research leaves humans as the primary point of comparison for ontogenetic trends in trabecular architecture, but *Homo sapiens* have their own caveats that complicate comparisons with other species. Beyond the obvious differences in locomotion, lifestyle, and size, significant changes in

trabecular architecture in older humans seems to be primarily driven by bone-related illnesses such as osteoporosis that affect reabsorption rates and trabecular production to a greater extent than diminished loading strain (Ryan & Krovitz 2006; McDonnel et al. 2007). The wild raccoon specimens used in this study showed no evidence of any bone pathologies and were likely unable to survive long enough in their natural habitat to develop these illnesses. As such, the gradual shifts in trabecular structures across ontogeny cannot be explained by the same causes as in humans. Additionally, ontogenetic studies of humans focused primarily on the very young (Ryan & Krovitz 2006) or elderly (McDonnel et al. 2007), with limited research conducted on the pubescent age range where the most significant changes appear to occur in raccoons. Finally, there has been minimal analysis of the development of the trabeculae of human humeri, which makes any direct comparisons to raccoon humeri problematic due to the noticeable differences in the trabecular characteristics of the fore- and hindlimb, to say nothing of how much more disparate these values likely would be in a bipedal species like *Homo sapiens.*

Humeral and Femoral Contrast

Though both the fore- and hindlimb elements show similar trends in the development of trabecular features across ontogeny, the frequent difference in absolute values of the metrics between the two bones suggests a difference in loading strain. Most non-primate mammal clades are defined by a "forelimb driven" quadrupedal gait, in which the forelimbs experience a stronger substrate reaction force (Demes et al. 1994; Schmitt and Hanna 2004; Young 2012). This loading pattern would lead to the expectation that the humeri of raccoons would feature a more dense trabecular matrix, with higher BV/TV, Tb.Th, Tb.N, and DA than the femur, to support this increased load, especially considering the smaller size and cortical density of these forelimb elements compared to the hindlimb. However, I observed the opposite pattern in

raccoons, with nearly all of these features significantly higher in the hindlimb, and Tb.N relatively comparable. Both the humerus and femur appear to be developing larger and thicker trabecular struts over time to support against higher strain even as Tb.N decreases, but the femur does so to a greater extent. That Tb.N is the only character to not show significant difference between the humerus and femur after two months suggests that the trabecular number within the articular heads of long limb elements is more strongly impacted by the overall mass of the animal than by the disparate strains experienced by the limbs. This difference in limb elements may be driven by the fact raccoons engage in a number of hindlimb dominated and exclusive behaviors that place significantly higher strains on the hindlimbs compared to other fully quadrupedal mammals (MacClintock & Thomas 1981; McClearn 1992). The impact of these specific behaviors could be further tested by sampling a wider range of raccoon populations. Individuals in regions of the Americas with less tree coverage may utilize hindlimb arboreal climbing less than their relatives from the more forested Great Lakes region, with that difference in behavior reflected in less dense and more isotropic femoral trabeculae. Future testing may also determine if these trends are present among "traditional" quadrupedal mammal species, which would imply that trabecular features may be impacted more by the overall size of the surrounding bone instead of the magnitude of forces applied to it.

Trabecular Orientation

Unlike the univariate trabecular metrics, which show a gradual shift in structure across ontogeny, primary trabecular orientation for both the humerus and femur can be divided into two distinct arrangements with clear divides between age groups. The struts arranged horizontally along the anterior/posterior axis in the youngest individuals rapidly undergo a shift to a more uniformly vertical orientation by the end of an individual's first year. This abrupt transition appears to be

caused by several factors. The full ossification of hyaline cartilage that comprised much of the articular head at two months ensures that loading strain exerted on the joint is no longer deflected laterally and instead bears down vertically on the structure in the direction of gravity. The infrequent and short excursions outside the den that two-month individuals can undertake increase in duration and distance with age, until individuals are engaging in foraging, walking and climbing behaviors that exert far greater strains on the limbs. This increase in stress helps to direct the trabeculae to align in a uniform vertical orientation, parallel to the force of gravity. Finally, this progression is further facilitated by an increase in vascularization within the bones during secondary endochondral ossification, as blood vessels invade the still developing epiphysis to transport osteoclast and osteoblast cells. These cells facilitate the growth and development of trabecular struts and allow the bone to more rapidly react to strains produced during locomotion (Streeter 1949; Charbord 1996).

Although this distinct shift from juvenile to adult orientations is present in both the humerus and femur, the rates at which this transition occurs vary between the two elements. Specifically, by four months the orientations of trabeculae within the humerus have been reoriented to the adult configuration, whereas this process lags in the femur until a full year has passed. The 4–12 month age range features femora with a trabecular azimuth with less variance than their younger peers, but it still retains a primarily horizontal plunge aligned parallel to the sagittal plane. Though I might expect a further gradual transition with age, by 14 months the trabecular orientations have progressed to the same vertical structures present in the humerus some 10 months earlier.

The causes of this transitional lag between the humerus and femur are unclear, and many of the factors that influence trabecular development and modification cannot be used as sole

explanations for this phenomenon. Differences in loading strain between the humerus and femur likely match those present in other mammal species during quadrupedal motion, with the humerus enduring higher substrate reaction forces. However, the utilization of hindlimb-dominated behaviors in raccoons, and the presence of larger more uniform trabecular struts in the femur suggest bipedal locomotion may have a stronger impact on trabecular development. Additionally, the timing and frequency of these behaviors in young raccoons further complicates matters. Although these high stress behaviors are not frequently observed in two-month-old individuals who are still working on getting their bearings, they are frequently observed by four to six months, when juveniles are far more independent. The impact of strain on trabecular structures can be influenced by several factors, but previous work has demonstrated that an increase in both strain magnitude and frequency have a significant impact on BV/TV and strut orientation (Keaveny et al 1999; Judex et al. 2007; Ozcivici et al. 2007; Barak et al. 2011). A possible explanation may be that before leaving the den, juvenile raccoons have ample time for their humeral trabeculae to adjust to stresses exerted during quadrupedal locomotion before incorporating more hindlimb-dominated movements. Nevertheless, it is unclear if the very sedentary lifestyle of very young raccoons provides enough activity to stimulate humeral trabecular development, and more testing will need to be done to quantify these transitions. Puberty, and the resulting release of hormones, has also been demonstrated to influence the development of trabecular structures. Several studies have demonstrated the use of hormonal antagonists to delay puberty in females can retard the growth of trabecular struts oriented in the direction of primary loading (Georgopoulos et al. 2001; Yingling et al. 2007). Additionally, both oestrogen and testosterone have been suggested to be integral in the bone formation and resorption process that creates trabeculae (Finkelstein 1996; Seeman 2002). It can therefore be

inferred that the production of these reproductive hormones during puberty has a significant effect on the trabeculae developing during endochondral ossification. However, these studies have shown no evidence to suggest the presence or absence of these hormones has a variable effect on trabeculae in different regions of the body. The orientation shift of humeral trabeculae occurs during the raccoon puberty window of 3-12 months, whereas femoral trabeculae still retain comparable orientations to younger, pre-puberty individuals. The production of hormones helping to influence trabecular growth would be expected to have a uniform effect between the humerus and femur and cannot account for the lag present during puberty.

Further studies focusing on ontogenetic changes in trabecular orientations within long limb elements are needed to assess whether any of the above factors or other, unknown factors influence the transition in orientation across ontogeny with variable effects on different bones. Additionally, future research should also investigate quadrupedal species outside of the genus *Procyon* to determine if this trend is consistent in other taxa, or exclusive to raccoons.

Conclusion

Procyon lotor undergoes a significant change in trabecular architecture of both the humerus and femur throughout the course of an individual's life, with a rapid change occurring during the eight month span over which puberty occurs. These changes tend towards a decrease in trabecular number and density as the space between struts increase, necessitating a higher percentage of struts to orient vertically to preserve internal support against strain exerted during generalist locomotor behaviors. Although these overall trends are consistent between the humerus and femur, the rate and extent of their changes vary significantly between the two bones. Several of these differences cannot be explained currently and additional research on the driving forces of trabecular remodeling during puberty is needed to resolve these issues.

Additionally, although *Procyon lotor* exhibits a generalist body plan that is comparable to a myriad of mammalian species, further research will need to be conducted to analyze if the trends seen in the species are consistent across other generalized and more specialized taxa.

Key differences in the ontogenetic development of BV/TV and DA in raccoons compared with humans and other primates highlight previously unexplored distinctions in trabecular structures. With the specific factors driving these differences still unclear, there is a need to sample additional taxa to quantify this variability and to understand the extent to which phylogeny, ecomorphotype and posture influence trabecular development. Quantifying this diversity will elucidate how various species develop trabecular structures to support differing loading strains, and if those structures can be used to predict behavior in older, fossilized species.

The differences between the fore- and hindlimbs also highlight the limitations in previous meta-analyses that combine distinct skeletal regions to bolster the size of datasets for meaningful statistical analysis. The overall trabecular growth trends can be similar between disparate bones, but the distinctions are wide enough in this work that I caution future researchers looking to combine elements in their research.

Chapter 3: Exploring Functional and Phylogenetic Variation in Limb Trabecular Structure Across Amniote Taxa

Abstract

Trabecular bone, a lattice of bony struts located within the cortical shell of many skeletal elements, plays a pivotal role in skeletal support by adjusting its architecture to withstand compressive forces. Research on trabecular morphology has historically concentrated on primates, with comparatively limited focus on other clades or on broad analysis of higher order groups. In this study, we investigate the trabecular architecture of a diverse range of terrestrial amniote taxa to examine how size, phylogenetic context, ecomorphology, and posture influence trabecular development in two limb elements. This comparative analysis was possible by establishing a uniform orientation method that can be applied to other amniote taxa. Our results demonstrate clear differences between the trabeculae of the humerus and femur in mammals that are not seen in reptiles. Although ecological niche and postural groups have limited influence on most traditional trabecular metrics, our results highlight striking differences in trabecular orientation between these groups. Posture was correlated with trabecular orientation, likely stemming from the varied angle of limbs and the resulting directions of stress exerted during locomotion. Future research into non-primate taxa should incorporate trabecular orientation to better understand trabecular diversity.

Introduction

The field of functional morphology seeks to understand the relationship between an organism's behavior and the ways its body is adapted to facilitate those actions. The wide range of activities in which vertebrates engage is reflected in a myriad of differing skeletal morphologies, each

adapted for unique behaviors and lifestyles. In cursorial animals, limb elongation, fusion of distal limb elements, and digit reduction are common features (Lull 1904; Stein & Casinos 1997; Smith et al., 2020). Fossorial species tend to have shorter forelimbs with higher mechanical advantages and a stout manus adapted for the powerful movements needed to move substrate (Shimer 1903; Elissamburu & De Santis 2011; Straehl et al. 2013). Arboreal species, in contrast, often develop ball-and-socket joints in the proximal limb elements, allowing for an increased range of motion (Dublin 1903; Arias-Martorell et al. 2015).

Over the last decade, advances in micro-CT technology have enabled researchers to analyze the form-function relationships of a different aspect of skeletal morphology: trabecular bone. Trabecular bone, also known as cancellous bone, supports the bone marrow of limb, vertebral, and cranial elements. It forms a complex lattice of rods and plates, which generally align parallel to the primary stress directions experienced by the bone, acting as supports while minimizing additional bone weight (Wolff 1892; Koch 1917; Fyhrie & Carter 1986). Individual trabeculae are small relative to the cortical bone that surrounds them, and bone-signaling osteocytes embedded within trabeculae allowing them to adapt to loading strains at a remarkable rate, usually within a timespan of just a few weeks (Parfitt 1988; Morgan et al. 2013). Although cortical bone does retain a level of plasticity in which remodeling can rapidly occur to repair microcracks or to maintain blood calcium homeostasis, larger scale morphological changes are limited by a need to maintain a minimum cortical thickness and by long-term evolutionary trends (Kivell 2016). For these reasons, research on trabecular bone has expanded, with scientists aiming to understand the factors driving the architecture of these bone struts across Amniota, and the relationships between trabecular bone structure and body size, postural group, ecological niche, substrate use, and growth.

Initial research on trabecular bone architecture focused on primates, with the goal of exploring both biomedical applications for humans and identifying trends specific to bipedal posture (Ryan & Krovitz 2006; Ryan & Raichlen 2017; Saers et al. 2017; Tsegai et al. 2018; Saers et al. 2022A; Nottestad et al. 1987; Rafferty 1998; Fajardo & Müller 2001; Morgan & Keaveny 2001; MacLatchy & Müller 2002; Ryan & Krovitz 2006; Fields et al. 2011; Wang et al. 2015). Building on the foundational research in primates and general trabecular analytic methods, studies have extended their focus to other primarily domesticated mammalian species, such as pigs, sheep, and cattle, to investigate how manual alterations in joint posture and locomotor loading influence trabecular bone architecture (Vander Sloten & Van der Perre 1989; Mori et al. 2003; van der Meulen et al. 2006; Polk et al 2008; Barak et al. 2011; Metzger et al. 2015; Yamada et al. 2022). These studies often involved controlled experiments where joint loading conditions are modified through surgical interventions, physical restraints, or exercise regimens, allowing researchers to directly assess the adaptive responses of trabecular bone to mechanical stimuli. However, recent work has highlighted the impact that captivity has on trabecular development, and it is likely that the trabeculae of wild individuals would differ significantly from the control groups in these studies (Chirchir et al. 2022; Zack et al. 2022). Other studies have sampled wild individuals to assess the diversity of trabecular structures in a non-controlled environment. Doube et al. (2011) found that trabecular thickness (Tb.Th) and spacing (Tb.Sp) scale positively with increasing body mass in mammals and birds, whereas non-avian dinosaurs exhibit the inverse trend (Aguirre et al. 2020). Several studies have also highlighted that variations in ecological niche within taxonomically restricted clades of mammals are reflected in their trabecular structures (Amson et al. 2017; Amson & Bibi 2021; Smith et al. 2023; Zack et al. 2023). Although these papers underscore the methods by which bone is modified and the

potential of trabecular analysis for ecological and functional insights, it remains unclear whether the relationships between these factors and trabecular structure hold true in a broader sample of mammals or other quadrupedal tetrapod clades. Mammals have been the subject of the vast majority of trabecular research, with minimal analysis of Aves and reptilian trabecular diversity (Plasse et al. 2019). Furthermore, studies comparing trabecular structures across multiple skeletal elements often select bones that differ greatly in structure and function (Amson & Bibi 2021) or compile different bones into a single dataset (Barak et al. 2013). This approach assumes that trabecular structures are similar across different limb elements, but research by Reinecke & Angielczyk (2024) found significant differences between the humerus and femur within the same species, suggesting that broad-scale comparisons should be limited to specific elements. Analyzing the trabecular architecture of several distinct bones in other species is important for determining whether previously noted trends are consistent in more specialized and non-mammalian taxa.

This study aims to expand on previous work by identifying trabecular diversity and quantifying the variation observed in two major amniote clades: Mammalia and Reptilia. I will address four research questions. First, I will sample both the humerus and femur to determine whether trabecular architecture is broadly consistent between the forelimb and hindlimb across species at this broad phylogenetic scale. Second, I will assess the effect of body mass on trabecular characteristics, and whether the scaling relationships of these characteristics are consistent between disparate amniote taxa. Third, I will quantify common trabecular metrics across Amniota to assess whether species grouped by ecological niche or postural group exhibit distinct trabecular characteristics. Finally, I will apply the methodology described by Reinecke & Angielczyk (2024) to investigate primary trabecular orientation and assess whether it can serve

as a more effective metric for linking trabecular architecture to factors such as limb posture and ecological niche compared to more commonly used metrics. This approach builds upon pre-existing systems for identifying trabecular rod eigenvectors and visualizing their orientation on a stereomorphic projection (Barak et al. 2011; Hébert et al. 2012; Nafei et al. 2000; Ryan et al. 2010, 2018; Zeininger et al. 2018) with methodology used to uniformly orient limb bones with highly disparate morphologies. I hypothesize statistically significant differences in trabecular architecture and primary orientation between the humerus and femur, as observed in a previous intraspecific analysis (Reinecke & Angielczyk 2024). Postural groups are likely to exhibit varied trabecular orientations given the differing angles at which species hold their limbs. I also expect to find a less pronounced but still notable contrast across ecological niches when sampling across mammals and reptiles given the disparate morphologies that have adapted to similar environments.

Methods

Taxon Sample and Categorization

One hundred and fourteen specimens representing fourteen species of reptiles and twenty-eight species of mammals were sampled (Fig. 3.1).

Figure 3.1
A temporally calibrated phylogeny of all sampled taxa sampled, modified from dos Reis et al. 2012; Pyron et al. 2013 and Thomson et al. 2021.

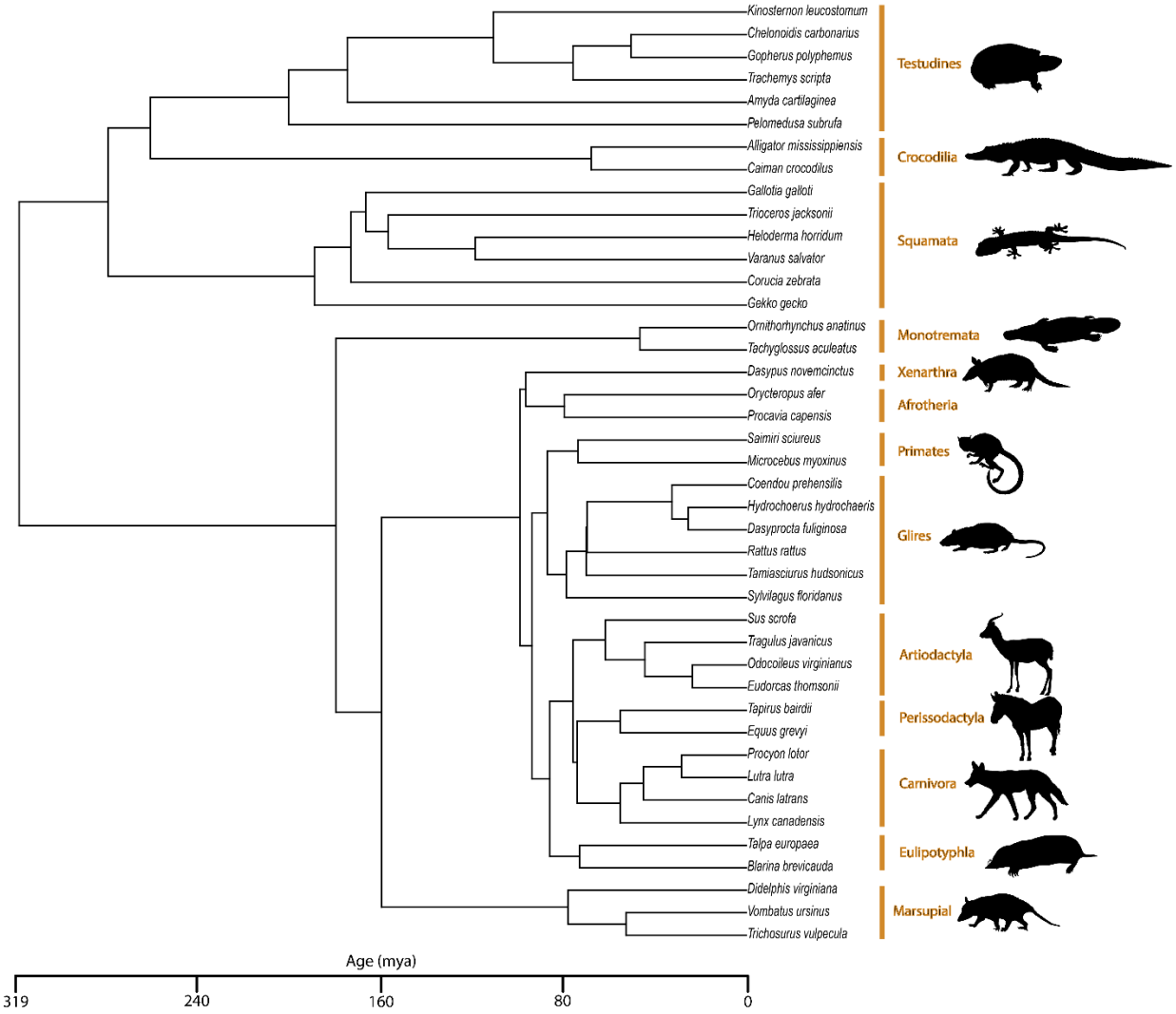

The majority of species were represented by three adult specimens each to remove ontogenetic variation while still providing information about levels of intraspecific variation. Species were selected to encompass the diversity in body mass, phylogeny, ecological niche, and postural groups of both clades. Particularly species-rich clades had additional species selected to more broadly cover the range of phylogenetic and morphological diversity. Fully aquatic and volant species were not included in the dataset as their locomotory mechanics and anticipated skeletal loading patterns differ greatly from more terrestrial species. Captive specimens were also

excluded as behavioral variance and limited mobility has been shown to have a discernible effect on trabecular development (Chirchir et al. 2022; Zack et al. 2022). Body mass estimates were determined for each specimen using the scaling equation developed by Campione and Evans (2012) for broad use across Tetrapoda. This method utilizes the midshaft circumference of both the humerus and femur and is an ideal model for the measurements collected for this study. A chronogram of all sampled taxa (Fig. 3.1) was created by integrating and modifying data from three previously published phylogenies (dos Reis et al. 2012; Pyron et al. 2013; Thomson et al. 2021).

Species were categorized using three criteria: major clade, ecological niche, and general postural groups. Ecological niche and postural groups for mammals and reptiles were obtained from various sources that detailed specific morphological features clearly associated with particular environments or behaviors (Baker 1985; Hildebrand 1985; Nowak 1999; International Union for Conservation of Nature 2023; Pianka et al. 2003; Pough 2003; Oskyrko et al. 2024). Set categories for ecological niche are not always fully defined, and individual interpretations were made when necessary. Ecological groups were identified based on a species' primary environment and any specialized morphological features suited for that specific ecological niche. In total, four specialist ecological niches were identified. Arboreal taxa exhibited characteristics suited for climbing, or were non-terrestrial species commonly found in dense forest environments. Cursorial taxa exhibited morphologies specialized for efficient long-distance locomotion and/or running, such as long, straight limbs. Fossorial taxa either possessed large robust limbs for digging or have been recorded as actively creating dens for burrowing, rather than co-opting dens previously made by other species. Similarly, semi-aquatic taxa either possessed limb morphologies suited for swimming or commonly lived in and around bodies of

water. Any species that could not be easily identified into one of these groups was instead categorized as “generalist”.

Posture was first identified as either sprawling or parasagittal based on the angle of the limbs held at mid-stance. Sprawling taxa exhibit abducted limbs compared to the adducted limbs of parasagittal taxa. For parasagittal taxa, species were further grouped by foot posture into plantigrade, digitigrade, and unguligrade groups. Although differences for these three groups are found primarily in the orientation and utilization of the carpals during locomotion, I hope to test if variations in ground reaction forces due to this variation are reflected in the trabeculae of proximal limb bones. Crocodilians exhibit a unique ability to shift the angle of their limbs to engage in different locomotory gaits that utilize disparate limb postures (Parrish 1987) and were classified as switch-gait. Given the wide variety of behaviors, skeletal morphology, and range of motion present in all these groups, I suspect the varied loading directions and magnitudes throughout the dataset will result in significant differences in trabecular architecture and orientation that may align with the group categorization.

Bone Scanning, Orienting, and Processing

The proximal articular head of the right humerus and femur were selected for analysis due to the relative similarities in structure. Across all sampled taxa, both proximal limb elements exhibit a distinct articular head that allows for a more consistent placement of a region of interest. Any bones that featured damage to the proximal head from injury or disease were excluded. If a viable right sided bone was not available for a particular specimen, the left element was selected and mirrored. In total, it was only necessary to mirror six humeri and seven femora.

All skeletal specimens were scanned using the University of Chicago's PaleoCT GE phoenix v | tome | x μCT (micro-computed tomography) scanner with a 240 kV micro-focus X-ray tube (RRID:SCR_024763). When possible, the entirety of the bone was scanned, with multiscans performed on larger specimens to retain a higher resolution. Scan resolutions range from 16.00 to 117.55 μm, with the maximum intraspecific variance in resolution remaining under 23 μm. The greatest disparities occurred in species where full-body scans were necessary, and the resolutions of nearly all species exhibited intraspecific variation under 10 μm. Voxel sizes for each scan were measured to ensure a size 3-4 times smaller than the average trabecular thickness to minimize the chance of scans omitting or warping trabecular struts (Bouxsein et al. 2010). Relative resolutions for each bone were calculated using methods described in Sode et al. (2008) and Smith et al. (2023) with the mean trabecular thickness (μm) divided by the scan resolution (μm). Relative resolutions remained consistent between scans and ranged in value from 0.02 to 0.12. Each scan was reconstructed within GE phoenix datos | x before the resulting image stacks were aligned within VGStudioMax 3.3.

The resulting tiff stacks were uniformly oriented and processed using Dragonfly 2022.2 (Dragonfly 2022). Bones were first oriented such that the midpoints of the proximal and distal metaphyses were vertical along the Z-axis. Metaphyseal midpoints were determined by creating lines perpendicular to the midshaft with endpoints contacting the lateral edges of cortical bone before identifying the midpoint of this line. Several lines were drawn for each axial view at the bone's distal and proximal ends to get an average "midpoint" for each region. The two midpoints for each bone were then aligned vertically. Following this, bones were rotated such that the center of the articular head pointed in the negative X-direction, and the lateralmost points of the articular surface were aligned along the Y-axis (Fig. 3.2).

Figure 3.2
Select specimens demonstrating application of the uniform orientation used to conduct analysis between species. (A) represents the vertical orientation and (B) represents the *in vivo* orientation for the humerus (left) and the femur (right) of *Dasyprocta fuliginosa* in cranial view. (C) and (D) represent the same orientations for the humerus (left) and the femur (right) of *Pelomedusa subrufa*. The red bars represent the primary trabecular orientation as measured in each bone's proximal ROI.

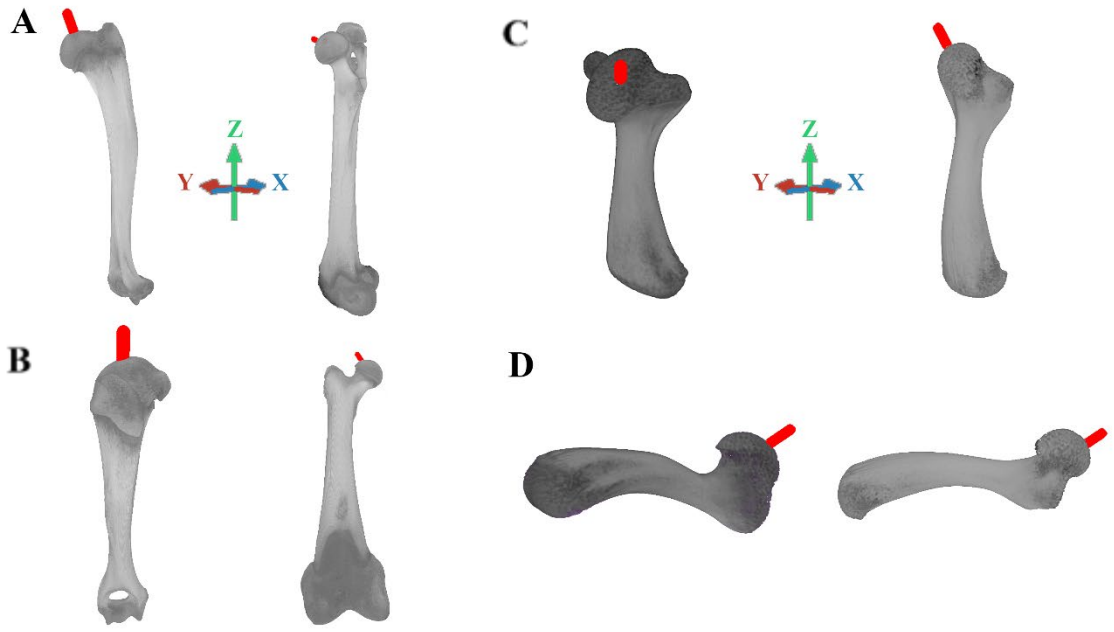

This alignment was chosen to provide a standard orientation for all species based on shared morphological features that facilitate consistent comparisons rather than reflecting how the limbs would be held in life. When detailing the orientation of bones within this chapter, "with respect to the limb" will refer to this standardized orientation and "with respect to the body" will refer to the actual *in-vivo* posture. This methodology expands on similar attempts to standardize limb bone orientations (Amson et al. 2017; Mielke et al. 2018; Reinecke & Angielczyk 2024) while broadening the scope to accommodate a diverse sample of amniote morphologies.

Following orientation, a box was drawn around the outermost edges of the joint surface to identify the center of the articular head. A spherical region of interest was expanded from this central point to maximize the number of sampled trabeculae while excluding cortical bone. Otsu sorting algorithms (Otsu 1979) were selected to segment and binarize the region of interest (ROI). Analysis of several sorting methods has demonstrated that Otsu segmentation typically preserves small individual trabecular struts without inflating the bone volume fraction (BV/TV) value of a sampled region (Smith & Angielczyk 2020).

BV/TV for each specimen was calculated within Dragonfly by comparing the volume of segmented trabeculae to the volume of the spherical region of interest. The spherical binarized trabeculae and non-trabecular space were imported into ImageJ (Rasband 1997) where the plugin BoneJ (Doube et al. 2010) was used to purify the scans and determine anisotropy, trabecular thickness (Tb.Th), and trabecular spacing (Tb.Sp). Following this step, the tiff image stacks were imported into Quant3D (Hoebeke & Trubuil 1999) to identify trabecular number (Tb.N) and primary trabecular eigenvectors. Mean intercept length (MIL) was the method chosen to describe the ROI's fabric tensor. Although MIL was initially created for analysis of polycrystalline materials it has subsequently been demonstrated to predict the mechanical properties of bone more accurately than other methods used to quantify structural anisotropy such as star volume distribution (Zysset 2003; Cowin & Doty 2007; Moreno et al. 2014). Finally, the trabecular eigenvectors were converted to azimuth and plunge measurements in R using the code of Amson et al. (2017). These measurements are commonly used in structural geology but can also be modified to reflect bony orientations. Azimuth describes the horizontal direction in which a feature trends, whereas plunge indicates the inclination of a line relative to the horizontal. To facilitate statistical testing, transformations were applied to the azimuth values using the formula

$||\alpha - 180| - 90|$, which converts the degree values of azimuth to a scale ranging from 0 to 90. Additional explanations of these features and how they are visualized are covered in the results section. A full list of specimens and their trabecular characteristics can be found in Supplementary Dataset S3.1.

Statistical Testing

Tests for normalcy found that several trabecular characteristics within this dataset exhibited a non-normal distribution within both Mammalia and Reptilia, resulting in the need for nonparametric Kruskal-Wallis (Kruskal & Wallis 1952) and Dunn tests (Dunn 1964). These tests were performed in R 4.2.3 using the kruskal.test (R Core Team 2023) and dunnTest (Dinno & Dinno 2017) packages and sought to assess if there are significant differences in the trabecular characteristics and orientations between the humerus and femur, for each of the two sampled major clades. Both limb elements were compared within and between Mammalia and Reptilia. Following the Kruskal-Wallis tests, Dunn tests were conducted for ecological and postural groups with more than two categories with a result considered significant at an $\alpha = 0.05$ significance level.

Phylogenetic generalized least squares (PGLS) analyses were performed to compare log-transformed body mass (logBM) values with species means for each trabecular characteristic in R using code for gls in nlme (Pinheiro 2011) and treeplyr packages (Harmon 2020) respectively. These PGLS analyses allow us to control for the non-independence of data points due to shared ancestry and provide more accurate estimates of trait correlations with body size. Previous analyses of trabecular structures have demonstrated that Tb.Th, BV/TV, and Tb.Sp scale with body mass at both inter- and intraspecific levels (Barak, Lieberman & Hublin 2013; Kim et al. 2017; Mazzetti et al. 2017; Reinecke & Angielczyk 2024**;** Saers 2017; Smith et al. 2023, 2024;

Zack et al 2023). Linear regression slopes were estimated for the species' averages of all trabecular characteristics able to be described by a single value versus body mass. Isometric regression slopes vary for each characteristic depending on their units: BV/TV and anisotropy are percentages and feature a slope of 0; Tb.N measures struts per mm and has an estimated slope of -1/3; Tb.Th and Tb.Sp scale cubically with volume and have an isometric slope of 1/3 (Mielke et al. 2018; Plasse et al. 2019; Smith et al 2023). Several additional PGLS models were also run that included ecological niche and postural group as predictor variables and replaced the models with solely logBM in the event an interaction between body mass and these groups was found to be significant ($p < 0.05$). As the sampled means were all found to be normally distributed, phylogenetic ANCOVAs were used to identify any statistically significant differences between ecological and postural groups.

Stereomorphic projections were utilized to visually represent the primary orientations of the trabecular structures for all sampled individuals. Axial definitions were modified to represent anatomical directions with respect to the limb elements themselves. A more detailed explanation of these directions and their implications for trabecular angles are provided in the results section.

Results

Humerus vs. Femur

When sampling all specimens, Kruskal-Wallis tests revealed significant differences between the humerus and femur for DA, BV/TV, Tb.Sp, and transformed azimuth values (Fig. 3.3; Table 3.1).

Figure 3.3

Violin plots from the full datatset comparing humeral and femoral trabecular metrics.: DA (A), BV/TV (B), Tb.Th (C), Tb.Sp (D), Tb.N (E), transformed azimuth values (F), and plunge (G). Characteristics showing a significant difference between bones are marked with an asterix. The horizontal lines within each violin plot are quartile lines.

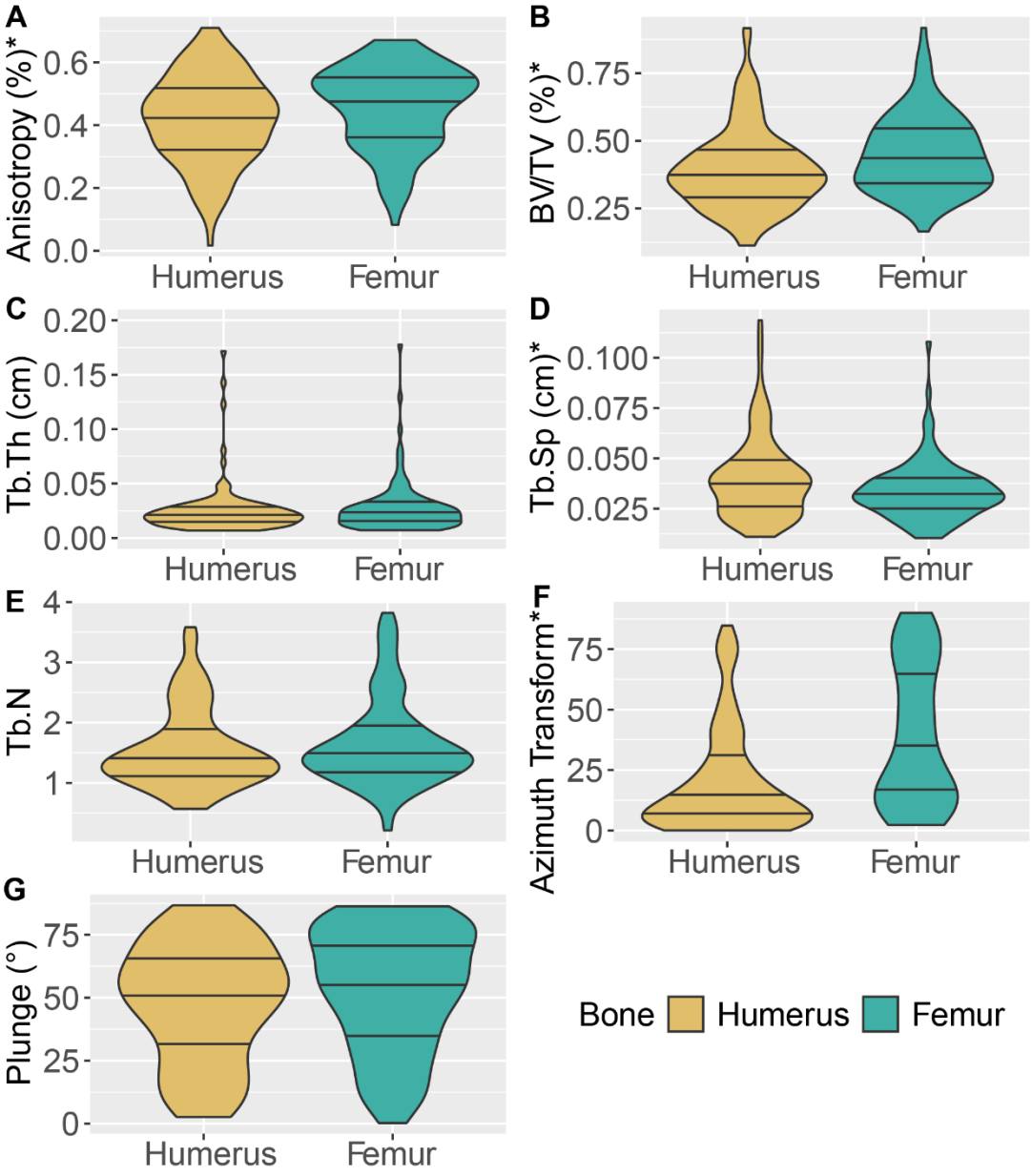

Table 3.1
Results from the Kruskal-Wallis tests on the raw values of several trabecular characteristics as separated by bone and class. Groups that demonstrated a statistically significant difference in values ($p < 0.05$) have been bolded.

Sample	Trabecular Characteristic	Chi-Squared	df	p-value
Humerus ~ Femur: All Sampled Taxa	Anisotropy	5.379	1	**0.02038**
	BV/TV	10.944	1	**0.0009389**
	Tb.Th	1.57	1	0.2101
	Tb.Sp	5.3511	1	**0.02071**
	Tb.N	1.7299	1	0.1884
	Azimuth Transform	33.166	1	**8.46E-09**
	Plunge	3.6928	1	0.05465
Humerus ~ Femur: Mammals	Anisotropy	4.2346	1	**0.03961**
	BV/TV	21.651	1	**3.27E-06**
	Tb.Th	3.2222	1	0.7948
	Tb.Sp	10.051	1	**0.001523**
	Tb.N	3.7046	1	0.05426
	Azimuth Transform	35.666	1	**2.34E-09**
	Plunge	1.1556	1	0.2824
Humerus ~ Femur: Reptiles	Anisotropy	1.0116	1	0.3145
	BV/TV	2.8859	1	0.08936
	Tb.Th	0.34662	1	0.556
	Tb.Sp	0.52369	1	0.4693
	Tb.N	0.29126	1	0.5894
	Azimuth Transform	1.7874	1	0.1812
	Plunge	4.2461	1	**0.03934**

For all sampled taxa, trabeculae in the femur tend to be more densely packed and point more uniformly along the cranial-caudal plane with respect to the limb than in the humerus, which exhibits lower DA, BV/TV, and transformed azimuth, and higher Tb.Sp values. When only mammals were considered, there were significant differences between the humerus and femur for those metrics as well (Fig. 3.4; Table 3.1). Humeral and femoral Tb.Th ranges were partly defined by several outlier individuals that when removed resulted in no significant difference in

Tb.Th between bones. By contrast, Reptilia only exhibited significant differences between the plunge values in the humerus and femur, with femoral trabeculae being aligned more vertically than their humeral counterparts.

Figure 3.4

Violin plots comparing boney trabecular metrics that showed a significant difference between the bones when the dataset was divided into mammals and reptiles. For mammals, significant differences were observed for anisotropy (A), BV/TV (B), Tb.Th (C), Tb.Sp (D), transformed azimuth values (F). For reptiles, only plunge values (G) differed significantly between the elements. Pairs of groups elements showing a significant difference are marked with an asterix. The horizontal lines within each violin plot are quartile lines.

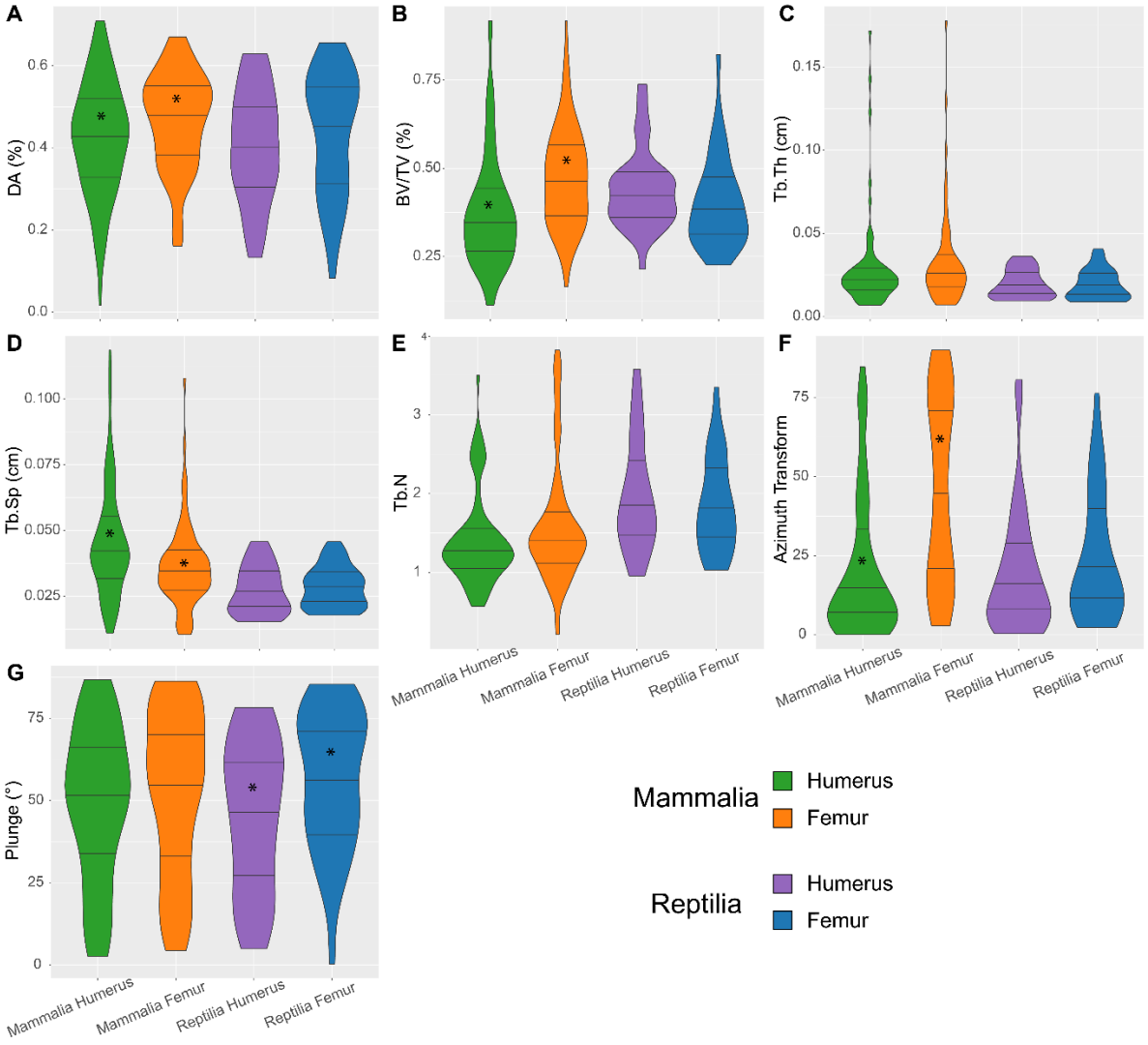

Trabecular Characteristics vs. Body Mass

Mammalian BV/TV, Tb.Th, Tb.Sp, and Tb.N exhibited significant allometric relationships with body mass in both long limb bones (Fig. 3.5; Table 3.2). The mammalian humerus also exhibited an allometric relationship with body mass. Tb.Th and Tb.Sp displayed negative allometry, with trabecular thickness and spacing increasing at slower rates than isometry. Tb.N decreased with body size but showed a positive allometric relationship with larger species having a greater number of trabeculae than expected under isometry. BV/TV and humeral DA were also found to exhibit positive allometry, though the regression slope explains a relatively low amount of variance. For reptiles, only DA (degree of anisotropy) scaled allometrically with a high R^2 value, with trabecular orientations becoming more uniform as logBM increased. Other reptile characteristics (Tb.Th, Tb.Sp, Tb.N) were also significant, but were associated with a low coefficient of determination ($R^2 < 0.3$). These low R^2 values indicates that the models explain only a small portion of the variance in the data, meaning that the relationships with mass are weak and there is a large amount of variance that is unaccounted for by the regressions. Reptile Tb.Th and Tb.Sp were found to be negative allometry, with both of these characteristics growing at a slower rate than was observed in mammals. Tb.N also exhibited a positive allometric relationship in which the number of struts decreases with body size, albeit at a slower rate than mammals. This means that a mid- to large-sized reptile will feature a higher number of trabeculae than a comparably sized mammal.

Figure 3.5

Scaling relationships of trabecular characteristics relative to log body mass for the humerus and femur of reptiles and mammals: DA (A), BV/TV (B), log Tb.Th (C), log Tb.Sp (D), and log Tb.N (E). The dotted lines represent the isometric slope for each metric. Slope formulas, R^2 and p-values are presented in table 3.2. P-Values reflect a null hypothesis in which the observed slope is equal to the isometric slope.

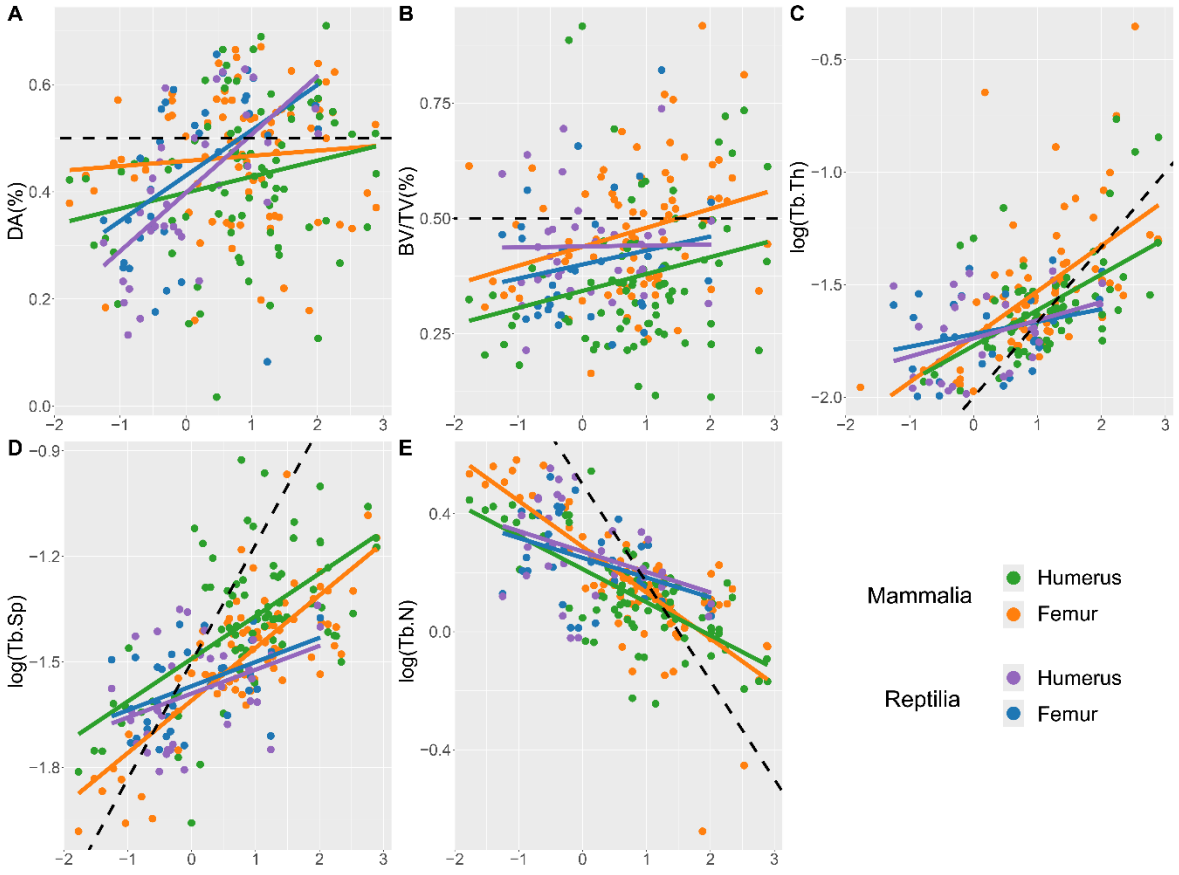

Table 3.2

Regression slope, R^2 and p-values for trabecular characteristics vs logBM as seen in figure 3.5. Any group that exhibited a statistically significant difference in slope from isometry ($p < 0.05$) and features R^2 values above 0.3 have been bolded. Groups that met only one of those two criteria have been marked with an asterix.

Trabecular Characteristic	Class	Bone	y	R^2	p
DA	Mammal	Humerus	0.03x+0.398	0.0488	0.049*
		Femur	0.01x+0.457	0.0069	0.464
	Reptile	Humerus	0.109x+0.398	0.443	**0.00447**
		Femur	0.085x+0.43	0.443	**0.0000177**
BV/TV	Mammal	Humerus	0.037x+0.343	0.055	0.0362*
		Femur	0.041x+0.439	0.0888	0.00727*
	Reptile	Humerus	0.002x+0.439	0.0003	0.929
		Femur	0.03x+0.4	0.0398	0.258
log(Tb.Th)	Mammal	Humerus	0.186x-1.815	0.497	**0.00000000101**
		Femur	0.226x-1.768	0.478	**0.000134**
	Reptile	Humerus	0.1x-1.76	0.204	0.000000177*
		Femur	0.098x-1.781	0.167	0.000000925*
log(Tb.Sp)	Mammal	Humerus	0.121x-1.491	0.375	**2.66e-19**
		Femur	0.15x-1.61	0.641	**7.48e-24**
	Reptile	Humerus	0.068x-1.59	0.159	6.04e-11*
		Femur	0.069x-1.569	0.235	1.9e-13*

Table 3.2 (cont.)

Trabecular Characteristic	Class	Bone	y	R^2	p
log(Tb.N)	Mammal	Humerus	-0.112x+0.212	0.497	**2.41e-28**
		Femur	-0.155x+0.288	0.579	**3.82e-19**
	Reptile	Humerus	-0.069x+0.272	0.146	3.53e-10*
		Femur	-0.067x+0.251	0.0267	2.55e-11*

Phylogenetic Comparative Methods

Phylogenetic ANOVAs of pooled data revealed a significant effect of ecological niche on humeral Tb.Sp (see Supplemental Dataset S3.2 for these results). The impact of ecological niche was also found to approach statistical significance ($0.05 < p < 0.076$) for humeral DA and femoral Tb.Th, and femoral Tb.Sp. Similar p-values were also observed for humeral BV/TV as grouped by posture. Subsequent Dunn post-hoc tests only found differences at a significance level of 0.05 for some of the included sub-groups (Fig. 3.6; Table 3.3). For ecological niche, the humeral Tb.Sp of semi-aquatic taxa were smaller compared to that of arboreal taxa. Femoral Tb.Th was also found to be statistically significantly smaller in fossorial taxa compared to cursorial species. None of the postural groups were found to be significantly different for any measured trabecular characteristics. Together, these results suggest that, although overall differences among groups may be present, specific contrasts between the majority of individual groups are subtle and do not reach statistical significance at the 0.05 level.

Figure 3.6

Boxplots of the residual values from pooled data of all statistically significant phylogenetic ANOVAs (p-value < 0.05) that tested for the effect of ecological niche. The boxes span from the first to the third quartile. The lines within the boxplots represent the median values for each group. Whiskers represent the range of data within 1.5 times the interquartile range (IQR) from the quartiles.

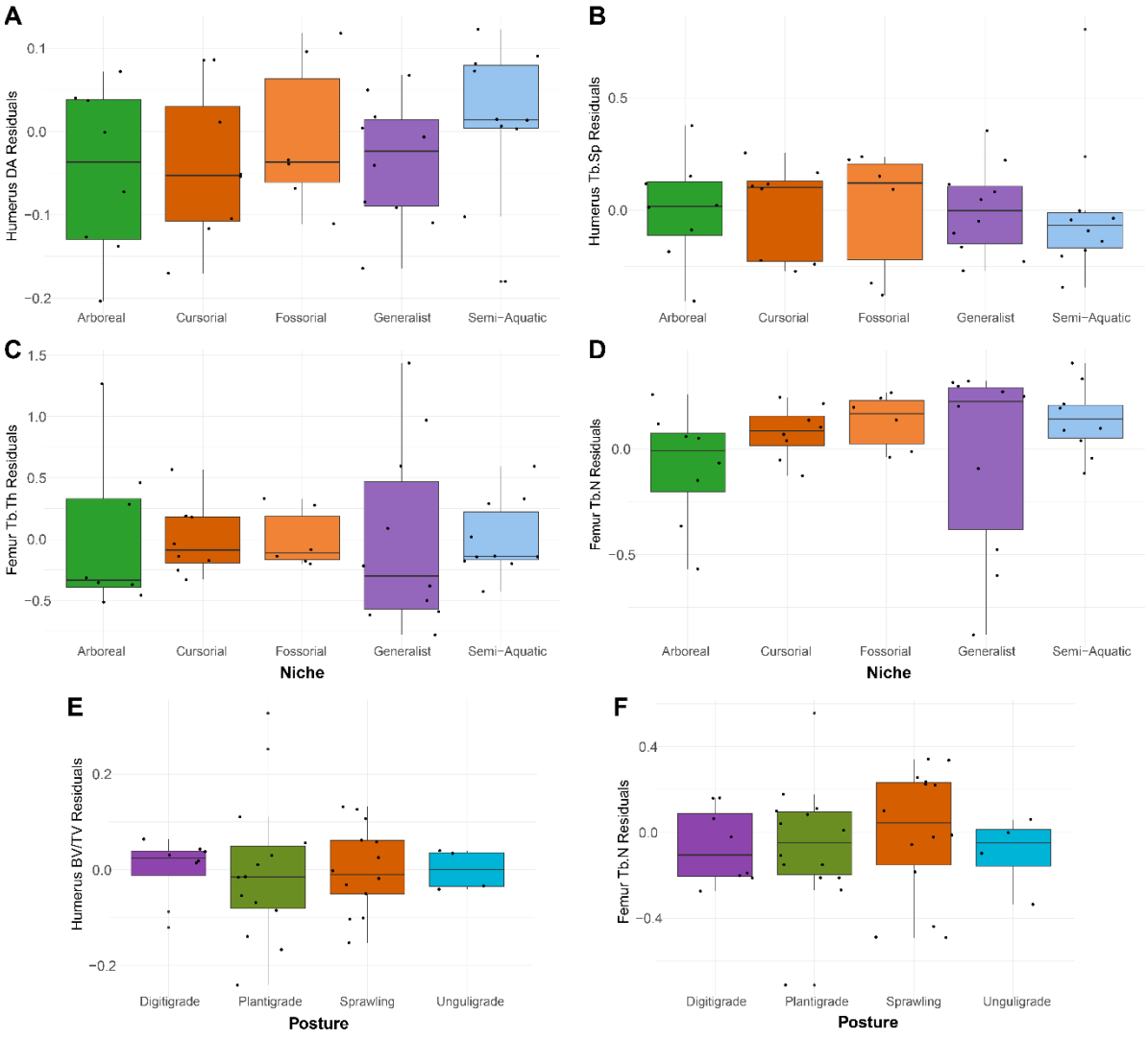

Table 3.3

Results of the post-hoc Dunn Test following Kruskal-Wallis tests of all residual values from PGLS. Paired groups that demonstrated a statistically significant difference in values ($p < 0.05$) have been bolded. The results of the Kruskal-Wallis tests can be found in Supplementary S2.2

Trabecular Characteristic	Comparison	Z	P unadjusted	P adjusted
Humerus Tb.Sp: Niche	Arboreal - Cursorial	0.122271	0.902685	1
	Arboreal - Fossorial	2.679086	0.007382	0.059059
	Arboreal - Generalist	1.452102	0.146473	0.585893
	Arboreal - Semi-Aquatic	2.929982	0.00339	**0.033898**
	Cursorial - Fossorial	2.565886	0.010291	0.072039
	Cursorial - Generalist	1.323217	0.185763	0.557289
	Cursorial - Semi-Aquatic	2.801097	0.005093	**0.045836**
	Fossorial - Generalist	-1.46801	0.1421	0.710501
	Fossorial - Semi-Aquatic	-0.1105	0.912016	0.912016
	Generalist - Semi-Aquatic	1.567528	0.116991	0.701948
Femur Tb.Th: Niche	Arboreal - Cursorial	-0.63173	0.527561	1
	Arboreal - Fossorial	3.069	0.002148	**0.01933**
	Arboreal - Generalist	0.601463	0.547532	0.547532
	Arboreal - Semi-Aquatic	1.804387	0.071171	0.427024
	Cursorial - Fossorial	3.653871	0.000258	**0.002583**
	Cursorial - Generalist	1.267367	0.205024	0.615072
	Cursorial - Semi-Aquatic	2.470293	0.0135	0.094502
	Fossorial - Generalist	-2.65716	0.00788	0.063042
	Fossorial - Semi-Aquatic	-1.5522	0.120614	0.60307
	Generalist - Semi-Aquatic	1.275895	0.201993	0.807971

Table 3.3 (cont.)

Trabecular Characteristic	Comparison	Z	P unadjusted	P adjusted
Humerus BV/TV: Posture	Digitigrade - Plantigrade	-0.20363	0.838646	1
	Digitigrade -Sprawling	-2.20047	0.027773	0.222186
	Plantigrade - Sprawling	-2.34151	0.019206	0.172852
	Digitigrade - Switch	-0.12888	0.897449	1
	Plantigrade - Switch	-0.0154	0.987709	0.987709
	Sprawling - Switch	1.155351	0.247947	1
	Digitigrade - Unguligrade	0.931782	0.351449	1
	Plantigrade - Unguligrade	1.165621	0.243768	1
	Sprawling - Unguligrade	2.726629	0.006398	0.063985
	Switch - Unguligrade	0.776524	0.437439	1
Humerus Tb.Sp: Posture	Digitigrade - Plantigrade	0.679848	0.496601	0.993202
	Digitigrade -Sprawling	1.927878	0.05387	0.430963
	Plantigrade - Sprawling	1.463445	0.143346	0.716729
	Digitigrade - Switch	1.714168	0.086498	0.518987
	Plantigrade - Switch	1.394124	0.16328	0.653121
	Sprawling - Switch	0.662401	0.507714	0.507714
	Digitigrade - Unguligrade	-1.24792	0.21206	0.636179
	Plantigrade - Unguligrade	-1.87937	0.060194	0.421357
	Sprawling - Unguligrade	-2.855	0.004304	**0.043037**
	Switch - Unguligrade	-2.44723	0.014396	0.129564

Table 3.3 (cont.)

Trabecular Characteristic	Comparison	Z	P unadjusted	P adjusted
Femur Tb.Sp: Posture	Digitigrade - Plantigrade	-0.1248	0.90068	0.90068
	Digitigrade -Sprawling	-1.78008	0.075062	0.450373
	Plantigrade - Sprawling	-1.94099	0.05226	0.365817
	Digitigrade - Switch	0.128885	0.897449	1
	Plantigrade - Switch	0.207963	0.835258	1
	Sprawling - Switch	1.178458	0.238614	0.954456
	Digitigrade - Unguligrade	-2.59568	0.00944	0.084964
	Plantigrade - Unguligrade	-2.70609	0.006808	0.068081
	Sprawling - Unguligrade	-1.4121	0.157922	0.789609
	Switch - Unguligrade	-1.95308	0.050811	0.406484

The slopes of several trabecular characteristics with respect to logBM were found to significantly differ among amniote niche and postural groups: humeral DA and femoral Tb.N with respect to posture, and femoral Tb.N with respect to ecological niche (Fig. 3.7; Tables 3.4, 3.5).

Figure 3.7

Allometric scaling relationships of trabecular characteristics versus log body mass for groups the phylogenetic ANOVA found to be statistically significant (p-value < 0.05). Specific groups are femoral Tb.Th with respect to Posture (A), humeral DA with respect to posture (B), and femoral Tb.N with respect to ecological niche (C). The dotted lines represent the isometric slope for each metric.

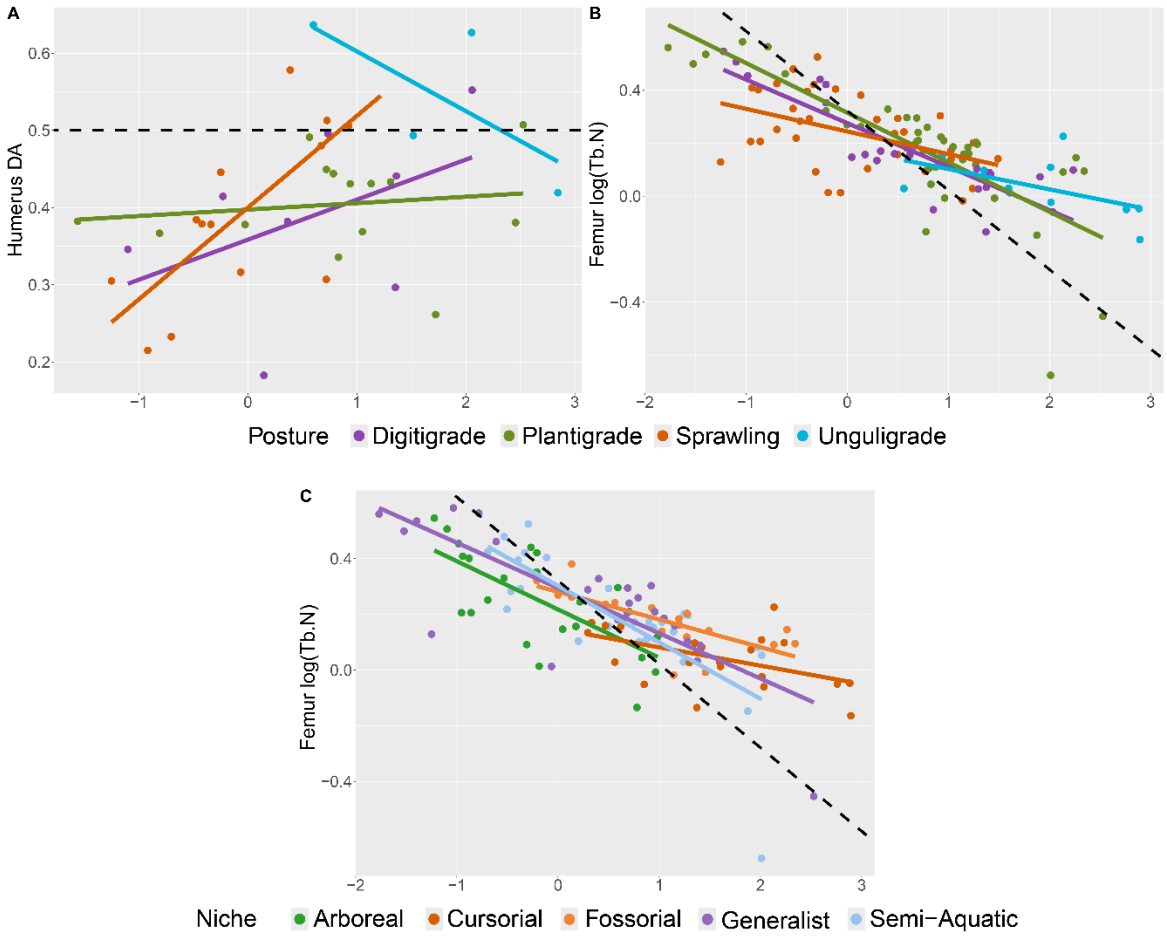

Table 3.4

Results of the post-hoc Dunn Test comparing the slopes of trabecular characteristics versus logBM in groups that Kruskal-Wallis testing found to demonstrate statistical differences in slope. Paired groups that demonstrated a statistically significant difference in values ($p < 0.05$) have been bolded.

Group	Trabecular Characteristic	Comparison	Z	P Unadjusted	P Adjusted
Niche	Humeral DA	Arboreal - Cursorial	-1.85444	0.063676	0.63676
		Arboreal - Fossorial	-0.99994	0.317339	1
		Cursorial - Fossorial	0.716939	0.473412	1
		Arboreal - Generalist	-0.96664	0.333726	1
		Cursorial - Generalist	0.988117	0.323095	1
		Fossorial - Generalist	0.157851	0.874574	1
		Arboreal - Semi-Aquatic	-1.20722	0.227347	1
		Cursorial - Semi-Aquatic	0.747532	0.454743	1
		Fossorial - Semi-Aquatic	-0.06314	0.949655	0.949655
		Generalist - Semi-Aquatic	-0.25518	0.798585	1
	Humerus Tb.Sp	Arboreal - Cursorial	0.305677	0.75985	1
		Arboreal - Fossorial	2.622486	0.008729	0.078562
		Cursorial - Fossorial	2.339484	0.01931	0.135173
		Arboreal - Generalist	1.490768	0.136022	0.816135
		Cursorial - Generalist	1.168556	0.242583	0.727748
		Fossorial - Generalist	-1.3733	0.169658	0.678632
		Arboreal - Semi-Aquatic	2.865539	0.004163	**0.04163**
		Cursorial - Semi-Aquatic	2.543327	0.01098	0.087842
		Fossorial - Semi-Aquatic	-0.1105	0.912016	0.912016
		Generalist - Semi-Aquatic	1.458165	0.144795	0.723975
	Femur Tb.Th	Arboreal - Cursorial	-0.48908	0.624783	1
		Arboreal - Fossorial	2.628775	0.008569	0.077124
		Cursorial - Fossorial	3.081578	0.002059	**0.020591**
		Arboreal - Generalist	0.386654	0.699012	0.699012
		Cursorial - Generalist	0.902194	0.366954	1
		Fossorial - Generalist	-2.39407	0.016662	0.133299
		Arboreal - Semi-Aquatic	1.29744	0.19448	0.972398
		Cursorial - Semi-Aquatic	1.81298	0.069835	0.488845
		Fossorial - Semi-Aquatic	-1.55746	0.119361	0.716163
		Generalist - Semi-Aquatic	0.966034	0.334027	1

Table 3.4 (cont.)

Group	Trabecular Characteristic	Comparison	Z	P Unadjusted	P Adjusted
Niche	Femur Tb.N	Arboreal - Cursorial	-0.40757	0.68359	1
		Arboreal - Fossorial	-1.90555	0.056709	0.56709
		Cursorial - Fossorial	-1.52821	0.12646	1
		Arboreal - Generalist	-0.91508	0.360148	1
		Cursorial - Generalist	-0.48547	0.627346	1
		Fossorial - Generalist	1.152312	0.249193	1
		Arboreal - Semi-Aquatic	-1.13848	0.254919	1
		Cursorial - Semi-Aquatic	-0.70887	0.478407	1
		Fossorial - Semi-Aquatic	0.947106	0.343585	1
		Generalist - Semi-Aquatic	-0.23695	0.812694	0.812694
Posture	Humerus BV/TV	Digitigrade - Plantigrade	-0.34813	0.727739	1
		Digitigrade - Sprawling	-2.25302	0.024258	0.21832
		Plantigrade - Sprawling	-2.23368	0.025504	0.204034
		Digitigrade - Unguligrade	0.865226	0.386915	1
		Plantigrade - Unguligrade	1.2067	0.227548	1
		Sprawling - Unguligrade	2.695819	0.007022	0.070216
	Femur Tb.N	Digitigrade - Plantigrade	-0.77838	0.436347	1
		Digitigrade - Sprawling	0.180636	0.856653	1
		Plantigrade - Sprawling	1.124542	0.260783	1
		Digitigrade - Unguligrade	-0.48253	0.62943	1
		Plantigrade - Unguligrade	0.087293	0.930438	0.930438
		Sprawling - Unguligrade	-0.6624	0.507714	1

Table 3.5

Regression slope, R^2 and p-values for trabecular characteristics vs logBM as seen in Figure 3.7. Any group that exhibited a statistically significant difference in slope from isometry ($p < 0.05$) and features R^2 values above 0.3 have been bolded. Groups that met only one of those two criteria have been marked with an asterisk.

Bone	Trabecular Characteristic	Posture/Niche	y	R^2	p
Humerus	DA	Sprawling	0.119x+0.4	0.563	**0.00198**
		Plantigrade	0.008x+0.397	0.0205	0.625
		Digitigrade	0.052x+0.358	0.203	0.262
		Unguligrade	-0.077x+0.68	0.476	0.31
Femur	Log(Tb.N)	Arboreal	-0.173x+0.218	0.486	**0.0038**
		Cursorial	-0.066x+0.147	0.263	0.000000007 18*
		Fossorial	-0.099x+0.281	0.527	**0.000000237**
		Generalist	-0.163x+0.295	0.624	**0.0000412**
		Semi-Aquatic	-0.203x+0.302	0.574	**0.0102**
	Log(Tb.N)	Sprawling	-0.085x+0.244	0.21	0.000000008 74*
		Plantigrade	-0.187x+0.315	0.612	**0.0000376**
		Digitigrade	-0.164x+0.276	0.747	**0.00000192**
		Unguligrade	-0.077x+0.179	0.312	**0.000236**

Trabecular Orientation

The stereomorphic projections measure two distinct values: azimuth and plunge. Azimuth values range from 0 to 360 and correlate to compass degrees, as described by the outer ring of the stereomorphic projection. For this study, an azimuth of 270° aligns with the midline of the articular head in both the humerus and femur, whereas a value of 0°/360° corresponds to the cranial portion of the long limb bone. The plunge ranges in value from 0° to 90° and describes the verticality of trabecular struts. A plunge value of 0° indicates the primary orientation for a species is perpendicular to the bone's midshaft, whereas a value of 90° indicates a completely vertical orientation aligned with the midshaft. Within the stereomorphic projection, the closer a point moves towards the center of the plot, the more parallel the trabecular orientation to the bone's midshaft.

The projections of the trabecular orientations for all specimens in the dataset reveal two distinct trends within the humerus and femur (Fig. 3.8). Regardless of posture, humeral trabecular orientations primarily settle around an azimuth of 270° with an average plunge of 39.18° from horizontal. For nearly all taxa sampled, this "western" direction points towards the glenoid cavity, though the exact location of the fossa may be found more vertically along the stereomorphic projection for species where the scapula is oriented dorsal-ventrally, such as the coyote (*Canis latrans)*. Parasagittal and sprawling taxa exhibit a high variance in humeral plunge values whereas switch-gait individuals feature a variance of only 6.36° with an average value of 75.43°.

Figure 3.8

Stereomorphic projections displaying the primary trabecular orientation of all sampled specimens. A and B present views of the humerus and femur, respectively, for two species from the same top-down view as the projections below. The blue circles represent the spherical ROI taken from each bone. The stereomorphic projections are grouped by posture (C and D) and general ecological niche (E and F). The size of each datapoint correlates to DA value with larger points indicating a higher DA. Directions for the X and Y planes have been included. The Z axis is oriented perpendicular to the plots, with the positive-Z direction projecting towards the reader.

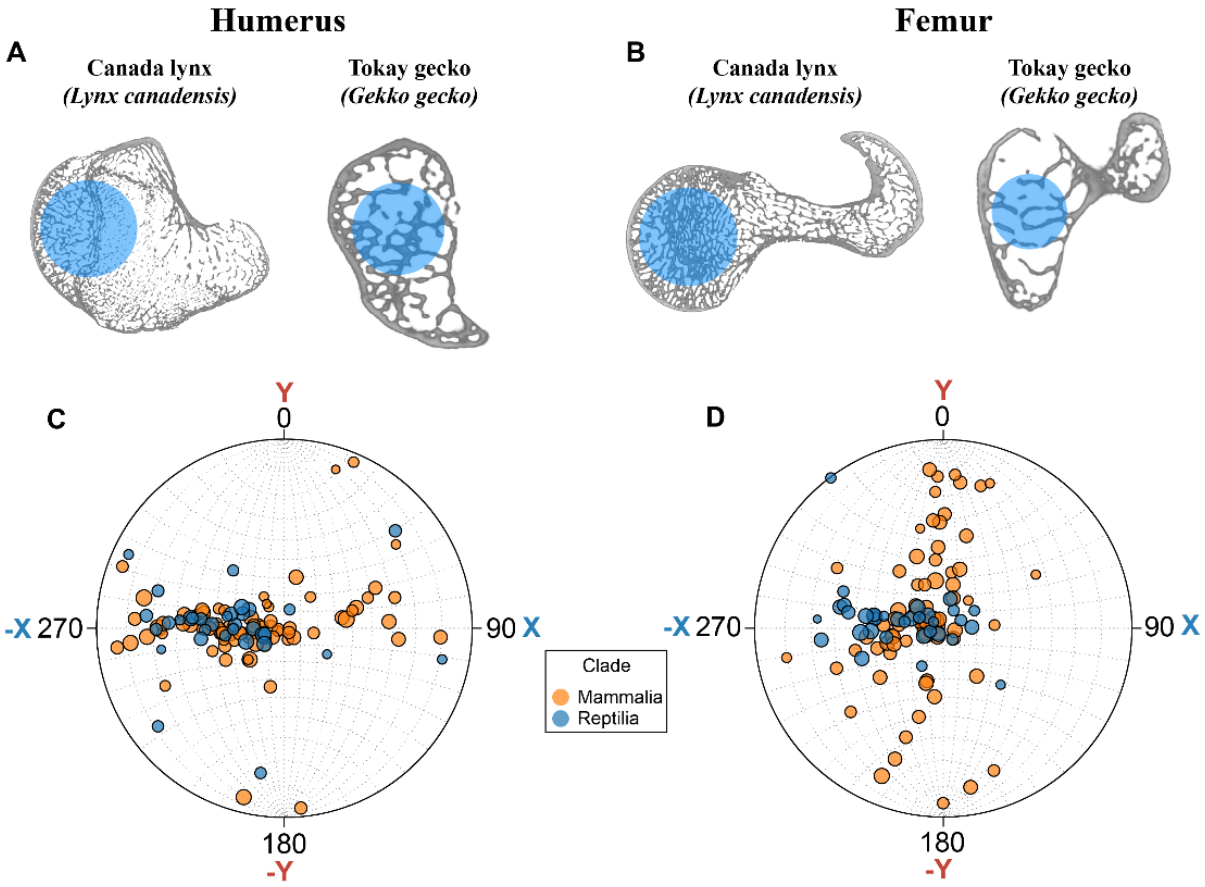

Figure 3.8 (cont.)

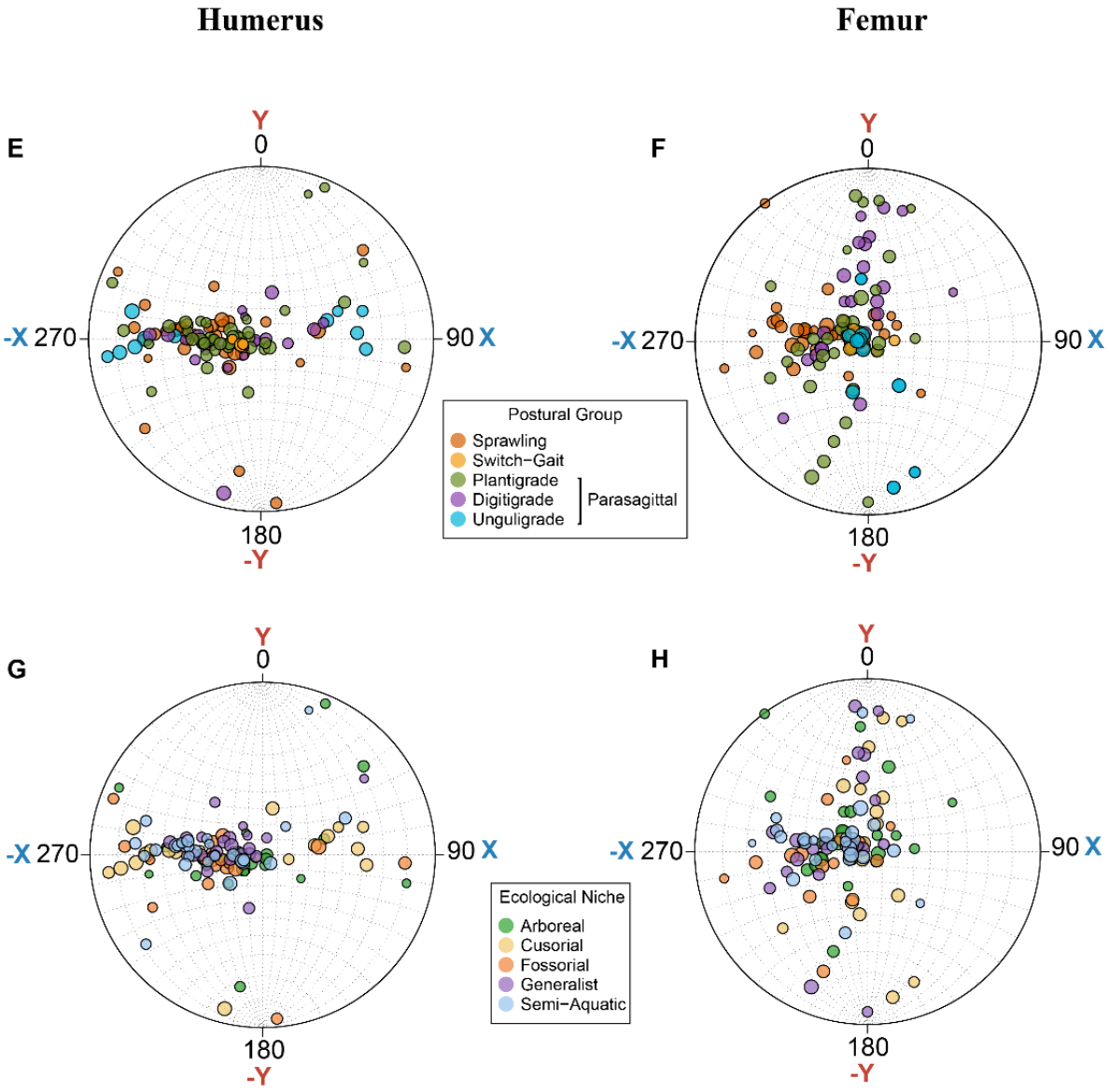

Compared to the humerus, femoral trabecular orientations exhibit distinct differences between postural groups visible on the stereomorphic projection. The femoral trabeculae of sprawling taxa feature similar trends to those seen in the humerus, settling along the western hemisphere of the stereomorphic projection with plunge values ranging from 4.36° to 82.95° degrees. Parasagittal species instead feature azimuths orienting towards the "north", or cranial direction of the overall body. About a third of parasagittal individuals cluster around the center of the plot with a nearly vertical strut orientation. The humeri and femora of switch-gait taxa demonstrate limited variance in their trabecular orientation, with struts typically aligned close to vertical.

Each of the three major clades within Reptilia show distinctive patterns when comparing humeral and femoral trabecular orientations (Fig. 3.9).

Figure 3.9
Stereomorphic projections displaying the primary trabecular orientation of all three sampled reptile orders for the humerus (A) and femur (B). The size of each datapoint corresponds to DA value with larger points indicating a higher DA. Directions for the X and Y planes have been included. The Z axis is oriented perpendicular to the plots, with the positive-Z direction projecting towards the reader.

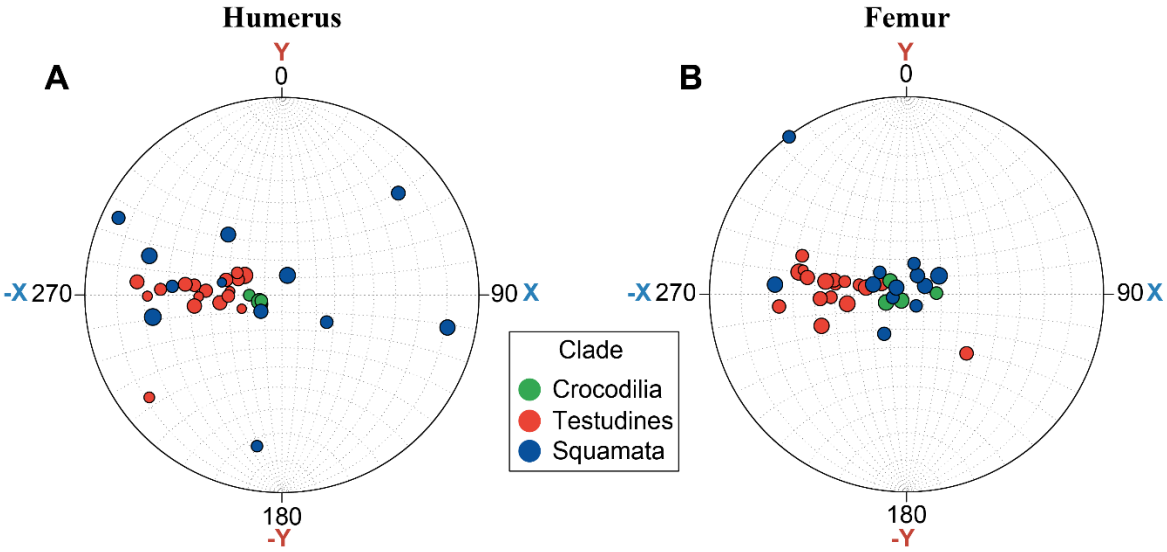

The humeral struts of Testudines retain a conserved range of azimuth values, with only one African helmeted turtle (*Pelomedusa subrufa)* featuring struts that stray more than 25° from the 272.28° average. Plunge values for turtles display much more variety, ranging from nearly horizontal (9.31°) to a maximum value of 65.94°. Crocodilian humeral orientations are even more conserved, with neither the azimuth nor plunge of any individual straying more than 14° from the average values of 256.05° and 75.43°, respectively. Squamata, by contrast, exhibits a much more variable range of trabecular orientations, albeit one that still trends towards horizontal struts oriented along the medial/lateral plane. Femoral trends for Testudines and Crocodilia mirror those seen in the humerus, whereas the squamates all show a very limited range of near-vertical orientations. To summarize, turtles and crocodilians display comparable trabecular orientations between their fore- and hindlimbs. Squamates exhibit humeral struts that trend laterally with respect to the limb bone itself, and dorsal-ventrally once the bone is oriented *in vivo*. By contrast, lizard femoral struts run parallel to the length of the limb bone, and face medially *in vivo.* A similar comparison was not performed for mammals due to the limited number of species within each comparable mammalian clade represented in the dataset.

Discussion

Trabecular bone is an integral part of the skeletal system acting to increase structural support by aligning parallel to the direction of stress (Wolff 1892; Koch 1917; Fyhrie & Carter 1986) and increasing in thickness to increase bone load-bearing capacity (van Rietbergen et al. 1995; Ruimerman et al. 2005). Given the wide diversity of behaviors and limb loading strain orientations present across terrestrial vertebrates (Lieberman et al. 2004), it has been suspected that differences in ecologically based behavior or postural group may be reflected in the structure of trabeculae themselves. Here, I measured several characteristics of trabeculae sampled from

within the articular heads of proximal limb elements in a broad sample of mammal and reptile species. Additionally, the bones were aligned to allow for a comparison of primary trabecular orientation between taxa. The results show significant differences in trabecular structures between the femur and humerus across Amniota, suggesting a wider diversity of structures within the skeleton than previously appreciated. Although trabecular characteristics such as DA, BV/TV, Tb.Th, Tb.Sp, and Tb.N proved to be minimally related to differences in ecological niche or posture, orientation was found to correlate strongly with these factors, reflecting adaptations to specific mechanical loading patterns and ecological pressures.

Differences between the Humerus and Femur

Previous research highlighted the potential differences in the trabecular architecture of the fore- and hindlimb (Reinecke and Angielczyk 2024). The results confirm statistically significant differences between these elements in DA, BV/TV, Tb.Sp, and transformed-azimuth across terrestrial quadrupedal amniotes (See Supplementary S3.2). Due to the small number of individuals sampled per species, outliers stemming from illness or injury that impacted trabecular structures were removed. These aberrant individuals exhibited issues visible from the cortical morphology and were identified through comparisons to others of comparable size and phylogenetic position, so the differences between the humerus and femur cannot be ascribed to the impact of potential outliers. Across a number of different ecological niches and postural groups within Mammalia, femoral trabeculae tend to be thicker and contribute to a higher bone volume fraction, whereas the humerus features wider spaces between trabeculae. Part of this distinction may stem from the fact that in most sampled taxa, the femur is the larger of the two bones. Increases in body mass correlate to higher Tb.Th values in single elements when compared across species, so larger elements may show a similar effect when comparing bones

within the same organism. While larger body mass also correlates with an increase in Tb.Sp values, the rising BV/TV values indicate this effect to not be as pronounced as the observed Tb.Th changes. The low R^2 for BV/TV ($R^2 < 0.3$) suggests that body size explains only a modest proportion of its variation, indicating potential influences from additional factors.

Reptiles exhibit far more conserved trabecular characteristics between the humerus and femur, with only the verticality of struts differing significantly. Compared to mammals, reptiles present less disparate gross morphologies between the fore- and hindlimb (Williston 1925; Romer 1956), as well as less variety in their use. Whereas mammals have evolved highly varied limb morphologies for the myriad of ecological niches the group inhabits, reptiles retain a more uniform limb anatomy. This is likely driven by the fact that many sprawling reptiles rely heavily on midbody lateral undulation to generate movement, using lateral flexion of the trunk to increase stride length and propel themselves forward (Reilly et al. 2005; Chong et al. 2022). The reliance on body undulation in a number of reptiles is likely reflected in the clade's trabecular structures as well, with less overall loading stress being exerted on the limbs (Farley & Ko 1997), leading to more uniform architecture. In contrast, parasagittal taxa, such as mammals, rely more heavily on their limbs for locomotion, necessitating a broader range of limb specializations for diverse forms of terrestrial, arboreal, and aquatic activity.

It is important to note the morphological differences between the articular heads of reptiles and mammals for the purpose of sampling out a specific region of interest for analysis. Nearly all mammal taxa, regardless of postural grade or phylogenetic position, exhibit relatively large spherical articular surfaces. For the femur, this articular surface is offset from the midshaft axis by an anatomical neck that varies in length between species. In humans and presumably other parasagittal mammals, the trabeculae within the femoral head are split between a nearly vertical

compressive group aligned parallel with the midshaft, and a more lateral tensile group that angles through the bone's neck (Sapthagirivasan & Mahadevan 2013). Although a similar morphology can be observed in turtles, other reptiles instead possess a more cylindrical head that rests directly above the bony midshaft and whose longest axis aligns with the cranial-caudal plane (Tsai & Holliday 2015). As such, secondary and tertiary trabecular orientations in the mammalian femur may be more disparate than those in the mammalian humerus or turtle limb elements, though future research will be necessary to assess the extent of these disparities and their biomechanical implications across a broader range of species and locomotor behaviors.

Trabecular Scaling with Size and Metabolism

Previous analysis of the scaling relationships between body mass and trabecular architecture of Mammalia have found varied results. Several publications found most trabecular characteristics exhibit a negative allometric relationship (Barak et al. 2013; Ryan & Shaw 2013; Christen et al. 2015), whereas others have found positive allometric relationships (Doube et al. 2011) or allometric patterns that vary between characteristics (Mielke et al. 2018; Amson & Bibi 2021). Findings by Smith et al. (2023) even suggest that these relationships may be dependent on the specific bone sampled or the size of an animal, with these trends shifting from negative to isometric as mass increases. The results uncovered negative allometric relationships for two mammalian characteristics (Tb.Th, Tb.Sp), and positive allometric relationships for BV/TV and Tb.N (Fig. 3.5; Table 3.2) with no obvious indication of changes to slope with respect to body size. Increases in trabecular spacing and a decrease in trabecular number appear to be balanced by an increase in intertrabecular thickness resulting in higher BV/TV values as body mass increases. As many of these previous studies have focused on a more limited range of mammalian taxa, results suggest that these allometric scaling relationships are broadly present

throughout the order and between long limb bones, while not discrediting the possibility for different relationships within lower order clades. Additionally, due to the size of the μCT scanner used for this study this dataset was unable to sample terrestrial mammal taxa above 450 kg. Mammals above this size range often feature adaptations for columnar limbs and reduced range of motion (Alexander 1985; Biewener 1989). This reduction in limb mobility paired with a high body weight likely impacts internal trabecular structures as more of the overall limb morphology and orientation is structured for weight bearing.

In focusing on mammalian taxa, comparably little work has been done to assess reptilian trabecular dynamics. Among reptiles, only DA was found to have a significant positive allometric relationship with body mass. Unlike mammals, which appear to retain a consistent level of trabecular isotropy, reptilian trabeculae orient more uniformly in a singular direction as body size increases. In comparing scaling patterns of trabecular elements between the two major clades, Ifind that as body size increases mammalian bones develop a smaller number of thicker struts that are more widely spaced compared to their reptilian counterparts. Increased trabecular thickness paired with a decrease in trabecular number are trends regularly seen in species with a higher mass, likely serving to support increased loading and compressive stress exerted on limb elements (Doube et al. 2011). Thicker struts distribute stress more evenly throughout the articular head while offering greater resistance to bending and buckling than thinner trabeculae (Currey 2002; Gibson 2005). Mammals typically engage in more vigorous and dynamic movement than reptiles and are more reliant on the limbs themselves to support the overall weight of the body, whereas the sprawling posture of reptile's spreads weight bearing onto the midbody as well (Blob 1999; Reilly et al. 2005). However, there is minimal change to the angle of proximal limb elements as body size increases in reptile. This ensures that increases in weight

result in a higher magnitude of stress being exerted on the proximal articular head. without the bone's midshaft located inferiorly to act in support against gravity. Due to this less vertical limb orientation, I suggest trabecular uniformity plays a larger role in strengthening reptilian limbs. Further testing will be necessary to assess the comparative strength of reptile bones to mammalian elements, and whether the reptilian midshaft is adapted to brace against bending strain as opposed to the compressive strain present in species with more vertical limbs.

Histological analyses of bones in humans have found that a decrease in metabolic rate correlates to a slowdown in bone remodeling (Wawrzyniak & Balawender 2022; Zhou et al. 2023). Between the two sampled clades, reptiles exhibit lower metabolic rates that may correspond to a reduced capacity for trabecular bone to change its architecture compared to similar sized mammals (Bennett & Ruben 1979; Nagy 2005). That is not to say no trabecular modification occurs in Reptilia, as analysis of both Squamata and Testudines has found significant remodeling within the medullary cavity (de Buffrénil & Houssaye 2021; Scheyer & Cerda 2021). Whether this remodeling rate is present within the denser proximal articular surfaces is unclear especially considering the far slower rates of cortical modification that could impact the volume of intertrabecular space. Further tests of trabecular remodeling rates throughout the limb in both Mammalia and Reptilia will be necessary to confirm potential differences between the two clades, and if these rates are uniform throughout the bone.

The Minor Impact of Ecology and Posture

Although I found significant differences in trabecular architecture between the forelimb and hindlimb in mammals, I observed minimal differences between groupings of species based on ecological niche or generalized postural group. The significant overall ANOVA results, phylogenetically corrected and adjusted for body size, suggest possible differences in Tb.Th for

both bones and Tb.Sp for the humerus across different ecological niches (Fig. 3.6), hinting at subtle ecological adaptations in trabecular bone structure. In much the same vein as differences in behavior and loading stress between mammals and reptiles, ecological niches that rely on repeated high stress limb movements, such as those seen in cursorial and fossorial taxa, logically could be expected to have larger individual struts to support against increased compressional stress. However, the presence of only a select few significant pairwise comparisons implies that measurable differences between distinct ecological groups are minimal, and that there is a great deal of overlap in the variance of limb stress between the groups. This lack of distinction between ecological groups may also be a result of the small sample of fossorial taxa present in this study (n=6). Although these species were sampled to feature a range of specialized and more generalist burrowing morphologies, the addition of more species may reveal more pronounced differences in trabecular bone microstructure that align with their specific ecological demands. A minimal impact of ecological niche on trabeculae has been observed in the vertebrae of several mammal clades (Smith et al. 2023; Zack et al. 2023), suggesting that this is a trend present in trabecular bone from other regions of the skeleton as well. In contrast, analysis of semi-aquatic and fully aquatic taxa has demonstrated significant differences in trabecular architecture (Houssaye et al. 2016). I suspect that this case may be an outlier, as aquatic limbs and fins typically endure a lower magnitude of stress compared to terrestrial limbs adapted to support the weight of the body while also facilitating movement (Dickson et al. 2021). Additionally, the skeletal structure of aquatic limbs, adapted for swimming with features such as elongated and streamlined elements, differs significantly from the structural diversity found in terrestrial limbs. These gross morphological differences likely further influence the variance in trabecular architecture, as the mechanical loading patterns in aquatic environments dominated by fluid

resistance contrast starkly with the magnitude and direction of forces experienced in terrestrial settings. Future work will be needed to assess if these assumptions are correct, and the degree to which loading regime and differences in gross morphology may account for different proportions of the variance observed between terrestrial and aquatic taxa.

The Impact of Posture on Trabecular Orientation

Unlike other trabecular characteristics, the primary orientation of struts within both the humerus and femur are largely unaffected by the size of an organism. Rather, postural group appears to be the primary factor driving trabecular orientation (Fig. 3.8). At first glance, the humeral trabecular orientations with respect to posture appear to be fairly consistent, with most sprawling and parasagittal taxa all exhibiting azimuth values oriented near 270° and with varying levels of verticality. *In vivo* however, this 270° measurement points caudally with respect to the overall body in parasagittal taxa and dorsally in sprawling taxa. The femoral stereomorphic projection more clearly reflects the differences between *in vivo* directions, with sprawling femoral trabeculae pointing dorsally, and parasagittal taxa exhibiting primarily cranially facing struts.

Within the parasagittal group**,** plantigrade taxa exhibit the widest range of trabecular orientation, whereas unguligrade trabeculae are fairly conserved in both the humerus and femur. I suspect that this distinction may be driven by differences in the limb's range of motion between these three postural groups. Plantigrade and digitigrade taxa retain several morphological features of the autopodium that favor lateral movements while allowing for adaptability for foot flexion, extension, abduction and adduction (Munteanu & Covașă 2018). Unguligrade taxa by contrast specialize towards a more columnar limb that optimizes forward momentum at the cost of mediolateral movement (Polly & Hall 2007). One might assume that the trabecular struts will

orient along the sagittal axis in the direction of this forward limb movement, but the unguligrade humerus is instead defined by heavily horizontal orientations along the medial-lateral axis. The rigid and columnar nature of the ungulate limb appears to effectively brace against the majority of dorsal-ventral stress exerted on proximal limb, diminishing the need for trabeculae to orient in that same direction. Instead, the trabeculae appear to be adapted to brace against lateral stress that the overall morphology of the limb is less suited to endure. Although this same trend can be observed in the femoral trabeculae of smaller unguligrade species, the larger individuals within this dataset exclusively exhibit vertical orientations aligned with the midshaft. Because the femoral head is not positioned directly above the midshaft, the femur is less effective at supporting the body's weight, resulting in increased dorsoventral stress on the femoral head. This stress appears minimal in smaller taxa, allowing for a primarily mediolateral orientation of the trabeculae, but in larger taxa, the trabeculae apparently play a critical role in resisting stress and are uniformly oriented vertically. Analysis of loading stress on the limb elements of various unguligrade taxa is limited, but studies of horse femora and humeri have found the primary stress angle in both bones to be comparable to the orientations found in my results (Pollock et al. 2008; Lang et al. 2024).

The size of the μCT scanner available for this study limited the size of bones that could be housed within the machine, which set an upper limit to the size of mammals that could be included in the dataset. Therefore, the trabecular orientations of many graviportal species are still unknown. Though the scaling relationships of trabeculae with respect to body mass are preserved in these larger taxa (Barak et al. 2011), how a columnar limb with a digitigrade to unguligrade foot posture associated with supportive soft tissue structures influence skeletal microanatomy has yet to be fully explored. Future analysis of these species via μCT machines with larger scan

volumes and higher radiation penetration depth may help to further expand our understanding of trabecular bone diversity and identify if trabecular orientation trends shift at the highest body masses.

Reptile Trabecular Diversity

Although less varied than mammals, the sampled reptiles show some major differences in limb morphology, especially when comparing the shapes of proximal limb elements in turtles to those of squamates and crocodilians. This distinction is present in trabecular morphology as well, with all three clades exhibiting distinct trends between the fore- and hindlimb (Fig. 3.9). Crocodilians exhibit highly conserved trabeculae in the humerus and femur that align with the distal condyles of bone, oriented laterally to the midbody *in vivo.* A similar trend can be seen in the squamate femur, but the humeri show the widest range of orientations among reptiles, ranging from near vertical to near horizontal. Additionally, there appears to be no distinct trend within the clade, as individuals within the same species can feature widely disparate orientations of humeral trabeculae (Fig. 3.9). Some lizard species, specifically in the genus *Anolis*, have been described as hindlimb dominant, and it may be that the use of the femur in running and jumping drives femoral trabeculae towards an optimal uniform orientation not required in the humerus (Losos 1990). However, further testing will be necessary to assess if this behavior is present in other squamate clades, or if the differences in loading strain between fore- and hindlimb are strong enough to "force" femoral trabeculae towards these orientations.

Trabecular orientations are conserved between the humerus and femur in Testudines, though their primary orientations are more dorsal *in vivo* compared to those of crocodilians. Unlike other sprawling reptiles, turtles have more vertically aligned limbs, which help support the additional

weight of their shell. The trabeculae appear to be oriented such that their struts align parallel to the force of gravity, likely to resist the stress exerted by the shell on the proximal articular heads of both limb elements. Further analysis is needed to establish a direct link between limb orientation and trabecular structure in turtles, but trabecular orientation may serve as a unique proxy for inferring the specific limb posture of reptiles.

Reptilian Plasticity and Analytical Challenges

Switch-gait behaviors, primarily observed in crocodilians, offer a unique model for studying the relationship between posture and trabecular bone architecture. Unlike the distinct parasagittal and sprawling postures seen in many vertebrates, crocodilians shift between a sprawling stance and a more upright "high-walk" gait. This behavioral flexibility reflects their evolutionary trajectory from parasagittal ancestors to a more sprawling stance that is similar to that of many other reptiles (Parrish 1987; Hutchinson 2006). Despite exhibiting some of the widest range of behaviors and limb orientations, crocodilian trabecular orientations were the most conserved of any clade, with both sampled species exhibiting nearly vertical struts in both the humerus and femur. Although this sample includes only two of the twenty-eight species of extant crocodilians, the strong similarities in skeletal morphology, behavior and ecological niche of all crocodilian species suggest that these trends are likely present throughout the clade.

I suspect two potential reasons for the apparent discrepancy between postural range and trabecular diversity. First, although trabecular bone typically aligns with the direction of primary stress, the different angles of stress in a sprawling posture versus a high walk may be comparable enough that trabeculae does not significantly trend towards one direction over another. In lieu of a particular singular direction, the trabeculae seem to settle on a “neutral” orientation aligned with the midshaft of the bone. Many of the other clades sampled appear to trend in this same

direction, suggesting that this may be the standard trabecular arrangement until sufficiently disparate loading stress during locomotion is exerted and the bone adjusts accordingly. However, it is possible that this orientation is defined during puberty as analysis of trabecular development across ontogeny has demonstrated a shift during prepubescent age in two separate taxa (Ryan & Krovitz 2006; Acquaah et al. 2015; Reinecke and Angielczyk 2024). Whether these trends are present in other mammal clades is still unclear and will require further analysis of ontogenetic trabecular development in more specialized species. Second, it may be that the semi-aquatic ambush hunting strategy and tail-dominated swimming behaviors of crocodilians do not exert enough loading stress on the limbs to drive trabecular reorientation. Future analyses of the forces acting on crocodilian limb bones during various locomotor behaviors could clarify whether specific activities generate higher stress levels, providing insights into how these forces influence trabecular structure and contribute to the observed patterns of vertical alignment and reduced variability.

Among the clades sampled, Squamata had the most specimens that were scanned but were unable to include for analysis in this study. This problem is in part due to the small size of many lizard species, and the nature of lizard limb elements, which tend to be smaller and less robust than those of other amniote clades. Several species, such as the viviparous lizard (*Zootoca vivipara*), have proximal limb elements so small that the resulting regions of interest are only a few voxels wide, far too small for any meaningful analysis. Scan resolutions for each of these lizards were comparable to those of other small species within the dataset, ensuring the issue is not a comparably low scan resolution. Even among somewhat larger taxa, the typical preservation of herpetological specimens as full-body wet specimens limits the ability to focus on specific bony elements, reducing the scan magnification below the level needed to record

very small trabeculae. This issue can be observed in the publicly available CT scans of full body squamate species on sites such as Morphosource (Boyer et al. 2016; Frýdlová et al. 2019). Despite the scans housed on these repositories being of generally excellent quality and high resolution, the need to preserve the entire body results in bony regions too small for analysis of trabecular structures. With a limited number of disarticulated skeletons housed in collections, this is an issue that is not so easily solved. Future research into squamate trabecular elements will need to prioritize scans that focus on just a few skeletal elements and utilize μCT machines with nano-focus x-ray tubes to maximize resolutions.

Implications for the Fossil Record

These results suggest that analysis of trabecular bone orientation within upper limb elements may provide insights for paleontologists studying postural evolution, who are inherently limited to skeletal elements. Traditional analysis of postural groups in extinct taxa has focused on range of motion (ROM) analysis (Hutson & Hutson 2012; White et al. 2015; Senter & Sullivan 2019; Gatesy et al. 2022; Brocklehurst & Pierce 2023). Although this approach can be useful in identifying a species' capacity for movement, it does not necessarily reflect frequent and consistent behaviors utilized by an organism. Humans have the capacity for incredible feats of flexibility and range of motion that the majority of individuals will never engage in, yet range of motion analysis has minimal means to separate frequent from infrequent behavior. By contrast, trabeculae instead react directly to habitual loading stress exerted on the limb, and more closely reflect an organism's standard behaviors by orienting struts parallel to these directions of loading. As analysis of trabecular bone becomes more widespread and robust in the field of paleontology, I advocate for a focus on orientation to help explore questions of postural

evolution, further refine the range of motion envelopes derived from model-based approaches, and to potentially identify limb orientations not seen in any extant clades.

This is not to suggest trabecular analysis is a foolproof method, as the capacity to accurately segment trabeculae in fossil bone is dependent on the composition and density of the surrounding rock matrix. For example, in the course of this study I experimented with early Permian non-mammalian synapsids, which are of particular interest in understanding postural evolution in the lineage including mammals. These specimens were collected in the American southwest and were found to be riddled with pyritic inclusions. These dense pyrite crystals produce bright artifacts in scans that skew contrast adjustments and obscure bone to the point that analysis of fossil elements becomes impossible (Racicot 2017). As trabeculae are such small elements, these obfuscations can completely negate any possible analysis (Appendix A3.1). It may therefore be difficult to include basal synapsids and other taxa preserved within "problematic" sediments in studies of trabecular bone architecture, and additional experimentation is needed to identify more suitably preserved specimens that span this transition.

Additionally, fossil elements will often undergo taphonomic deformation during the fossilization process. Although this can have a dramatic effect on gross morphology (e.g., Angielczyk & Sheets 2007; Kammerer et al. 2020) the microstructures nestled within presumably are even more susceptible to compaction and shearing, which could alter trabecular shape, orientation, or spatial distribution. The effects of deformation on larger, more visually distinct structures can be subtle, implying that it will likely be difficult or even impossible to detect changes in trabecular architecture without non-deformed specimens for comparison. Consequently, studies of fossil trabeculae likely will need to utilize a much larger dataset than comparable studies of extant

taxa—potentially double the size—to account for the approximate rate of deformation observed in fossil specimens (Kammerer et al. 2020).

Limitations

Due to the cost and time investment needed to collect, scan, and process the specimens for this study, this dataset was limited with regards to both the number of individuals sampled per species, as well as the breadth of species sampled from each major clade. Due to the reactive nature of trabeculae to significantly change their structure due to illness or injury, outliers can exert a particularly strong influence on results. An example of the magnitude of these differences can be seen in Figure 3.8, where the femoral plunge of one Jackson's chameleon (*Trioceras jacksonnii)* is over 60 degrees lower than its contemporaries and placing the point marking its orientation along the edge of the graph. Although these outliers have been identified and removed where appropriate, their presence further shrinks this dataset and lessens the power of statistical analyses. As trabecular research expands to measure more clades of amniotes, my hope is that researchers will provide high quality scans to online repositories to allow others with limited time, funds, or access to μCT scanners the means to acquire larger robust datasets less influenced by outlier individuals.

As described in Bouxsein et al. (2010), the voxel size of a μCT scan should be a minimum of 3-4 times smaller than a measured object in order to avoid significant errors in preserving trabecular morphology. While the scan resolutions are within this window with respect to the average Tb.Th value of each specimen, there is the possibility that the higher resolutions of larger specimens may slightly warp or omit smaller trabeculae. While I believe the potential impact of this on my data to be minimal if at all present, it should be noted that future research focusing on larger amniote taxa should emphasize utilization of multiscans and prioritization of scans

focused exclusively on proximal or distal elements to further lower voxel sizes and minimize these potential effects.

Conclusion

This work analyzes the trabecular architecture of proximal limb elements to assess potential differences in structure across a broad sample of terrestrial amniote taxa. Along with quantifying variation between the humerus and femur, I also looked to identify trends in trabecular architecture that correlated with ecological niche and general postural group. I found a statistically significant difference in DA, BV/TV, and Tb.Sp between the humerus and femur within Mammalia, but less variation between the limb elements of reptiles, likely due to the limited morphological diversity in limb structure of the group. Traditionally measured trabecular characteristics were generally found to exhibit only a few statistically significant differences among ecological groups and no differences among postural groups. Trabecular orientation did exhibit trends for both sets of groups, with lateral trabeculae in both reptile limbs and mammalian humeri while the mammalian femur featured anteriorly facing struts. The size, number, and uniformity of trabecular struts appear to be influenced by a myriad of factors that vary strongly across such a broad phylogenetic sample, to the extent that future analyses will likely need to focus on smaller clades to meaningfully measure their differences. By comparison, trabecular orientation appears to be driven primarily by the direction and magnitude of loading stress, making it a more viable characteristic to assess variation in highly disparate clades. Although determining trabecular orientation can be difficult in species of differing skeletal morphology, I hope the methodology I utilized in this paper serves as a foundation for future analyses seeking to broaden our understanding of trabecular diversity and the factors that influence their growth and complex organization.

Chapter 4: Identifying Trabecular Diversity Among Long Limb Elements in Didelphids

Abstract

Trabecular bone, a network of small bony struts located within larger cortical structures, has been studied to identify the ways in which bone reacts and adjusts to loading strains exerted on the skeleton. Despite the presence of trabeculae in numerous different skeletal elements, research has generally focused on a limited number of proximal limb bones, leading to general assumptions of trabecular uniformity in other bones. In this study, I utilize the group Didelphidae to investigate if the trabecular architectures of lower limb elements are significantly different from those of the humerus and femur, and what factors may drive potential structural heterogeneity. My results indicate that distal long limb bones exhibit thicker trabecular struts that are more densely packed together, but less uniformly oriented than their upper limb counterparts. I hypothesize that these differences are likely driven by a more conserved directionality of loading stresses on distal limb elements, paired with an increased magnitude of stress from the weight of the body as compared to the humerus and femur. Surprisingly, the heterogeneity of trabeculae between the humerus and femur observed broadly across Mammalia was not present in didelphids, underscoring the need to explore the trabecular diversity of more restricted clades in detail.

Introduction

The mammalian body is a living, reactive system that actively modifies its structure based on the influences of outside factors. Although this principle is commonly observed in features such as muscle and organs, bone is an equally dynamic tissue. The responsive nature of bone was first

described in 1893 by Julius Wolff who stated that the bones of healthy animals will alter their structures to adapt to loads exerted on them (Wolff 1893). To explain these modifications, Wolff drew comparisons between the loading beams of construction cranes and the complex latticework of bony struts nestled within the outer cortical shell that I now refer to as trabecular bone. Trabecular bone, commonly found in the skull, vertebrae, and limb bones, will remodel itself to resist loading, typically through a widening of trabecular struts that are oriented in the direction of stress (Wolff 1893; Koch 1917; Fyhrie & Carter 1986). Technical advancements in high resolution microCT scanning and computational programs have allowed scientists to measure a number of trabecular characteristics and how factors such as ontogenetic stage (Tanck et al. 2001; Ryan & Krovitz 2006; Reinecke & Angielczyk 2024) body size (Doube et al. 2011; Barak et al. 2013; Zack et al. 2023; Smith et al. 2024), phylogeny (Amon & Bibi 2021; Smith et al. 2023), ecomorphotype (Amson et al. 2017; Mielke et al 2018), and postural grade (Reinecke & Angielczyk In Review) impact their structure.

The majority of these studies have focused their scope on one or two bones, often the femur, to draw direct comparisons to biomedical analyses that measure the same features in humans and primates (Ryan & Krovitz 2006; Ryan & Shaw 2013; Saers et al. 2017; Tsegai et al. 2018; Alfieri et al. 2025)**.** Therefore, our understanding of the diversity of trabecular structures across limb elements is limited, especially with regards to distal long limb bones. The loading regimes of these bones can vary significantly from those the proximal limb elements endure, such as higher bending strain exerted on the tibia and radius (Lieberman et al. 2004; Taylor et al. 2004), and it is likely the trabeculae have adapted to these stresses in ways distinct from those of the more commonly studied limb bones. Analyses that have compared two disparate limb elements have highlighted the differences in trabeculae between bones within the same species (Amson et

al. 2017; Reinecke & Angielczyk 2024, In Review), raising the possibility that similar variation is present in other under-sampled elements. As I continue to evaluate additional taxa and develop a more robust understanding of trabecular architecture, sampling multiple bones will be integral in highlighting the range of diversity possible throughout the mammalian skeleton.

This study aims to develop a more robust understanding of trabecular diversity by comparing the proximal regions of five limb bones: the humerus, femur, radius, ulna, and tibia. The Marsupial family Didelphidae was selected as the study group due to the range of body sizes and ecomorphotypes the clade encompasses while generally exhibiting conserved cortical structures to minimize the effect of gross bone morphology on the trabeculae within. I analyzed several commonly measured trabecular characteristics along with primary trabecular orientation, which has been demonstrated to have a significant correlation to general ecological niche (Reinecke & Angielczyk In Review). I hypothesize that opossums will be distinct in their humeral and femoral trabecular structures that are comparable to those observed in other comparably sized mammals found to inhabit similar ecological niches. The distal limb elements are expected to demonstrate statistically significant differences between bones in characteristics such as trabecular strut size and spacing due to the varied loading strains exerted on these bones during locomotion. In comparing the proximal and distal limb elements, I predict the former will exhibit a higher density of larger trabecular struts in more isometric directions due to the greater magnitude of strain originating from a more conserved range of directions.

Methods

Twenty-five specimens representing ten species within the clade Didelphidae were sampled for this study (A full list of specimens and their trabecular characteristics can be found in Supplementary Dataset S4.1.). Six of the sampled species were represented by three specimens

each; of the remaining four species two were represented by two specimens each and two were represented by single specimens. All sampled specimens were adults to eliminate the confounding effects of ontogenetic trabecular changes (Ryan et al. 2006; Tsegai et al. 2018) and due to the limited interspecific variation present in adult individuals compared to juveniles (Reinecke & Angielczyk 2024). Additionally, captive individuals were excluded from this study as the sedentary lifestyle and nutritional deficiencies of zoo specimens have been demonstrated to have a measurable effect on trabecular growth and architecture when compared to wild contemporaries (Chirchir et al. 2022; Zack et al. 2022). Body size estimates were obtained using the scaling equation described in Champione & Evans (2012), which utilizes the midshaft circumference of the humerus and femur to derive a log-transformed body mass.

A cladogram of all sampled didelphid species based on Jansa et al. 2014 was used to provide a phylogenetic framework (Fig. 4.1). Generalized ecological niches were sourced from Nowak (1999) and placed on a ranked ordinal scale from one to four, with one representing an arboreal species found almost exclusively in heavily forested environments, and four representing terrestrial taxa inhabiting grasslands and riverbanks. Species given a value of two primarily inhabit forest environments but have been observed in more open spaces, whereas three represents the opposite.

Figure 4.1
A cladogram of all sampled taxa modified from a time-scaled tree made for Jansa et al. 2014. Branch lengths have been colored based on average logBM for each species. Each species includes a ranked number from 1-4 indicating their ecological niche score. A value of 1 indicates a species that is entirely arboreal, and a value of 4 indicates an entirely terrestrial species. A value of 2 indicates a species that prefers an arboreal lifestyle but will still engage in more terrestrial activities. The inverse applies to species in with a score of 3.

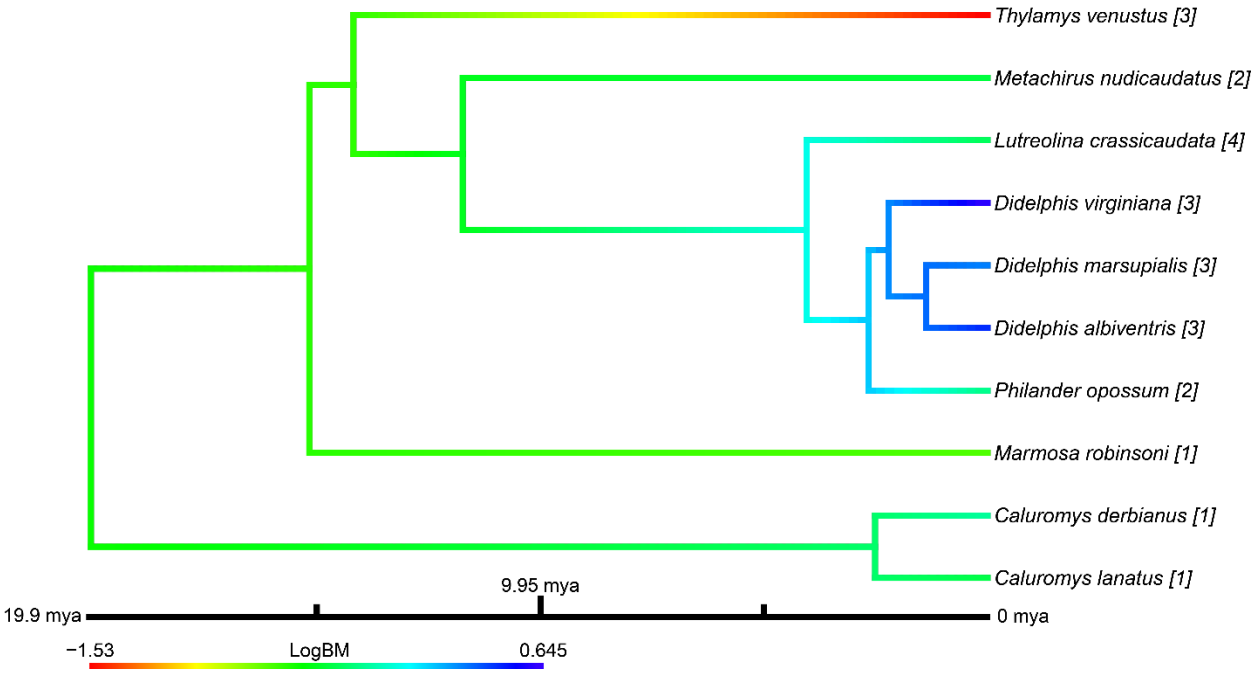

µCT Scanning

Five limb elements were selected for analysis: the humerus, radius, ulna, femur and tibia. All limb elements were scanned with the University of Chicago's PaleoCT GE phoenix phoenix v | tome | x µCT (micro-computed tomography) scanner. A 240 kV micro-focus X-ray tube was used for larger specimens such as *Didelphis virginiana*, whereas smaller species such as *Thylamys venustus* were scanned with a 180 kV micro-focus tube to resolve finer trabecular elements. Scans resolutions for all specimens range from 21.627 to 57.822 µm. Voxel sizes for each scan were determined to be at least 3-4 times smaller than the average trabecular thickness in order to avoid issues of scans warping or omitting trabecular elements (Bouxsein et al. 2010).

Scans were reconstructed using GE phoenix datos | x before being imported into VGStudio Max 3.3 for image stack alignment. Following these steps, the resulting tiff stacks were brought into Dragonfly 2022.2 (Dragonfly 2022) for orientation and analysis. A standard vertical orientation for the bones were utilized in order to minimize the differences in trabecular direction due to overall midshaft angle. This orientation model was sampled from previous work into trabecular diversity (Reinecke & Angielczyk 2024, In Review) with slight modifications to ensure the direction of the articular surfaces more closely reflect their *in vivo* locations. All bones are first pivoted such that the midpoint of the proximal and distal metaphyses align vertically along the Z-axis. Bones were then rotated to orient the articular surfaces in the same directions as they would be held *in vivo*. The humerus was positioned such that the center of the proximal articular surface aligned in the -Y direction, corresponding to the posterior direction. The femoral head was rotated to face the -X direction, corresponding to the medial direction. The radius, ulna, and tibia were rotated to have the radial tuberosity, ulnar trochlear notch, and the tibial tuberosity face the +Y direction corresponding to the anterior direction. These general orientations can be seen in Figure 4.2.

Figure 4.2
Standard orientations for the humerus (A), Femur (B), radius (C), ulna (D), and tibia (E). The 3D model illustrates the view of the bone from the posterior direction and the 2D cross-section corresponds to the orientation displayed in the stereomorphic projections in Figure 2.1. The blue circles represent the spherical region of interest (ROI) sampled from each bone.

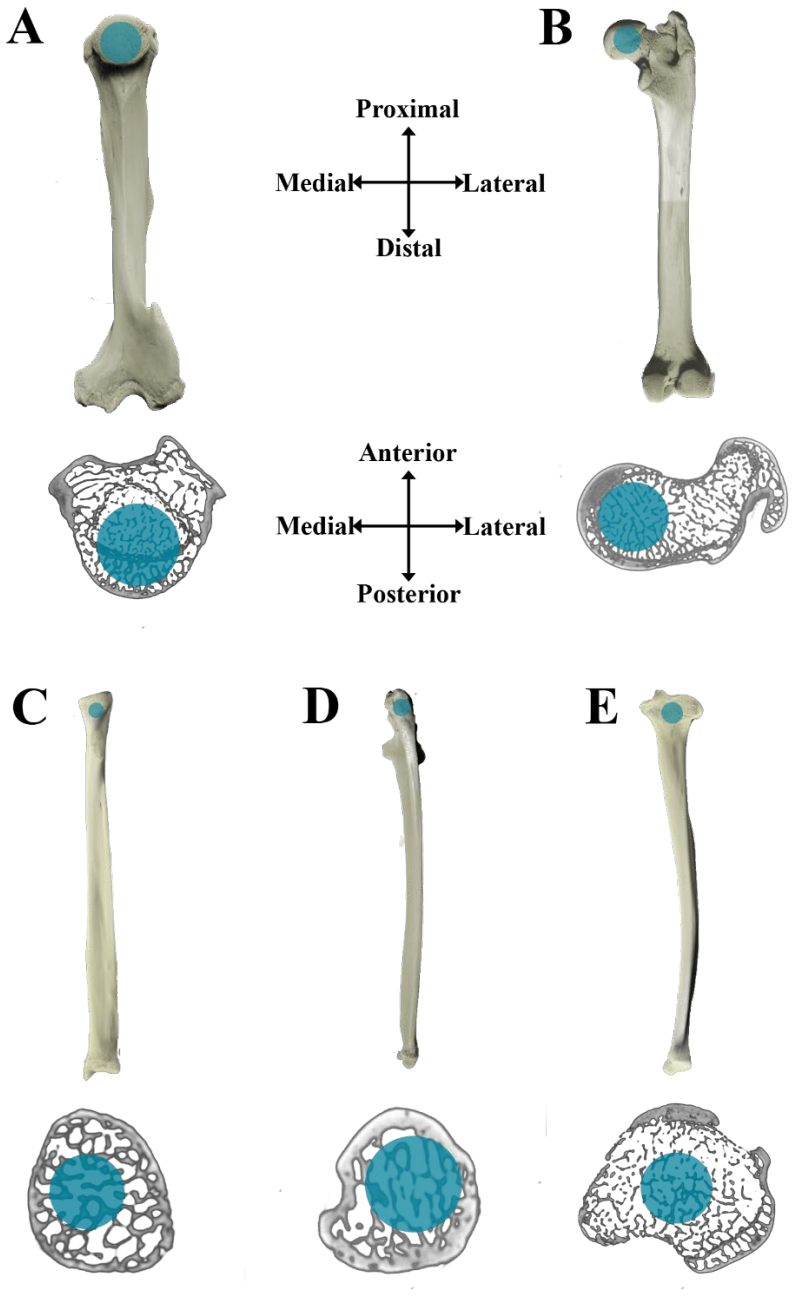

A spherical region of interest (ROI) was selected to minimize edge effects, ensuring a more accurate representation of the trabecular microarchitecture (Kivell 2011). In upper limb elements the middle of this ROI was placed in the center of the articular head. The edges were then expanded to maximize the volume of sampled trabecular bone while excluding all cortical structures. In the radius and tibia, a cropping box was drawn to contact cortical edges of the proximal bone, such that the upper and lower box faces contact the proximal tip and lower portions of the tuberosity respectively. A spherical ROI was then expanded out from the center of this cube, shifted proximally in some individuals in the event that trabecular structures were found to be located exclusively above the tuberosity. For the ulna, the region of space adjacent to the trochlear notch was too small for meaningful analysis of trabecular structures, resulting in the cropping box instead being aligned along the edges of the olecranon process and the lateralmost tip of the coronoid process. Given the concave shape of the olecranon in several opossum species, the spherical ROI would often be shifted laterally from the center of this cube in order to remain within trabecular space. Examples of all ROI locations can be seen in Figure 4.2.

Outsu sorting algorithms (Otsu 1979) within Dragonfly were utilized to segment and binarize the ROI. Outsu segmentation has been demonstrated to be useful for trabecular analysis as it will prioritize preservation of small trabecular struts while preserving the overall bone volume fractions (BV/TV) of a sampled region (Smith & Angielczyk 2020). Bone volume fraction (BV/TV) was calculated for each specimen in Dragonfly by comparing the volume of segmented trabeculae to that of the overall spherical region of interest. The binarized images of trabeculae and non-trabecular spaces were subsequently imported into Fiji (Rasband 1997), where the BoneJ plugin (Doube et al. 2010) was used to refine the scans and compute anisotropy (DA), trabecular thickness (Tb.Th), and trabecular spacing (Tb.Sp). The processed tiff image stacks

were then analyzed in Quant3D (Hoebeke & Trubuil 1999) to determine trabecular number (Tb.N) and principal trabecular eigenvectors. The fabric tensor, reflecting anisotropy within the region of interest, was quantified using the mean intercept length (MIL) method. MIL has been shown to more accurately predict bone mechanical properties compared to other anisotropy metrics (Zysset 2003; Cowin & Doty 2007; Moreno et al. 2014). Finally, the trabecular eigenvectors were converted into angular trend and plunge measurements in R using the workflow described by Amson et al. (2017). Azimuth values were transformed using the formula $\left||X-180|-90\right|$, converting the degrees values to a scale ranging from 0 to 90, with 90 indicating an orientation along the anterior-posterior plane, and 0 indicating an orientation along the medial-lateral plane.

Statistical Testing

Shaprio-Wilk tests found a non-normal distribution for the majority of trabecular characteristics. Therefore nonparametric Kruskal-Wallis tests (Kruskal & Wallis 1952) using the kruskal.test function (R Core Team 2023) and Dunn tests (Dunn 1964) with the dunnTest package (Dinno & Dinno 2017) were utilized to determine if there are significant differences in trabecular characteristics between bones.

Phylogenetic generalized least squares (PGLS) were used to assess the effects of log-transformed body mass and ecological niche on the trabecular characteristics of all sampled bones. Additionally, these analyses address the issue of non-independence among data points caused by shared evolutionary history, providing a more reliable assessment of the relationship between trabecular traits and body size. These tests were run in R using the packages nlme (Pinheiro et al. 2022) and treeplyr (Harmon 2020). Predicted isometric linear regression slopes between log-transformed body mass (logBM) and each trabecular characteristic were also estimated. DA and

BV/TV are percentage-based measurements and exhibit an isometric slope of 0. Tb.Th and Tb.Sp are linear measurements that scale at a rate 1/3 relative to volume, resulting in an expected isometric slope of 1/3. Tb.N is measured as the number of struts per cubic mm of bone, and has a expected isometric slope of -1/3. Comparable isometric slope values have been used in previous work that served as the basis for these values (Mielke et al. 2018; Plasse et al. 2019; Smith et al 2023; Reinecke & Angielczyk 2024, In Review).

Stereomorphic projections on a stereonet were used to illustrate the primary orientations of trabecular features for all sampled specimens on a 2D plane (Amson et al. 2017; Mielke et al. 2018; Reinecke & Angielczyk 2024). These projections measure two values to present an angular measurement: azimuth and plunge. Azimuth values span from 0 to 360 degrees and represent angular measurements**.** Plunge values, ranging from 0° to 90°, indicate the degree of vertical alignment of trabecular struts. A plunge of 0° signifies a completely horizontal orientation, whereas 90° represents a fully vertical alignment. On the stereomorphic projection, points closer to the center of the plot reflect more vertical trabecular orientations, with the outermost ring defining the angular direction for each individual.

As in other works analyzing trabecular orientation, axial definitions were changed to represent anatomical directions (Barak at al. 2011; Mielke et al 2018; Reinecke & Angielczyk 2024). These axes represent the three anatomical planes with respect to the general direction each limb element would face *in vivo*. The X-axis represents the medial-lateral plane, with the medial direction pointing “west” in the -X direction. The Y-axis represents the anterior-posterior plane, with the anterior direction pointing “north” in the Y direction. The Z-axis represents the superior-inferior plane, with superior pointing “up” out of the page in the Z direction. An illustration demonstrating these orientations can be seen in Figure 4.2.

Results

Kruskal-Wallis tests comparing the mean values of the five limb elements found significant differences in all trabecular metrics (Fig. 4.3; Table 4.1). Subsequent Dunn tests (Table 4.2) revealed that the humerus has a significantly lower degree of anisotropy (DA) compared to the radius and ulna, both the radius and tibia exhibit significantly ($p < 0.05$) low bone volume fraction (BV/TV) values, and the tibia possesses significantly fewer trabecular struts relative to the upper limb elements. Dunn tests also indicate generally consistent values for both Tb.Th and Tb.Sp in the majority of sampled bones, with only the radius and tibia exhibiting significant differences with a single element for each respective metric.

Figure 4.3

Violin plots of the trabecular characteristics for all bones sampled across all taxa. Bars represent the 25th, 50th, and 75th quartile.

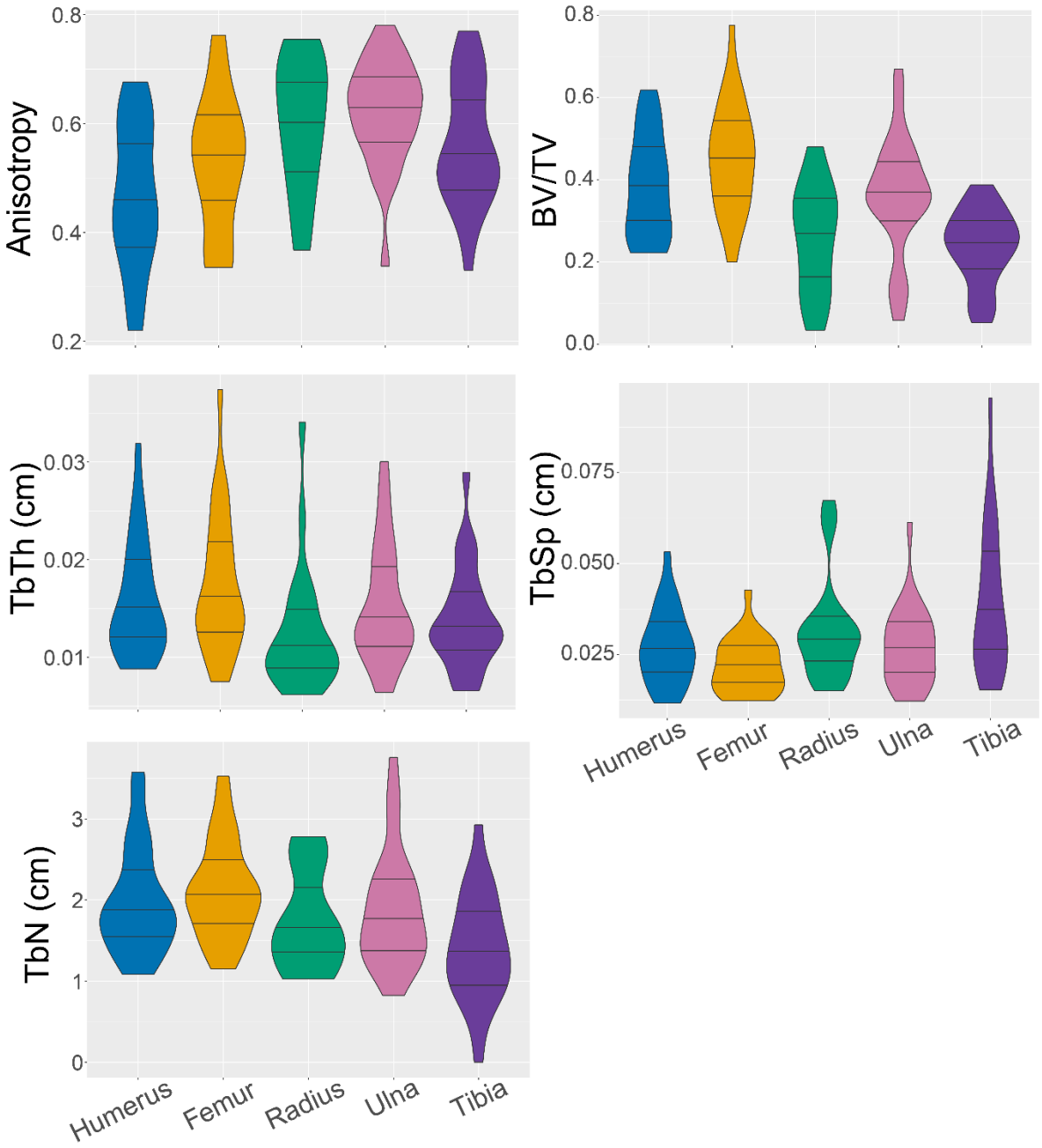

Table 4.1
A table of Kruskal-Wallis test statistics for all trabecular characteristics. Any characteristics with a p value < 0.05 have been bolded.

Trabecular Characteristic	Chi Squared	df	P value
DA	19.60678587	4	**0.000597**
BV/TV	36.08999868	4	**2.77E-07**
Tb.Th	10.85015832	4	**2.83E-02**
Tb.Sp	17.04520809	4	**1.89E-03**
Tb.N	15.40899225	4	**3.92E-03**
Azimuth Transform	34.19569649	4	**6.79E-07**
Plunge	13.88788518	4	**0.007662**

Table 4.2

A table of statistics from the Dunn post-hoc test comparing each bone to one another for all measured trabecular characteristics. Any characteristics with a p value < 0.05 have been bolded.

Trabecular Characteristic	Comparison	Z	P Unadjusted	P Adjusted
DA	Femur - Humerus	1.340437668	0.180103096	0.720412385
	Femur - Radius	-1.896376056	0.057910336	0.347462015
	Humerus - Radius	-3.191361873	0.001416038	**0.012744342**
	Femur - Tibia	-0.859582251	0.390019363	0.780038725
	Humerus - Tibia	-2.200019919	0.027805482	0.194638373
	Radius - Tibia	1.065940706	0.286450446	0.859351339
	Femur - Ulna	-2.642577117	0.008227773	0.065822181
	Humerus - Ulna	-3.983014785	6.80E-05	**0.000680465**
	Radius - Ulna	-0.656595983	0.511440732	0.511440732
	Tibia - Ulna	-1.782994866	0.074587139	0.372935695
BV/TV	Femur - Humerus	1.572372334	0.115864226	0.347592679
	Femur - Radius	4.248247253	2.15E-05	**0.000193905**
	Humerus - Radius	2.72919126	0.006348987	**0.038093921**
	Femur - Tibia	5.219254852	1.80E-07	**1.80E-06**
	Humerus - Tibia	3.646882518	0.000265441	**0.00212353**
	Radius - Tibia	0.794031974	0.427176817	0.854353635
	Femur - Ulna	1.859612206	0.062940411	0.251761645
	Humerus - Ulna	0.287239872	0.773928659	0.773928659
	Radius - Ulna	-2.451691181	0.014218663	0.071093316
	Tibia - Ulna	-3.359642647	0.000780433	**0.005463034**
Tb.Th	Femur - Humerus	0.825539389	0.40906543	1
	Femur - Radius	3.100918419	1.93E-03	**0.019292143**
	Humerus - Radius	2.303371598	0.021257944	0.191321499
	Femur - Tibia	1.859591305	6.29E-02	4.41E-01
	Humerus - Tibia	1.034051915	0.301111894	1
	Radius - Tibia	-1.304382539	0.192103185	1
	Femur - Ulna	1.144691215	0.252337092	1
	Humerus - Ulna	0.319151826	0.749611386	0.749611386
	Radius - Ulna	-1.995041642	0.046038338	0.368306707
	Tibia - Ulna	-0.71490009	0.474670782	0.949341563

Table 4.2 (cont.)

Trabecular Characteristic	Comparison	Z	P Unadjusted	P Adjusted
Tb.Sp	Femur - Humerus	-1.770228793	0.076689035	0.460134207
	Femur - Radius	-2.715652797	6.61E-03	0.059530721
	Humerus - Radius	-1.005449305	0.314680548	0.629361097
	Femur - Tibia	-3.961737997	7.44E-05	**7.44E-04**
	Humerus - Tibia	-2.191509203	0.028414964	0.198904751
	Radius - Tibia	-1.111749729	0.266245772	1
	Femur - Ulna	-1.765973436	0.077400306	0.387001528
	Humerus - Ulna	0.004255358	0.996604726	0.996604726
	Radius - Ulna	1.009560372	0.312705964	0.938117891
	Tibia - Ulna	2.195764561	0.028108799	0.224870396
Tb.N	Femur - Humerus	0.797881059	0.424939516	1
	Femur - Radius	2.080203336	3.75E-02	0.262548205
	Humerus - Radius	1.309377001	0.190406678	0.761626713
	Femur - Tibia	3.655359092	2.57E-04	**2.57E-03**
	Humerus - Tibia	2.857478033	0.004270222	**0.038431997**
	Radius - Tibia	1.451209047	0.146721659	0.733608293
	Femur - Ulna	1.504271757	0.132511408	0.795068449
	Humerus - Ulna	0.706390698	0.479945204	0.959890409
	Radius - Ulna	-0.626938752	0.530699384	0.530699384
	Tibia - Ulna	-2.151087335	0.031469307	0.251754456
Azimuth Transform	Femur - Humerus	-5.417070322	6.06E-08	**6.06E-07**
	Femur - Radius	-2.975237256	0.00292762	**0.020493342**
	Humerus - Radius	2.258149871	0.023936317	0.143617904
	Femur - Tibia	-4.097909443	4.17E-05	**0.000333519**
	Humerus - Tibia	1.31916088	0.187115334	0.935576668
	Radius - Tibia	-0.983719385	0.325253506	0.650507012
	Femur - Ulna	-4.344720188	1.39E-05	**0.000125508**
	Humerus - Ulna	1.072350134	0.283562796	0.850688389
	Radius - Ulna	-1.222161218	0.221646667	0.886586667
	Tibia - Ulna	-0.246810745	0.805054694	0.805054694

Table 4.2 (cont.)

Trabecular Characteristic	Comparison	Z	P Unadjusted	P Adjusted
Plunge	Femur - Humerus	-0.276598249	0.782088609	0.782088609
	Femur - Radius	-2.554733924	0.0106269	0.095642097
	Humerus - Radius	-2.287514629	0.022165803	0.155160618
	Femur - Tibia	-1.561716267	0.118354845	0.710129069
	Humerus - Tibia	-1.285118018	0.198751046	0.99375523
	Radius - Tibia	1.045972671	0.29557365	0.886720951
	Femur - Ulna	0.791496528	0.428654302	0.857308603
	Humerus - Ulna	1.068094777	0.285477762	1
	Radius - Ulna	3.319392216	0.000902136	**0.009021362**
	Tibia - Ulna	2.353212795	0.01861198	0.148895837

PGLS

Phylogenetic ANOVAs indicate that the trabeculae of all five bones are impacted by changes in body mass (see Table 4.3). Tb.Th, Tb.Sp and Tb.N were the most consistently influenced by body mass, with all bones except the radius reaching a statistically significant level of 0.05 with at least two of the characteristics. The radius demonstrated a single significant relationship between logBM and Tb.Th. DA and BV/TV by comparison show little to no influence from body mass, with only the DA of tibial trabecular showing a statistically significant relationship with logBM. Ecological niche, as defined by niche score, had almost no impact on the measured characteristics, with only ulnar DA and tibial Tb.N demonstrating a significant relationship with niche.

Table 4.3

Results of the Phylogenetic Generalized Least Squares (PGLS) analysis, including ANOVA statistics, for the relationship of trabecular characteristics with logBM and ecological niche accounting for phylogenetic non-independence among species. The model was fitted using a maximum likelihood approach, with the phylogenetic tree and branch lengths incorporated to correct for evolutionary relationships. Significant predictors ($p < 0.05$) are highlighted, indicating their contribution to explaining variation in the dependent variable.

Bone	Trabecular Characteristic		Df	Sum Sq	Mean Sq	F value	Pr(>F)
Humerus	DA	logBM	1	8.67E-07	8.67E-07	0.001715	0.968306154
		Niche_Score	1	0.000529	0.000529	1.046514	0.345774215
		logBM:Niche_Score	1	0.0011	0.0011	2.177028	0.190535975
	BV /TV	logBM	1	5.39E-05	5.39E-05	0.132639	0.728202009
		Niche_Score	1	3.54E-05	3.54E-05	0.087233	0.77767937
		logBM:Niche_Score	1	4.12E-06	4.12E-06	0.010131	0.923104993
	Tb. Th	logBM	1	0.000533	0.000533	5.491547	0.057575211
		Niche_Score	1	9.15E-06	9.15E-06	0.094354	0.769095745
		logBM:Niche_Score	1	2.59E-06	2.59E-06	0.026667	0.875642643
	Tb. Sp	logBM	1	0.002076	0.002076	21.78636	**0.003440065**
		Niche_Score	1	1.88E-05	1.88E-05	0.197807	0.67209143
		logBM:Niche_Score	1	2.01E-05	2.01E-05	0.210944	0.662197838
	Tb. N	logBM	1	0.10326	0.10326	77.43887	**0.000119474**
		Niche_Score	1	0.000173	0.000173	0.129532	0.73124701
		logBM:Niche_Score	1	0.000192	0.000192	0.144063	0.717345124
Femur	DA	logBM	1	0.000241	0.000241	0.339885	0.581
		Niche_Score	1	0.001295	0.001295	1.823892	0.225560618
		logBM:Niche_Score	1	0.003562	0.003562	5.014825	0.066403619
	BV /TV	logBM	1	0.000252	0.000252	0.725615	0.426994045
		Niche_Score	1	0.000281	0.000281	0.806816	0.403666054
		logBM:Niche_Score	1	6.92E-06	6.92E-06	0.019896	0.892445164
	Tb. Th	logBM	1	0.000751	0.000751	10.80882	**0.016662042**
		Niche_Score	1	9.66E-07	9.66E-07	0.013902	0.909988373
		logBM:Niche_Score	1	1.6E-05	1.6E-05	0.229612	0.648775963
	Tb. Sp	logBM	1	0.000954	0.000954	15.1801	**0.008019411**
		Niche_Score	1	6.77E-06	6.77E-06	0.107762	0.753859703
		logBM:Niche_Score	1	2.77E-05	2.77E-05	0.441189	0.531230789
	Tb. N	logBM	1	0.071589	0.071589	32.68607	**0.001240728**
		Niche_Score	1	9.32E-08	9.32E-08	4.26E-05	0.995005838
		logBM:Niche_Score	1	0.004891	0.004891	2.233023	0.185709641

Table 4.3 (cont.)

Bone	Trabecular Characteristic		Df	Sum Sq	Mean Sq	F value	Pr(>F)
Radius	DA	logBM	1	0.000112	0.000112	0.24779	0.639752466
		Niche_Rank	1	1.26E-05	1.26E-05	0.027801	0.874111574
		logBM:Niche_Rank	1	0.000929	0.000929	2.055881	0.211072717
	BV /TV	logBM	1	0.001318	0.001318	2.494133	0.175105888
		Niche_Rank	1	0.000336	0.000336	6.36E-01	0.461328316
		logBM:Niche_Rank	1	9.31E-09	9.31E-09	1.76E-05	0.996812447
	Tb. Th	logBM	1	7.67E-04	0.000767	8.407561	**0.033807256**
		Niche_Rank	1	0.000116	0.000116	1.271115	0.310735807
		logBM:Niche_Rank	1	2.11E-06	2.11E-06	0.023104	0.885129237
	Tb. Sp	logBM	1	3.84E-05	3.84E-05	0.049263	0.833130772
		Niche_Score	1	1.73E-05	1.73E-05	0.022221	0.887326866
		logBM:Niche_Score	1	1.94E-05	1.94E-05	0.024942	0.880691619
	Tb. N	logBM	1	2.82E-02	0.028168	4.32E+00	0.092274488
		Niche_Score	1	2.95E-03	0.002952	0.452679	0.530902197
		logBM:Niche_Score	1	0.000307	0.000307	0.047127	0.836720528
Ulna	DA	logBM	1	0.000405	0.000405	4.971032	0.076205122
		Niche_Score	1	0.000795	0.000795	9.765252	**0.026106128**
		logBM:Niche_Score	1	4.31E-06	4.31E-06	0.052868	0.827255946
	BV /TV	logBM	1	0.001364	0.001364	2.841216	0.152686967
		Niche_Score	1	3.79E-05	3.79E-05	0.078874	0.790079657
		logBM:Niche_Score	1	6.5E-05	6.5E-05	0.13534	0.728017999
	Tb. Th	logBM	1	0.000849	0.000849	10.06642	**0.024738148**
		Niche_Score	1	3.13E-05	3.13E-05	0.371271	0.568934592
		logBM:Niche_Score	1	8.83E-06	8.83E-06	0.104665	0.759395318
	Tb. Sp	logBM	1	0.000663	0.000663	7.714128	**0.039020472**
		Niche_Score	1	2.02E-05	2.02E-05	0.235296	0.648130082
		logBM:Niche_Score	1	9.37E-06	9.37E-06	0.109005	0.754664473
	Tb. N	logBM	1	0.074946	0.074946	82.26123	**0.00027249**
		Niche_Score	1	4.35E-04	0.000435	0.476926	0.520560567
		logBM:Niche_Score	1	6.04E-04	0.000604	0.663372	0.452403583

Table 4.3 (cont.)

Bone	Trabecular Characteristic		Df	Sum Sq	Mean Sq	F value	Pr(>F)
Tibia	DA	logBM	1	0.074946	0.074946	82.26123	**0.00027249**
		Niche_Score	1	4.35E-04	0.000435	0.476926	0.520560567
		logBM:Niche_Score	1	6.04E-04	0.000604	0.663372	0.452403583
	BV /TV	logBM	1	4.34E-05	4.34E-05	0.218122	0.660119225
		Niche_Score	1	0.000158	0.000158	0.793041	0.413974437
		logBM:Niche_Score	1	1.90E-05	1.9E-05	0.095556	0.769695941
	Tb. Th	logBM	1	0.000566	0.000566	11.17192	**0.020497616**
		Niche_Score	1	4.50E-05	4.5E-05	0.888745	0.38910316
		logBM:Niche_Score	1	1.40E-05	1.4E-05	0.276811	0.621292394
	Tb. Sp	logBM	1	0.004103	0.004103	10.98857	**0.021126274**
		Niche_Score	1	0.001471	0.001471	3.939908	0.103922455
		logBM:Niche_Score	1	0.000426	0.000426	1.140478	0.334376398
	Tb. N	logBM	1	0.024106	0.024106	1.30E+01	**0.015517039**
		Niche_Score	1	0.021431	0.021431	11.53232	**0.019336377**
		logBM:Niche_Score	1	6.32E-05	6.32E-05	0.034002	0.860948944

Trabecular Architecture with Respect to Body Mass

Regression analysis indicated no relationship between body mass and DA and BV/TV in all five bones (Fig. 4.4; Table 4.4). Tb.Th values in all five bones were found to correlate with body mass, and exhibited negative allometry, indicating the thickness of trabecular struts in these elements increases at a slower rate than overall logBM. For Tb.Sp, only the humerus and femur were found to demonstrate a negatively allometric growth rate, indicating that larger opossums have narrower spacing between trabecular struts in upper limb bones. The humerus, femur and ulna exhibited positive allometric scaling in a decreasing trend for Tb.N with respect to body mass, indicating that while the number of trabecular rods and cones decrease with size, this rate of change is slower than that observed for body mass.

Figure 4.4

Scaling relationships of trabecular characteristics relative to log body mass for all sampled bones. Specific trabecular characteristics are DA (A), BV/TV (B), log Tb.Th (C), log Tb.Sp (D), and log Tb.N (E). The dashed lines represent the isometric slope for each metric. Slopes were included for any characteristics that demonstrated a $R^2 > 0.3$ and a p-value < 0.05. Slope formulas, R^2 and p-values are presented in Table 13.

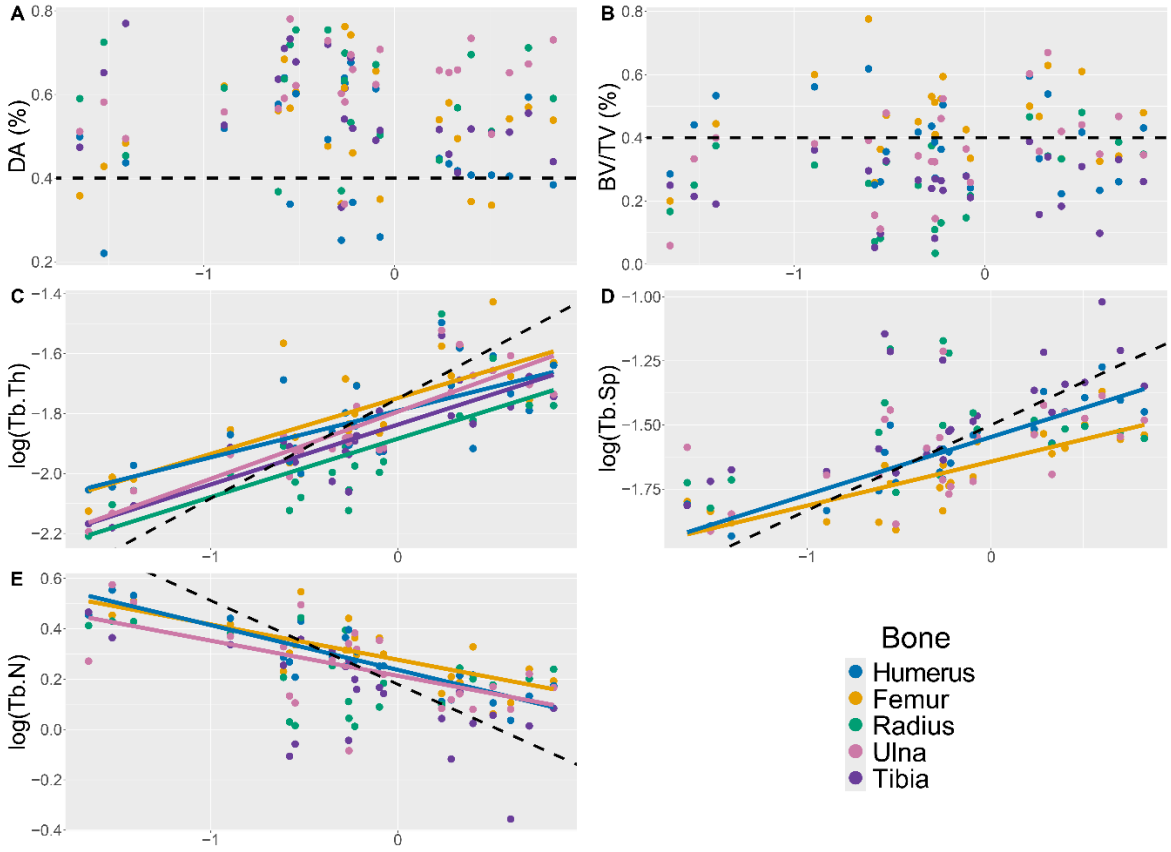

Table 4.4

Table of the regression formulas for the scaling relationships between logBM and trabecular characteristics as seen in Figure 4.4. Trabecular characteristics that have a $R^2 > 0.4$ and $p < 0.05$ have been bolded. Characteristics that exhibit $p < 0.05$, but $R^2 < 0.3$ have been marked with an asterisk.

Trabecular Characteristic	Bone	y	R^2	P
DA	Humerus	0.468	0.000000423	0.998
	Femur	0.007x+0.529	0.00134	0.865
	Radius	-0.002x+0.597	0.0000746	0.97
	Ulna	0.059x+0.635	0.17	0.045
	Tibia	-0.078x+0.545	0.214	0.0229
BV/TV	Humerus	-0.035x+0.377	0.0368	0.37
	Femur	0.034x+0.463	0.0305	0.415
	Radius	0.067x+0.28	0.123	0.12
	Ulna	0.092x+0.384	0.182	0.0375
	Tibia	0.014x+0.241	0.0113	0.621
Tb.Th	Humerus	0.156x-1.791	0.477	**0.000415**
	Femur	0.187x-1.748	0.547	**0.00504**
	Radius	0.195x-1.884	0.551	**0.0177**
	Ulna	0.224x-1.794	0.783	**0.00654**
	Tibia	0.2x-1.837	0.715	**0.00123**
Tb.Sp	Humerus	0.225x-1.547	0.79	**0.00618**
	Femur	0.172x-1.643	0.639	**0.000125**
	Radius	0.098x-1.504	0.143	0.0016*
	Ulna	0.13x-1.569	0.261	0.0014*
	Tibia	0.215x-1.404	0.478	0.0889
Tb.N	Humerus	-0.178x+0.237	0.767	**0.00000749**
	Femur	-0.141x+0.227	0.584	**0.00000248**
	Radius	-0.1x+0.189	0.217	0.0002*
	Ulna	-0.14x+0.213	0.359	**0.00057**
	Tibia	0.603x-0.015	0.0832	0.046*

Trabecular Orientation

Among all sampled bones, the radius exhibited the highest average plunge value at 75.73 degrees, less than 15 degrees from a fully vertical orientation (Fig. 4.5). The olecranon process of the ulna exhibited the most horizontal average orientation at 63.34 degrees. Average azimuth values reflected the orientation of the articular head of three bones as they are located *in vivo*. The trabeculae of the femoral head point medially towards the center of the body, whereas those of the humerus face anteriorly. As the articular disk of the radius braces directly against compressive strain from the superior humerus, the majority of specimens exhibited a vertical trabecular orientation. *Metachirus nudicaudatus* and *Thlamys venustus* were two exceptions, however, with an average radial azimuth pointing in the anterior and medial directions, respectively. The ulnar trabeculae faced anteriorly and were oriented roughly parallel to the triceps tendon that connects to the olecranon. Although the tibial tuberosity points anteriorly, the average trabecular azimuth of the tibia instead faced in the posterior direction.

Figure 4.5
Stereomorphic projection displaying the primary trabecular orientation of all sampled specimens. The size of each datapoint correlates to DA value with larger points indicating a higher DA. Directions for the X and Y planes have been included. The Z axis is oriented perpendicular to the plots, with the positive-Z direction projecting towards the reader.

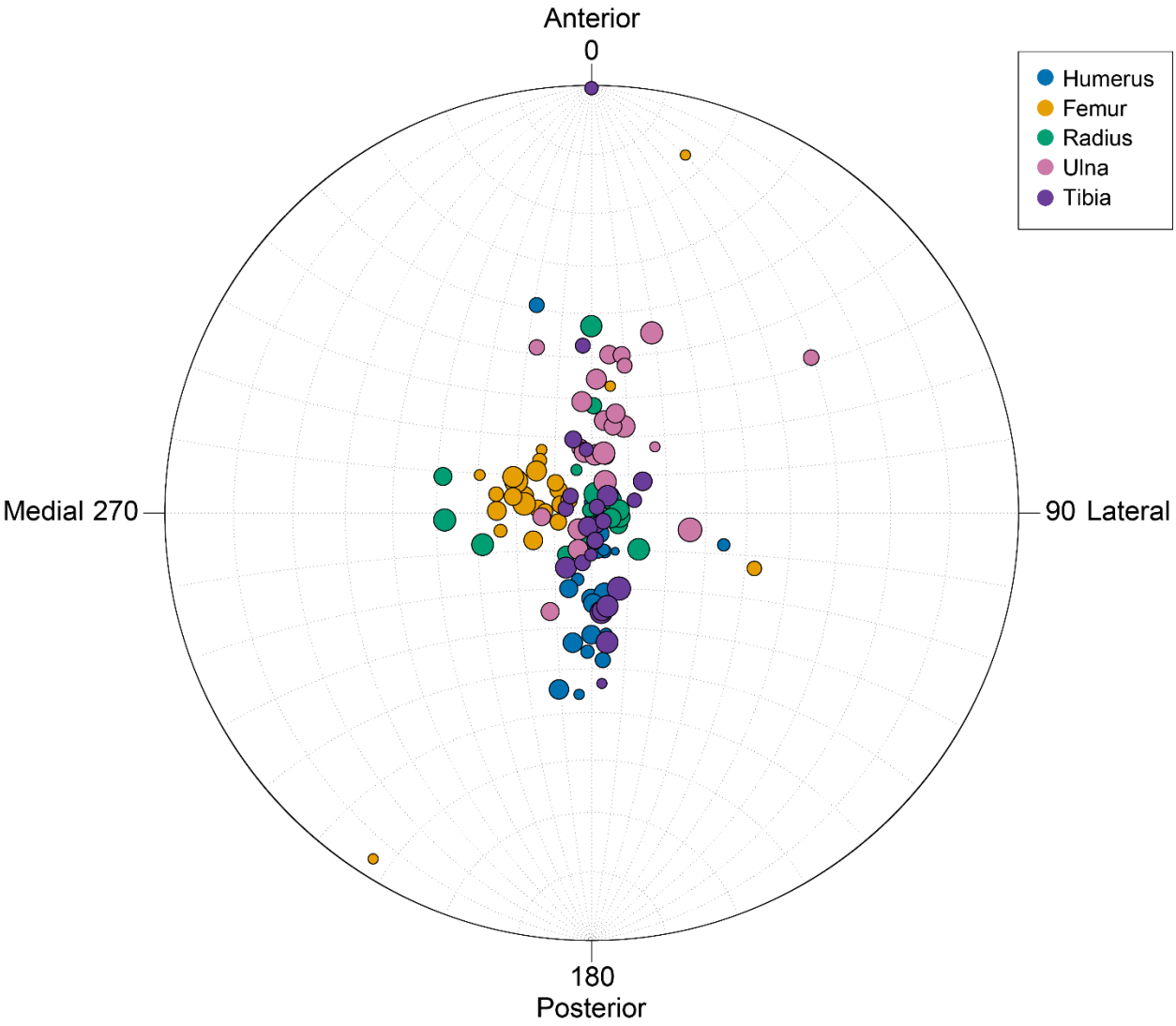

Discussion

In this study, I examined the trabecular bone architecture of the proximal head of long limb elements across a diverse sample of didelphid species, representing a range of body sizes and

ecological adaptations. Building on prior studies that compared trabecular structures across various bones (Ryan & Walker 2010; Ryan & Shaw 2013; Amson et al. 2017; Reinecke & Angielczyk 2024), I aim to identify potential disparities in these elements and the factors shaping their architecture. These findings reveal minimal statistically significant differences ($p < 0.05$) in most trabecular characteristics among the five bones studied, with the most notable distinctions observed in proximal versus distal limb elements. This contrasts with analyses of other mammalian groups, where significant variations were identified between the humerus and femur. These results suggest that trabecular structures in opossums are more uniform compared to other sampled mammalian clades, and that architectural differences across major clades may be more pronounced than previously thought. Additionally, these findings suggest that future analysis of trabecular structures in multiple elements will have to consider the types and magnitude of stress experienced by the elements and its disparate impacts on bone development.

Femur and Humerus

Statistically significant differences in the trabeculae of the humeral and femoral articular head have been observed in primates (Ryna & Walker 2010; Doershuk et al. 2019) and other mammal species (Reinecke & Angielczyk 2024, In Review). Specifically, the femur is characterized as possessing thicker, more densely packed and uniform trabecular struts than the humerus. While the humerus, and by extension the forelimb, endures a higher magnitude of strain in quadrupedal species compared to the hindlimb (Rubin & Lanyon 1982; Biewener 1990), the articular head of the humerus is located directly superior to the midshaft. This placement ensures that the midshaft of the bone can act to brace against this strain. The femoral head is placed medially to midshaft, ensuring that the articular head and anatomical neck endure the brunt of a marginally weaker

strain. This lack of overall support results in the larger trabecular struts compacted together to protect against injury.

In contrast, analysis of family Didelphidae found no significant difference in the trabecular architecture of these bones. Given the assumption that trabecular architecture is primarily driven by behavior, it can initially be hypothesized that the generalist nature of opossum species is what drives this lack of diversity in trabeculae. Larger opossum species are found in a wide range of environments and engage in a myriad of behaviors as they navigate through grasslands, forests, urban centers, and other locations. Although smaller opossum species inhabit a more specialized arboreal niche, many species utilize a prehensile tail that lessens the strain exerted on the appendages compared to species relying entirely on their limbs to brace and grip branches during climbing (O'Connell 1983; Nowak 1999). Whether arboreal or generalist, the opossum limb morphology is associated with a less ecomorphologically specialized mammalian structure, so much so that the clade is often considered to be a "living fossil", comparable to a more ancestral therian state (Jenkins 1984; Krause & Krause 2006; Bishop & Pierce 2024). This explanation, however, is complicated by comparisons with other generalist mammals, such as raccoons (*Procyon lotor*), which exhibit significant differences in trabecular architecture between the femur and humerus despite sharing a similar ecological niche and limb morphology (Reinecke & Angielczyk 2024). Raccoons, like opossums, are highly adaptable and engage in diverse behaviors, including climbing, foraging, and swimming, yet their trabecular bone structure shows clear adaptations to the distinct loading patterns of their forelimbs and hindlimbs. This may be due in part to the limited home range of opossum species. Analysis of *Didelphis virginiana* has shown individuals of the species to inhabit a home range of less than 1.5 square miles (Gillette 1980), indicating a limited ability for an individual to move through and be

influenced by disparate ecological regions. While I was unable to identify comparable home range studies performed on other opossum species, it is reasonable to assume that smaller species are likely to inhabit an even smaller range. It could be argued that the constraints of marsupial limbs during early development related to the need for climbing and grasping behaviors might limit the variance of trabecular structures compared to placentals, even considering adult opossums and raccoons engage in comparable behaviors. However, the ability for trabeculae to rapidly change their structure in a matter of weeks means that this ontogenetic limitation may be lost when an individual enters adulthood and engages in a wider range of adult behaviors. Additionally, wombat specimens sampled by Reinecke & Angielczyk (In Review) indicate at least one other marsupial species exhibits significant differences between femoral and humeral trabeculae, more in line with those observed in placentals. Further analysis of a broader sample of marsupial taxa and their changes across ontogeny will be necessary to determine if this trabecular homogeneity is more prevalent within the clade or a unique feature of didelphids.

Distal Limb Elements

Analysis revealed almost no statistically significant differences in the trabecular architecture among the lower limb elements, despite their varied morphologies and functional roles within the limbs. Both the radius and tibia function as the primary load bearers in the zeugopodium, resulting in high magnitudes of bending and compressive strain (Taylor 2004). In contrast, the ulnar olecranon process does not serve as a weight bearing structure, but rather as the insertion site for the tendons of the triceps brachii. As an animal extends the elbow joint during the walk cycle or grasping behaviors, the olecranon receives the brunt of this proximally directed tension.

The lack of significant differences in trabecular architecture among the distal limb elements could, in part, be attributed to the fact that the bending strain seen in the radius and tibia is

primarily exerted on the midshaft of the bones, rather than the articular regions where trabecular bone is predominantly located (Burr et al. 1996; Ruff 2000; Lieberman et al. 2004). Trabeculae typically coalesce in the distal and proximal ends of bones, with the central midshaft comprised primarily of thick cortical bone for support. These results suggest that the compressive strain focused on the proximal end of these bones is insufficiently varied among elements to result in distinct differences between trabecular regions. BV/TV differences between the ulna and tibia are the one exception, with the former exhibiting a significantly higher bone volume fraction. Previous work has highlighted that the yield strength of trabeculae is 30% lower for tensile than compressive strength **(**Keaveny et al. 1994), suggesting a higher density of trabeculae is needed to support the higher tensile strain experienced by the olecranon process. The overall homogeneity in trabecular structures also may be attributed to the small size of these animals, where spatial constraints and a standardized Tb.Th with respect to body size limit the extent to which trabecular architecture can vary. At such a scale, it would appear there is minimal space for the addition of more trabecular struts or intertrabecular space, and variation instead comes from the direction of primary strain to which the trabeculae orient themselves.

It is possible that the distal portions of these elements contain more varied trabecular architectures given the complex variation of stresses exerted at the carpus and tarsus joints. Although future research into these structures may highlight differences between elements, the small size of these elements makes analysis difficult in small mammal species. Many xCT scans of small mammals available in public archives consist of full-body scans at resolutions that are too low for trabecular analysis, so future limb-focused scans are needed to facilitate additional research.

Proximal versus Distal

Comparisons between proximal and distal limb elements revealed that the BV/TV values of the femur and humerus were significantly higher than those of both the radius and tibia, indicating greater trabecular bone density in the proximal regions of the upper limb bones. The primarily compressive strain exerted on the humerus and femur (Taylor et al. 1996; Iijima et al. 2024) appears to be more centralized at the proximal end of the bone, resulting in a greater bone volume fraction within the articular head. For the distal limb bones, differences appear to be driven by distinct trabecular microstructural characteristics: thinner trabeculae (Tb.Th) in the radius compared to the femur, and fewer, more widely spaced trabeculae (Tb.N and Tb.Sp) in the tibia compared to the femur and humerus. However, no significant differences were found between the tibia and radius for any trabecular metrics, suggesting that while both bones exhibit lower BV/TV compared to the femur and humerus, the underlying mechanisms influencing further trabecular development may differ and warrant further investigation.

Trabecular Orientation

The average trabecular orientation of each limb element appears to reflect both the range of behaviors in which each bone participates, and the types of strain experienced by the proximal region. The radius and tibia endure compressive strain from both proximal limb elements channeling the body's weight down onto the articular head and ground reaction forces pressing upwards against the joint surface. As a result, both the radius and tibia exhibit the most vertical trabeculae of the sampled elements. Of the two, the tibial trabeculae are slightly more posteriorly facing as the acute angle of the knee joint orients the femoral condyles more posterior to the center of the tibia. Although no study has been performed to measure the trabecular orientation of the tibia in humans, I predict that these structures would be more vertical than are seen in the sampled opossum species as the human leg is a more columnar structure that directs its

compressive strain more vertically. For the radius, it is likely the trabeculae of the distal portion of the bone, having to endure more disparate strain directions caused by the flexibility of the wrist, will average towards a more horizontal and anisotropic trabecular orientation. The humerus and femur, the two bones with the least vertical trabecular orientations, are subjected to far more multidirectional forces due to the bones' increased ranges of motion, shear forces from muscle attachments, and compressive forces from body weight that are spread across a wider volume of bone. With all of these loading directions averaged together, the trabeculae in both bones orient themselves primarily in the direction of the socket connecting the articular surface to the midbody. For the femur, the trabeculae point medially to meet with the acetabulum. In the humerus, trabeculae are faced posteriorly and more horizontal given the angled nature of the midshaft in opossums and other quadrupedal mammals of similar size.

Effects of Body Size

In measuring the effect body size has on trabecular architecture, the humerus and femur exhibit trends comparable to those observed in other mammalian taxa of a similar size (Doube et al. 2011; Reinecke & Angielczyk In Review). Specifically, as body mass increases, trabecular thickness and intertrabecular distance decrease while the overall number of trabeculae increase. Lower limb elements, conversely, seem far less impacted by body mass, with only Tb.Th being significantly impacted by changes in weight across all five bones. This difference can potentially be attributed to the distinct mechanical environments of the upper and lower limbs. Lower limb bones endure higher magnitudes of stress due to their weight-bearing role, yet they often exhibit thinner cortical structures compared to upper limb bones. As a result, trabecular thickness of the lower limb increases at a faster rate than the femur and humerus while both Tb.Sp and Tb.N follow an isometric growth rate in all but the ulna. Despite the increased growth rate of

trabecular thickness in lower limb elements, without spacing or number to act as a "counterbalance" BV/TV remains constant in all skeletal elements. This suggests that in lower limb bones, more factors that are yet unknown may be at play leading to this consistency in trabecular density. For the humerus and femur, increasingly large trabecular struts are offset by wider inter-trabecular space and a decrease in trabecular number, though which of these two has a stronger impact is unclear. Additionally, these results highlight that differences in the relationship between body mass and trabeculae are not just present between higher order clades of vertebrae (Mammalia, Aves, and non-avian Reptilia), but also within these clades as well. Given that this study has identified several ways opossum trabeculae differ from those of other mammals, further analysis of lower limb bones across more mammalian taxa will be necessary to determine whether these trends are consistent in other groups or unique to Didelphidae.

The Impact of Ecological Niche

Trabecular bone architecture is widely understood to be primarily driven by mechanical loading and behavioral patterns, as it dynamically adapts to the forces exerted upon it during an organism's lifetime (Ruff et al. 2006; Fajardo et al. 2013). Given this relationship, I would expect to observe distinct differences in trabecular morphology across species or populations occupying different ecological niches, reflecting variations in niche-specific behavior. In theory, the relative uniformity in cortical bone morphology within Didelphidae should make them a good test case to determine the degree to which trabeculae can respond to ecological and behavioral influences. Nevertheless, the results of this study only identified niche to have a significant impact on ulnar DA and tibial Tb.N. These findings are in line with those of other works measuring the effect of ecological niche on trabeculae, which found scattered but

generally minimal relationships between an organism's environment and their trabecular architecture (Smith et al. 2023; Reinecke & Angielczyk In Review).

The findings of this study do not necessarily imply that ecomorphology does not play any role in determining trabecular structure, but rather that measurable differences are probably only apparent in more morphologically and ecologically specialized taxa whose cortical structures have gone through significant modifications. Analysis of earthworm mice found trabecular differences to be more striking among more ecologically specialized taxa (Smith et al. 2023), and it is likely that the possum species sampled for this study lack sufficient morphological distinction to result in comparable levels of variation. Part of this observed homogeneity may also be due to the problematic and simplistic ways in which I define the ecology of a species. I recognize that defining ecology often involves categorizing species into discrete niches or functional groups, such as 'arboreal,' 'terrestrial,' or 'generalist.' However, such classifications can oversimplify the complex and dynamic nature of ecological behavior and habitat use, especially in less specialized species (Wisniewski et al. 2023). The majority of specimens sampled for this study have been seen to inhabit several different kinds of ecosystems, and it is likely that range has increased the diversity of trabecular architecture within each species. Ideally, future research would seek to identify the specific home ranges of each individual, and create ranked categories based on the frequency they inhabit a specific ecological and environmental regime. Given the high cost and time invested needed to tag, track, and collect wild specimens, I propose a more viable alternative that could involve targeting species with a wide range with detailed sampling of distinct populations from different ecoregions. An example could be a study measuring the trabecular differences in coyote remains collected from temperate forests on the eastern coast, the great plains, western deserts, and urban environments across North America. Although Iare

only beginning to understand the degree to which trabecular architecture may capture an ecological or environmental signal, at present it seems any additional insight could already be determined through considerations of gross cortical morphology.

Conclusion

This study investigates trabecular bone architecture in the proximal heads of long limb elements across a diverse sample of didelphid species. Trabecular characteristics in the humerus and femur exhibited a homogeneity not previously reported in other mammal taxa. The distal limb elements were similarly uniform in their trabecular architectures but showed some differences with proximal elements. This variation appears to be driven by differences in the types of strain each bone endures. Proximal limb elements create dense matrices of cancellous bone to resist compressional strain at the articular head, whereas the bending strain exerted on the midshaft of lower limb bones requires less trabeculae to be present near their articular regions. Trabeculae typically orient towards the direction of joints, or tendons in the case of the ulnar olecranon, while still retaining a relatively vertical direction.

The unique trabecular makeup of Didelphidae compared to other quadrupedal species highlights the diversity in cancellous structures within mammals and establishes that there are likely more factors at play influencing their development than the primary direction of loading. Future analysis of trabeculae within other clades will need to both sample a broader range of skeletal elements and consider the complex interplay of loading regimes. Additionally, developing a more robust system for defining ecological spaces will be necessary to identify the possible relationship between niche and trabecular growth beyond those seen in more specialized species.

Chapter 5: Conclusions and Future Research Directions

The narrative surrounding trabecular bone and its impact on the skeleton has long been a relatively basic one, dating back to 1892 when Julius Wolff first described how struts within long limb bones would orient parallel to the direction of stress. This simplistic view of trabecular bone has long endured within the field of osteology, even as new technologies and analysis began to quantify and analyze these structures in more detail. My dissertation work, in looking to expand our understanding of trabecular architecture and the factors driving its development and evolution, has highlighted the complexity of both of these topics.

Chapter two addressed the ontogenetic development of trabeculae within raccoons and found varied growth rates and trabecular characteristics between individual bones. Although the introduction of novel adult behaviors as an individual ages impacts trabecular bone, other currently unrecognized factors occurring during puberty influence these struts as well. Additionally, by adulthood the humerus and femur exhibit distinct trabecular structures that can only partly be explained by the forelimb dominated nature of raccoons and other quadrupedal mammals. Chapter three sought to identify how variation in behaviors and loading regimes across phylogenetic, ecological and postural groups alter bony architecture. Although differences were found between higher clades, likely driven by variations in posture, metabolic rate and cortical morphologies, no significant differences were observed between postural and ecological groups. Distinctions along ecological niche have been observed in more restricted clades, suggesting that even slight alterations to the gross morphology of cortical bone can have a considerable impact on trabeculae, but that levels of disparity observed across higher clades may overwhelm our ability to recover a consistent signal at that level. Chapter four sought to determine the variation in trabeculae among upper and lower long limb elements in opossums.

Differences were found between upper and lower limb bones, in which the former's increased range of motion, larger size, and lessened magnitude of stress lead to thicker, more densely packed struts that are less uniformly oriented. However, the heterogeneity between upper limb bones that had been ubiquitous among other mammal groups, including those of comparable size and lifestyle to Didelphidae, was not observed in opossums. This trabecular homogeneity was not observed in other marsupial species sampled in chapter three, suggesting other factors drive the unique bony architecture found in opossums.

Although this dissertation serves as a foundational piece of work in understanding the broad diversity of trabeculae within long limb elements across amniotes, there are still a number of unanswered questions warranting further research. Statistically significant distinctions were not observed between the mean values of trabecular characteristics of ecological and postural categories, but my results did identify a large amount of variance within these groups, as seen in the data of chapters three and four. This high intragroup variation persists despite the relatively low intraspecific variation observed within individual species, further suggesting that behavioral and ecological classifications do not capture the functional and mechanical diversity of trabecular bone. One possible explanation for this variation is that differences in behavior may account for trabecular structural diversity in some, but not all, sampled groups. The limb bone trabeculae of specialized cursorial taxa tend to exhibit more conserved patterns, likely due to the biomechanical constraints imposed by their high-speed, parasagittal limb movements. In contrast, generalist species or those occupying a broader ecological niche may display greater variability in trabecular organization, reflecting the wider range of mechanical demands they encounter.

This discrepancy highlights the need to re-examine how ecological and functional groups are defined in comparative skeletal studies. Traditional categorical classifications (e.g., "arboreal," "fossorial," or "terrestrial") likely oversimplify the continuum of locomotor behaviors and habitat use seen in nature. Many species engage in multiple locomotor modes or occupy home ranges with varied terrain, leading to trabecular bone adaptations that do not fit neatly into rigid categories. Therefore, future research should shift toward a more nuanced analytical framework that considers the spectrum of behaviors a single species may employ, as well as the range of mechanical loads experienced across different microhabitats. By incorporating continuous variables we may better explain the observed variation in trabecular architecture.

Looking beyond the activity and home ranges of amniotes, this dissertation research also sought to isolate trabecular features from other non-trabecular elements. In reality, the parts of the skeletal system are not removed from one another, and the shape and size of cortical elements can both impact the stresses driving trabecular growth as well as limit the space trabecular struts are able to inhabit. The impact of this issue can likely be observed in the differing trabecular architectures seen between mammal fore and hindlimbs that is not present in reptiles, which have more homogeneous gross morphologies. Additionally, cortical bone itself serves to protect against loading stress and variations in its thickness can diminish or increase the need for trabeculae. The trabecular thickness of all sampled species scaled at a lower rate than body mass, suggesting that animals of extremely large or small size may exhibit very novel ratios of trabecular and cortical thickness as compared to those in this dataset. Hints of this were observed in squamata, where several species featured trabeculae that would have been comparable in thickness to the cortical bone itself, had the former not been nearly absent from the proximal regions of limb bones. Beyond these extremes, a better understanding of the relationships

between cortical and trabecular thickness may help to present a more nuanced and cohesive lens into the broader ways bone reacts to stress and strain. To that end, new methodology utilizing finite element analysis and stress heatmapping could create clear visualizations that illustrate these concepts.

Identifying these issues and directions for future work could not have been possible without the data collected in this dissertation, and it is my hope that the methods and results presented here serve as inspiration for those looking to "unravel" the complex web that is trabecular bone. The bone orientation methodology in particular should provide researchers the means to compare diverse taxa and focus on trabecular orientations that appear more diagnostic than traditional trabecular characteristics.

Appendix

Figure A2.1A
Bones are isolated and oriented such that the midpoint of the proximal and distal metaphysis are aligned along the Z-axis. Once the bone has been made vertical, the widest points on either end of the articular head are aligned such that the resulting line rests on the Y-axis, and the articular head faced the -X direction.

Figure A2.1B
Once the bone has been oriented, a cubic clipping box is drawn around the articular head to crop it from the rest of the bone.

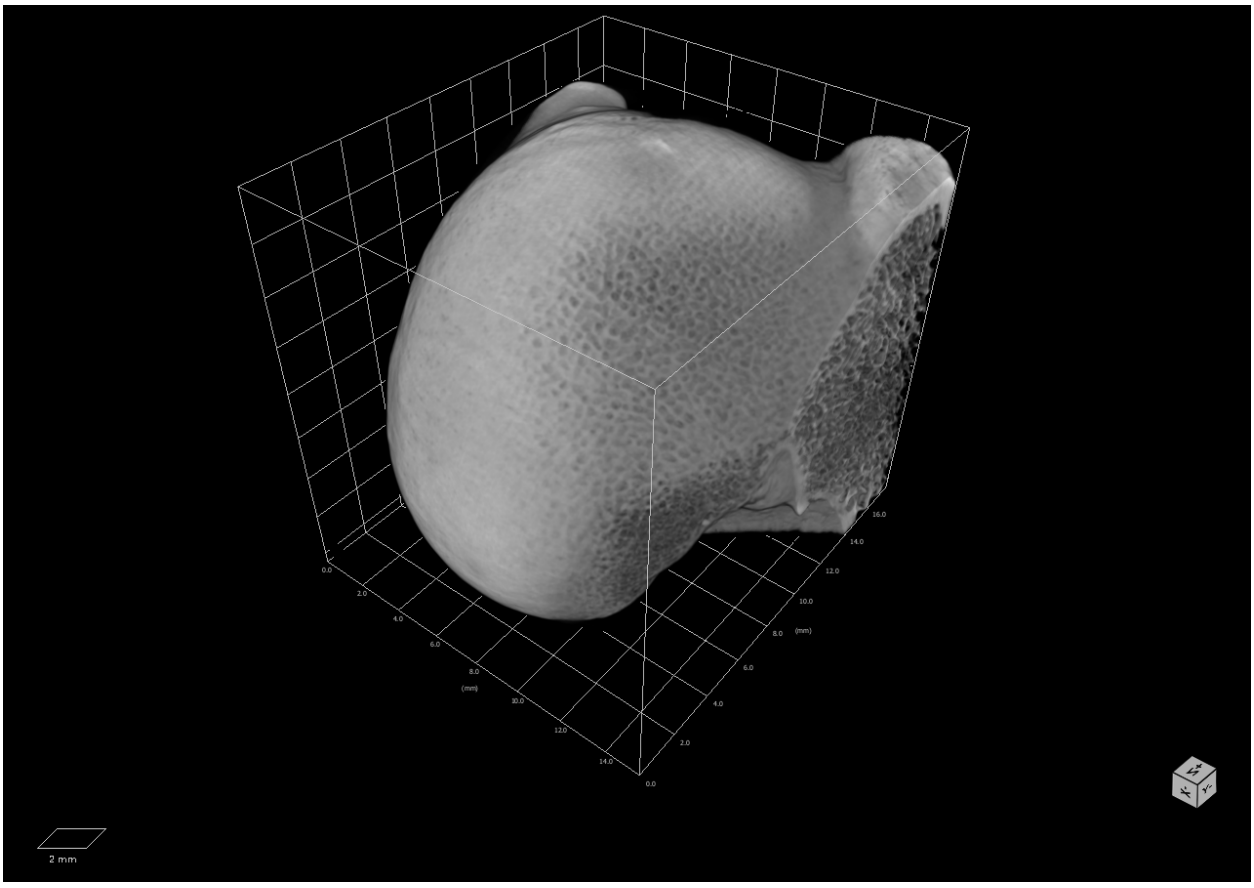

Figure A2.1C
From this isolated articular head, Dragonfly's "Sphere" shapes tool can be used to place a sphere in the center of the articular surface. The sphere is then expanded or contracted to maximize the amount of sampled trabecular bone with excising any cortical elements.

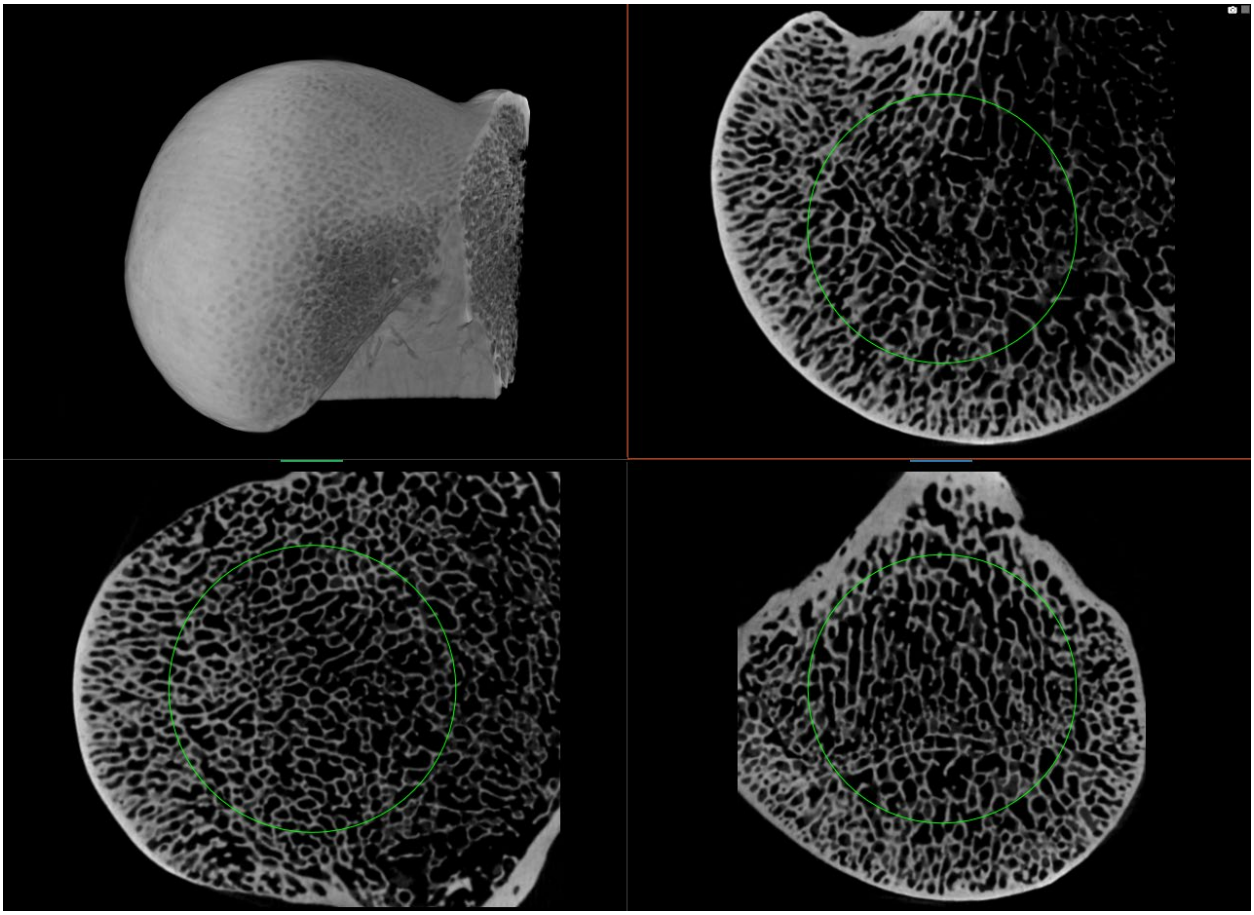

Figure A2.1D
From Dragonfly's "Segment" tab, the otsu sorting algorithm is used to isolate and select the trabecular bone from the surrounding space. This trabecular ROI is also inverted to select the non-trabecular space

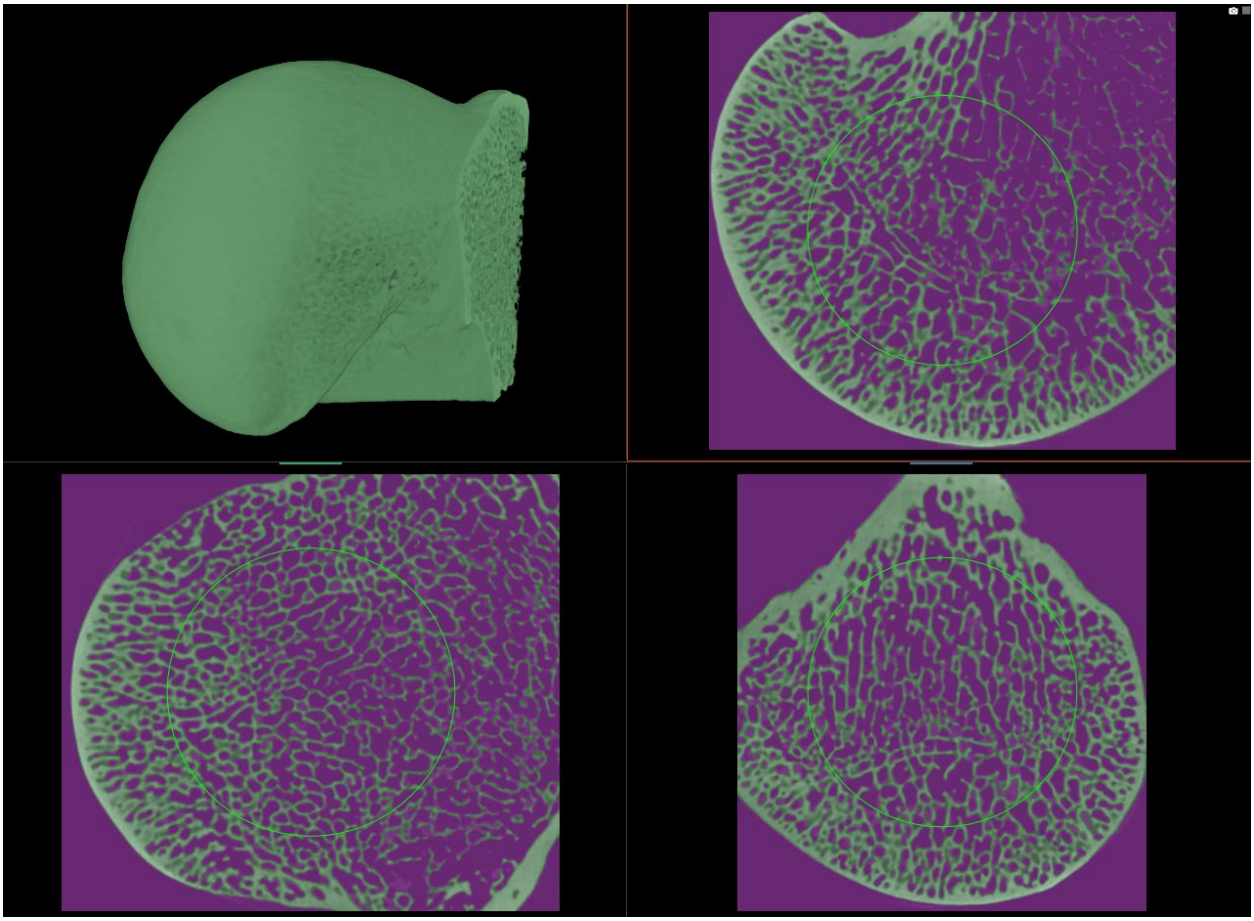

Figure A2.1E

A specific section of both the trabecular and non-trabecular ROI is selected using the sphere tool, before it is binarized and exported for analysis in other programs. The volume of both of these cropped ROI is also recorded to determine BV, TV, and BV/TV

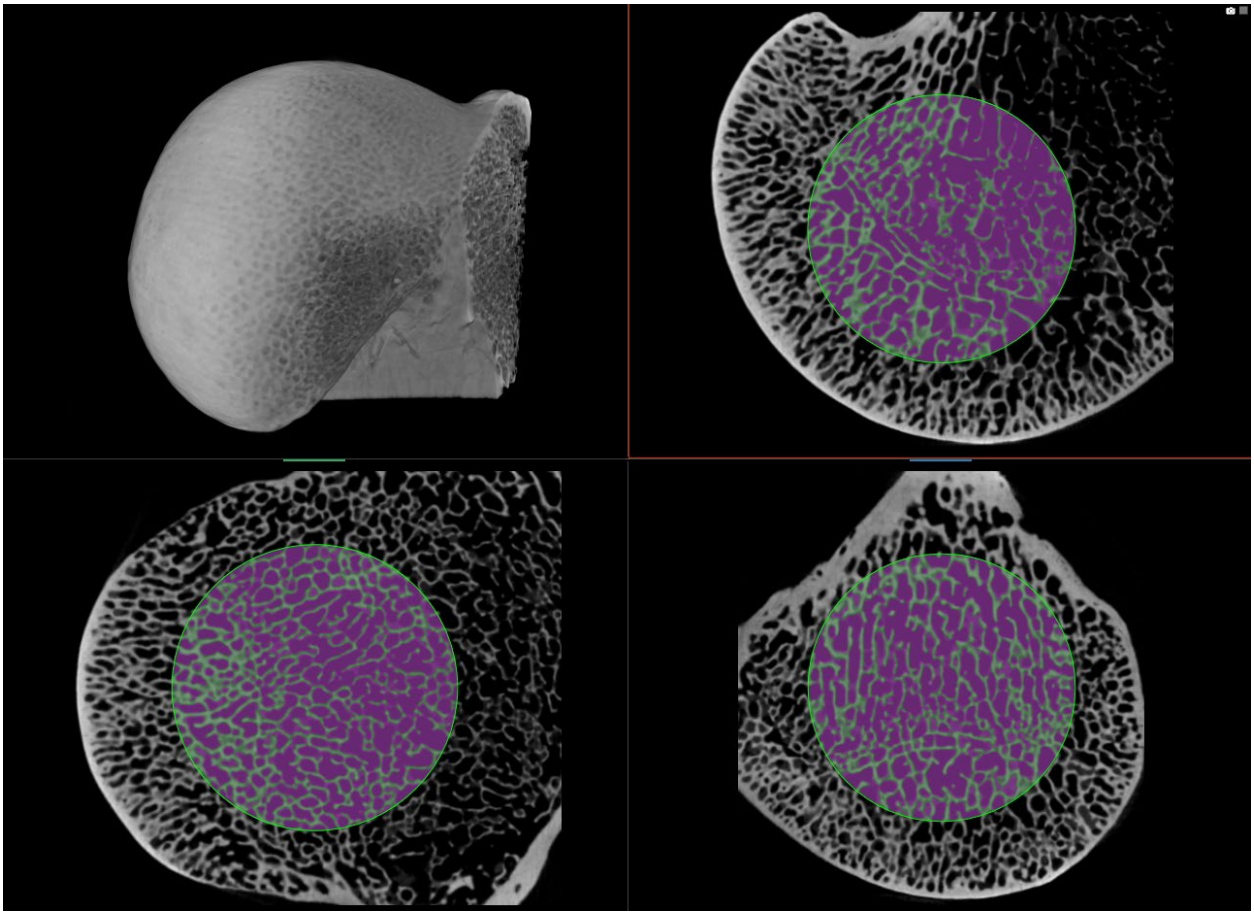

Table A2.2
A table of the Dunn post-hoc results tests performed and illustrated in Table 2.3

Bone	Trabecular Characteris-tic	labels for each pairwise comparison	Z test statis-tic values	unadjusted p-values	adjusted p-val-ues
Hu-merus	DA	2 Months - 4-12 Months	-3.37648	7.34E-04	5.14E-03
		2 Months - 14-24 Months	-3.90511	9.42E-05	8.48E-04
		2 Months - 26-38 Months	-3.56269	3.67E-04	2.94E-03
		2 Months - 46+ Months	-5.08878	3.60E-07	3.60E-06
		4-12 Months - 14-24 Months	-0.59351	5.53E-01	1.00E+00
		4-12 Months - 26-38 Months	-0.59352	5.53E-01	1.00E+00
		4-12 Months - 46+ Months	-1.43149	1.52E-01	9.14E-01
		14-24 Months - 26-38 Months	-0.05609	9.55E-01	9.55E-01
		14-24 Months - 46+ Months	-0.7667	4.43E-01	1.00E+00
		26-38 Months - 46+ Months	-0.62604	5.31E-01	1.00E+00
	BV/TV	2 Months - 4-12 Months	-4.47604	7.60E-06	7.60E-05
		2 Months - 14-24 Months	-2.67456	7.48E-03	5.24E-02
		2 Months - 26-38 Months	-1.03589	3.00E-01	6.01E-01
		2 Months - 46+ Months	-1.13351	2.57E-01	7.71E-01
		4-12 Months - 14-24 Months	1.622078	1.05E-01	5.24E-01
		4-12 Months - 26-38 Months	2.788213	5.30E-03	4.24E-02
		4-12 Months - 46+ Months	3.467578	5.25E-04	4.73E-03
		14-24 Months - 26-38 Months	1.297361	1.95E-01	7.78E-01
		14-24 Months - 46+ Months	1.66262	9.64E-02	5.78E-01
		26-38 Months - 46+ Months	0.105946	9.16E-01	9.16E-01
	Tb.Th	2 Months - 4-12 Months	-4.2491	2.15E-05	2.15E-04
		2 Months - 14-24 Months	-3.99414	6.49E-05	5.84E-04
		2 Months - 26-38 Months	-3.16326	1.56E-03	1.09E-02
		2 Months - 46+ Months	-3.8965	9.76E-05	7.81E-04
		4-12 Months - 14-24 Months	0.138961	8.89E-01	1.00E+00
		4-12 Months - 26-38 Months	0.533164	5.94E-01	1.00E+00
		4-12 Months - 46+ Months	0.595534	5.51E-01	1.00E+00
		14-24 Months - 26-38 Months	0.533164	5.94E-01	1.00E+00
		14-24 Months - 46+ Months	0.432884	6.65E-01	1.00E+00

		26-38 Months - 46+ Months	-0.03853	9.69E-01	9.69E-01

Table A2.2 (cont.)

Bone	Trabecular Characteristic	labels for each pairwise comparison	Z test statistic values	unadjusted p-values	adjusted p-values
Humerus	Tb.Sp	2 Months - 4-12 Months	-0.0927	9.26E-01	9.26E-01
		2 Months - 14-24 Months	-1.93714	5.27E-02	2.64E-01
		2 Months - 26-38 Months	-3.00671	2.64E-03	2.11E-02
		2 Months - 46+ Months	-4.95611	7.19E-07	7.19E-06
		4-12 Months - 14-24 Months	-1.77792	7.54E-02	3.02E-01
		4-12 Months - 26-38 Months	-2.83683	4.56E-03	3.19E-02
		4-12 Months - 46+ Months	-4.64356	3.42E-06	3.08E-05
		14-24 Months - 26-38 Months	-1.20689	2.27E-01	6.82E-01
		14-24 Months - 46+ Months	-2.64253	8.23E-03	4.94E-02
		26-38 Months - 46+ Months	-1.07872	2.81E-01	5.61E-01
	Tb.N	2 Months - 4-12 Months	-2.03612	4.17E-02	2.50E-01
		2 Months - 14-24 Months	-0.32647	7.44E-01	7.44E-01
		2 Months - 26-38 Months	1.312418	1.89E-01	5.68E-01
		2 Months - 46+ Months	2.430862	1.51E-02	1.05E-01
		4-12 Months - 14-24 Months	1.594805	1.11E-01	5.54E-01
		4-12 Months - 26-38 Months	2.99779	2.72E-03	2.45E-02
		4-12 Months - 46+ Months	4.394076	1.11E-05	1.11E-04
		14-24 Months - 26-38 Months	1.527159	1.27E-01	5.07E-01
		14-24 Months - 46+ Months	2.592998	9.51E-03	7.61E-02
		26-38 Months - 46+ Months	0.693463	4.88E-01	9.76E-01
	Plunge	2 Months - 4-12 Months	-5.27621	1.32E-07	1.32E-06
		2 Months - 14-24 Months	-3.96789	7.25E-05	6.53E-04
		2 Months - 26-38 Months	-3.62853	2.85E-04	2.28E-03
		2 Months - 46+ Months	-3.36314	7.71E-04	5.39E-03
		4-12 Months - 14-24 Months	1.127273	2.60E-01	1.00E+00
		4-12 Months - 26-38 Months	0.952318	3.41E-01	1.00E+00
		4-12 Months - 46+ Months	2.149757	3.16E-02	1.89E-01
		14-24 Months - 26-38 Months	-0.06514	9.48E-01	9.48E-01
		14-24 Months - 46+ Months	0.90238	3.67E-01	1.00E+00
		26-38 Months - 46+ Months	0.87646	3.81E-01	7.62E-01

Table A2.2 (cont.)

Bone	Trabecular Characteris-tic	labels for each pairwise comparison	Z test statis-tic values	unadjusted p-values	adjusted p-val-ues
Femur	DA	2 Months - 4-12 Months	-2.60081	9.30E-03	6.51E-02
		2 Months - 14-24 Months	-4.60257	4.17E-06	3.76E-05
		2 Months - 26-38 Months	-3.69584	2.19E-04	1.75E-03
		2 Months - 46+ Months	-5.11193	3.19E-07	3.19E-06
		4-12 Months - 14-24 Months	-1.99221	4.63E-02	2.32E-01
		4-12 Months - 26-38 Months	-1.37986	1.68E-01	6.71E-01
		4-12 Months - 46+ Months	-2.24231	2.49E-02	1.50E-01
		14-24 Months - 26-38 Months	0.41255	6.80E-01	1.00E+00
		14-24 Months - 46+ Months	-0.07969	9.36E-01	9.36E-01
		26-38 Months - 46+ Months	-0.51047	6.10E-01	1.00E+00
	BV/TV	2 Months - 4-12 Months	-3.7707	1.63E-04	1.63E-03
		2 Months - 14-24 Months	-3.18824	1.43E-03	1.29E-02
		2 Months - 26-38 Months	-1.36363	1.73E-01	5.18E-01
		2 Months - 46+ Months	-1.41667	1.57E-01	6.26E-01
		4-12 Months - 14-24 Months	0.466234	6.41E-01	1.00E+00
		4-12 Months - 26-38 Months	1.87278	6.11E-02	3.67E-01
		4-12 Months - 46+ Months	2.479715	1.31E-02	1.05E-01
		14-24 Months - 26-38 Months	1.424021	1.54E-01	7.72E-01
		14-24 Months - 46+ Months	1.921058	5.47E-02	3.83E-01
		26-38 Months - 46+ Months	0.20226	8.40E-01	8.40E-01
	Tb.Th	2 Months - 4-12 Months	-3.09519	1.97E-03	1.38E-02
		2 Months - 14-24 Months	-4.72928	2.25E-06	2.25E-05
		2 Months - 26-38 Months	-3.94457	7.99E-05	6.40E-04
		2 Months - 46+ Months	-4.54651	5.45E-06	4.91E-05
		4-12 Months - 14-24 Months	-1.65065	9.88E-02	5.93E-01
		4-12 Months - 26-38 Months	-1.20213	2.29E-01	1.00E+00
		4-12 Months - 46+ Months	-1.19912	2.30E-01	9.22E-01
		14-24 Months - 26-38 Months	0.284081	7.76E-01	1.00E+00
		14-24 Months - 46+ Months	-1.19912	2.30E-01	1.00E+00
		26-38 Months - 46+ Months	0.211891	8.32E-01	8.32E-01

Table A2.2 (cont.)

Bone	Trabecular Characteris-tic	labels for each pairwise comparison	Z test statis-tic values	unadjusted p-values	adjusted p-val-ues
Femur	Tb.Sp	2 Months - 4-12 Months	-1.05375	2.92E-01	5.84E-01
		2 Months - 14-24 Months	-2.87318	4.06E-03	2.44E-02
		2 Months - 26-38 Months	-4.28401	1.84E-05	1.65E-04
		2 Months - 46+ Months	-5.38797	7.13E-08	7.13E-07
		4-12 Months - 14-24 Months	-1.77792	7.54E-02	3.02E-01
		4-12 Months - 26-38 Months	-3.26102	1.11E-03	7.77E-03
		4-12 Months - 46+ Months	-4.07921	4.52E-05	3.62E-04
		14-24 Months - 26-38 Months	-1.62306	1.05E-01	3.14E-01
		14-24 Months - 46+ Months	-2.09335	3.63E-02	1.82E-01
		26-38 Months - 46+ Months	-0.14447	8.85E-01	8.85E-01
	Tb.N	2 Months - 4-12 Months	1.101697	2.71E-01	1.00E+00
		2 Months - 14-24 Months	3.120888	1.80E-03	1.44E-02
		2 Months - 26-38 Months	3.70169	2.14E-04	1.93E-03
		2 Months - 46+ Months	4.088835	4.34E-05	4.34E-04
		4-12 Months - 14-24 Months	1.971429	4.87E-02	2.43E-01
		4-12 Months - 26-38 Months	2.65576	7.91E-03	4.75E-02
		4-12 Months - 46+ Months	2.788548	5.29E-03	3.71E-02
		14-24 Months - 26-38 Months	0.85767	3.91E-01	1.00E+00
		14-24 Months - 46+ Months	0.633174	5.27E-01	1.00E+00
		26-38 Months - 46+ Months	-0.34673	7.29E-01	7.29E-01
	Plunge	2 Months - 4-12 Months	-0.78632	4.32E-01	8.63E-01
		2 Months - 14-24 Months	-2.45082	1.43E-02	9.98E-02
		2 Months - 26-38 Months	-3.08718	2.02E-03	1.62E-02
		2 Months - 46+ Months	-4.22062	2.44E-05	2.44E-04
		4-12 Months - 14-24 Months	-1.62208	1.05E-01	5.24E-01
		4-12 Months - 26-38 Months	-2.32714	2.00E-02	1.20E-01
		4-12 Months - 46+ Months	-3.2352	1.22E-03	1.09E-02
		14-24 Months - 26-38 Months	-0.845	3.98E-01	1.00E+00
		14-24 Months - 46+ Months	-1.43649	1.51E-01	6.03E-01
		26-38 Months - 46+ Months	-0.38526	7.00E-01	7.00E-01

Figure A3.1
An individual slice from a µCT of a *Dimetrodon* vertebrae selected to highlight the effect geologic inclusions can have in masking skeletal elements. Pyritic inclusions are circled in blue and were dense enough to create disruptive scattering that reduced contrast of fossil remains. This scan did utilize filters to further increase contrast between fossils and the surrounding matrix.

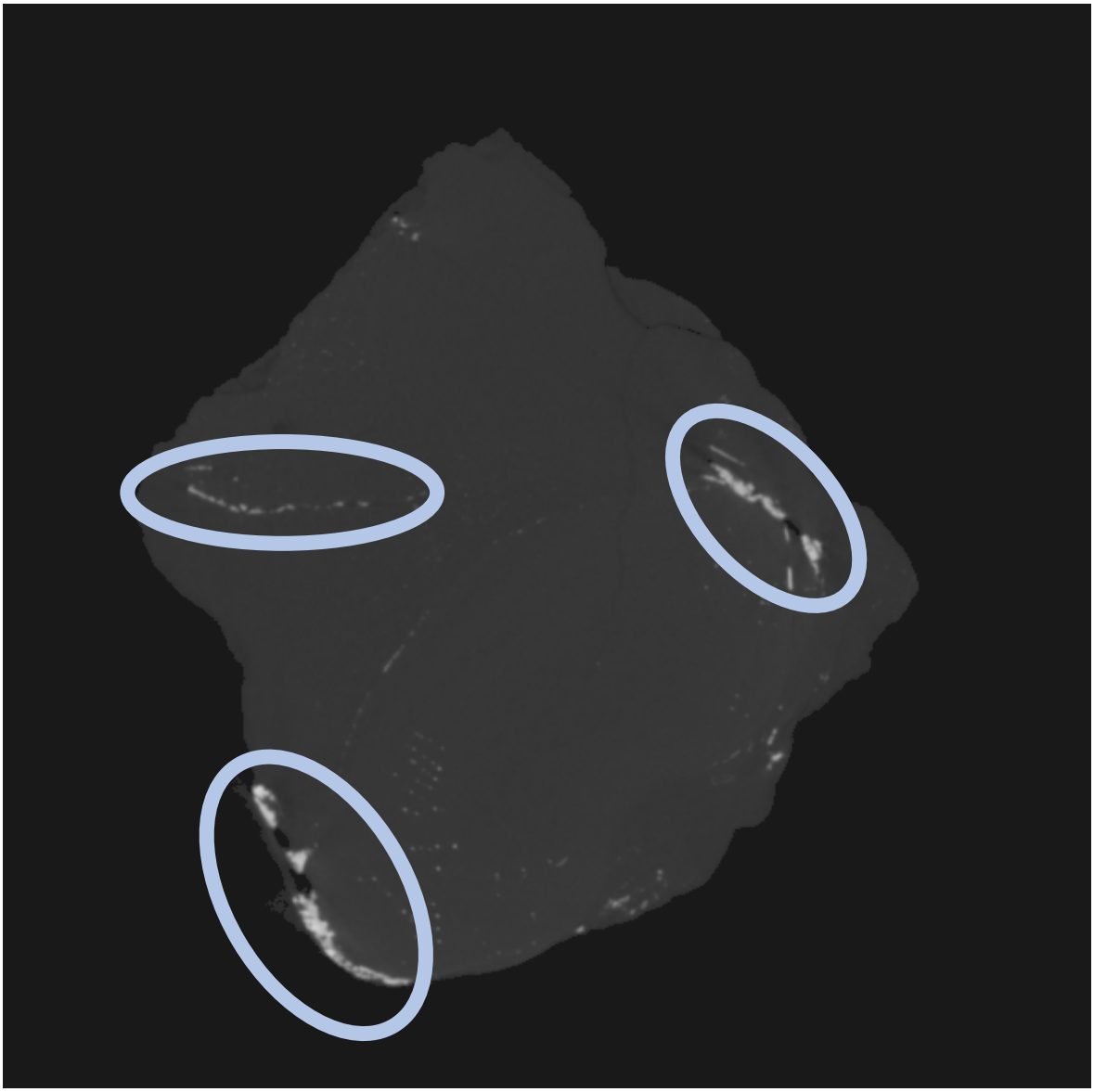

Bibliography

Acquaah, Frank, et al. "Early trabecular development in human vertebrae: overproduction, constructive regression, and refinement." *Frontiers in Endocrinology* 6 (2015): 67.

Aguirre, Trevor G., et al. "Differing trabecular bone architecture in dinosaurs and mammals contribute to stiffness and limits on bone strain." *PLoS One* 15.8 (2020): e0237042.

Alfieri, Fabio, et al. "The relationship between primate distal fibula trabecular architecture and arboreality, phylogeny and size." *Journal of Anatomy*.

Amson, Eli, et al. "Trabecular architecture in the forelimb epiphyses of extant xenarthrans (Mammalia)." *Frontiers in Zoology* 14 (2017): 1-17.

Anderson, H. Clarke. "Matrix vesicles and calcification." *Current rheumatology reports* 5.3 (2003): 222-226.

Angielczyk, Kenneth D., and H. David Sheets. "Investigation of simulated tectonic deformation in fossils using geometric morphometrics." *Paleobiology* 33.1 (2007): 125-148.

Arias-Martorell, Julia, et al. "Like father, like son: Assessment of the morphological affinities of AL 288–1 (A. afarensis), Sts 7 (A. africanus) and Omo 119–73–2718 (Australopithecus sp.) through a three-dimensional shape analysis of the shoulder joint." *Plos one* 10.2 (2015): e0117408.

Arikan, Hüseyin, and Kerim Cicek. "Haematology of amphibians and reptiles: a review." *North-Western journal of zoology* 10.1 (2014): 190-209.

Baker, Robert J. "Macdonald, D.(ed.) The encyclopedia of mammals. facts on file, inc., 460 Park Ave. South, New York 10016. xlviii+ 895 pp., 1984. Price (hardbound), $43.00." (1985): 830-831.

Barak, Meir M. "Cortical and trabecular bone modeling and implications for bone functional adaptation in the mammalian tibia." *Bioengineering* 11.5 (2024): 514.

Barak, Meir M., Daniel E. Lieberman, and Jean-Jacques Hublin. "A Wolff in sheep's clothing: trabecular bone adaptation in response to changes in joint loading orientation." *Bone* 49.6 (2011): 1141-1151.

Barak, Meir Max, Daniel E. Lieberman, and Jean-Jacques Hublin. "Of mice, rats and men: Trabecular bone architecture in mammals scales to body mass with negative allometry." *Journal of Structural Biology*, vol. 183, no. 2, 2013, pp. 123-31.

Baum, T., et al. "Automated 3D trabecular bone structure analysis of the proximal femur—prediction of biomechanical strength by CT and DXA." *Osteoporosis International*, vol. 21, 2010, pp. 1553-64.

Bennett, Albert F., and John A. Ruben. "Endothermy and activity in vertebrates." *Science* 206.4419 (1979): 649-654.

Biewener, Andrew A. "Biomechanics of mammalian terrestrial locomotion." *Science*, vol. 250, no. 4984, 1990, pp. 1097-1103.

Bishop, Peter J., and Stephanie E. Pierce. "Late acquisition of erect hindlimb posture and function in the forerunners of therian mammals." *Science Advances*, vol. 10, no. 43, 2024, eadr2722.

Blair, Harry C., et al. "Balanced regulation of proliferation, growth, differentiation, and degradation in skeletal cells." *Annals of the New York Academy of Sciences*, vol. 1116, no. 1, 2007, pp. 165-73.

Blob, Richard W., and Andrew A. Biewener. "In vivo locomotor strain in the hindlimb bones of *Alligator mississippiensis* and *Iguana iguana*: implications for the evolution of limb bone safety factor and non-sprawling limb posture." *Journal of Experimental Biology* 202.9 (1999): 1023-1046.

Bonewald, Lynda F. "The amazing osteocyte." *Journal of bone and mineral research* 26.2 (2011): 229-238.

Bouxsein, Mary L., et al. "Guidelines for assessment of bone microstructure in rodents using micro–computed tomography." *Journal of bone and mineral research* 25.7 (2010): 1468-1486.

Boyer, Doug M., et al. "Morphosource: archiving and sharing 3-D digital specimen data." *The Paleontological Society Papers* 22 (2016): 157-181.

Boyle, William J., W. Scott Simonet, and David L. Lacey. "Osteoclast differentiation and activation." *Nature* 423.6937 (2003): 337-342.

Brocklehurst, RJ, and SE Pierce. "Musculoskeletal modelling untangles the origins of mammal forelimb function and posture; Society of Experimental Biology Centenary Conference Abstract Book." Society of Experimental Biology, (2023).

Brocklehurst, Robert, Magdalen Mercado, and Stephanie Pierce. "Adaptive landscapes reveal complex evolution of forelimb posture in stem mammals (Synapsida)." *Integrative and comparative biology* 63. Supplement 1 (2023).

Brommage, R. "Perspectives on using nonhuman primates to understand the etiology and treatment of postmenopausal osteoporosis." *J Musculoskelet Neuronal Interact* 1.4 (2001): 307-325.

Burr, David B., et al. "In vivo measurement of human tibial strains during vigorous activity." *Bone* 18.5 (1996): 405-410.

Campione, Nicolás E., and David C. Evans. "A universal scaling relationship between body mass and proximal limb bone dimensions in quadrupedal terrestrial tetrapods." *BMC biology* 10 (2012): 1-22.

Carter, Dennis R., and Gary S. Beaupré. "Skeletal function and form." *(No Title)* (2000).

Chagin, Andrei S., and Tsz Long Chu. "The origin and fate of chondrocytes: cell plasticity in physiological setting." *Current Osteoporosis Reports* 21.6 (2023): 815-824.

Charbord, Pierre, et al. "Early ontogeny of the human marrow from long bones: an immunohistochemical study of hematopoiesis and its microenvironment [see comments]." (1996): 4109-4119.

Chen, Huayue, et al. "Age-related changes in trabecular and cortical bone microstructure." *International journal of endocrinology* 2013.1 (2013): 213234.

Chirchir, Habiba, et al. "Effects of reduced mobility on trabecular bone density in captive big cats." *Royal Society Open Science* 9.3 (2022): 211345.

Choi, K., et al. "The elastic moduli of human subchondral, trabecular, and cortical bone tissue and the size-dependency of cortical bone modulus." *Journal of biomechanics* 23.11 (1990): 1103-1113.

Choi, K., and Steven A. Goldstein. "A comparison of the fatigue behavior of human trabecular and cortical bone tissue." *Journal of biomechanics* 25.12 (1992): 1371-1381.

Chong, Baxi, et al. "Coordinating tiny limbs and long bodies: Geometric mechanics of diverse undulatory lizard locomotion." *arXiv preprint arXiv:2201.09312* (2022).

Christen, Patrik, Keita Ito, and Bert van Rietbergen. "A potential mechanism for allometric trabecular bone scaling in terrestrial mammals." *Journal of anatomy* 226.3 (2015): 236-243.

Cowin, Stephen C., and Stephen B. Doty. *Tissue Mechanics*. Springer Science & Business Media, (2007).

Crewe, Albert V. "Scanning Electron Microscopes: Is high resolution possible? Use of a field-emission electron source may make it possible to overcome existing limitations on resolution." *Science* 154.3750 (1966): 729-738.

Culmann, K. *Die Graphische Statik*. Verlag Von Meyer & Zeller, 1865.

Currey, John D. *Bones: structure and mechanics*. Princeton University Press, 2002.

de Buffrénil, Vivian, and Alexandra Houssaye. "Lepidosauria." *Vertebrate skeletal histology and paleohistology* (2021): 399-424.

Demes, B., et al. "The kinetics of primate quadrupedalism:" hindlimb drive" reconsidered." *Journal of Human Evolution* 26.5-6 (1994): 353-374.

DeSilva, Jeremy M., and Maureen J. Devlin. "A comparative study of the trabecular bony architecture of the talus in humans, non-human primates, and *Australopithecus*." *Journal of Human Evolution* 63.3 (2012): 536-551.

Dickson, Blake V., et al. "Functional adaptive landscapes predict terrestrial capacity at the origin of limbs." *Nature* 589.7841 (2021): 242-245.

Dinno, Alexis, and Maintainer Alexis Dinno. "Package 'dunn. test'." *CRAN Repos* 10 (2017): 1-7.

Doershuk, Lily J., et al. "Complex variation of trabecular bone structure in the proximal humerus and femur of five modern human populations." American Journal of Physical Anthropology 168.1 (2019): 104-118.dos Reis, Mario, et al. "Phylogenomic datasets provide both precision and accuracy in estimating the timescale of placental mammal phylogeny." *Proceedings of the Royal Society B: Biological Sciences* 279.1742 (2012): 3491-3500.

Doube, Michael, et al. "BoneJ: free and extensible bone image analysis in ImageJ." *Bone* 47.6 (2010): 1076-1079.

Doube, Michael, et al. "Trabecular bone scales allometrically in mammals and birds." *Proceedings of the Royal Society B: Biological Sciences* 278.1721 (2011): 3067-3073.

Dragonfly. Version 2022.2, Comet Technologies Canada Inc., 2022, https://www.theobjects.com/dragonfly.

Dublin, Louis I. "Adaptations to aquatic, arboreal, fossorial and cursorial habits in mammals. II. Arboreal adaptations." *The American Naturalist* 37.443 (1903): 731-736.

Dunn, Olive Jean. "Multiple comparisons using rank sums." *Technometrics* 6.3 (1964): 241-252.

Elissamburu, Andrea, and Luciano De Santis. "Forelimb proportions and fossorial adaptations in the scratch-digging rodent Ctenomys (Caviomorpha)." *Journal of Mammalogy* 92.3 (2011): 683-689.

Elliott, Jim C., and S. D. Dover. "X-ray microtomography." *Journal of microscopy* 126.2 (1982): 211-213.

Evans, Richard H. "An analysis of criterion variable reliability in conjoint analysis." *Perceptual and motor skills* 82.3 (1996): 988-990.

Fajardo, R. J., and Ralph Müller. "Three-dimensional analysis of nonhuman primate trabecular architecture using micro-computed tomography." *American Journal of Physical Anthropology: The Official Publication of the American Association of Physical Anthropologists* 115.4 (2001): 327-336.

Fajardo, Roberto J., et al. "Nonhuman anthropoid primate femoral neck trabecular architecture and its relationship to locomotor mode." *The Anatomical Record: Advances in Integrative Anatomy and Evolutionary Biology: Advances in Integrative Anatomy and Evolutionary Biology* 290.4 (2007): 422-436.

Farhi, Diane C. "Pathology of bone marrow and blood cells." *(No Title)* (2009).

Farley, Claire T., and T. Christine Ko. "Mechanics of locomotion in lizards." *Journal of Experimental Biology* 200.16 (1997): 2177-2188.

Feldkamp, Lee A., et al. "The direct examination of three-dimensional bone architecture in vitro by computed tomography." *Journal of bone and mineral research* 4.1 (1989): 3-11.

Fields, Aaron J., et al. "Influence of vertical trabeculae on the compressive strength of the human vertebra." *Journal of Bone and Mineral Research* 26.2 (2011): 263-269.

Fiero, Brad C., and B. J. Verts. "Comparison of techniques for estimating age in raccoons." *Journal of Mammalogy* 67.2 (1986): 392-395.

Finkelstein JS. "A longitudinal evaluation of bone mineral density in adult men with histories of delay puberty." *J Clin Endocrinol Metab* 81 (1996): 1152-1155.

Foster, Kathleen L., and Timothy E. Higham. "How forelimb and hindlimb function changes with incline and perch diameter in the green anole, *Anolis carolinensis*." *Journal of Experimental Biology* 215.13 (2012): 2288-2300.

Frost, H. M. "A chondral modeling theory." *Calcified Tissue International* 28 (1979): 181-200.

Frost, H. M. "Skeletal structural adaptations to mechanical usage (SATMU): 4. Mechanical influences on intact fibrous tissues." *The anatomical record* 226.4 (1990): 433-439.

HM, FROST. "The mechanostat: a proposed pathogenic mechanism of osteoporoses and the bone mass effects of mechanical and non mechanical agents." *Bone Miner* 2 (1987): 73-85.

Frýdlová, Petra, et al. "Universality of indeterminate growth in lizards rejected: The micro-CT reveals contrasting timing of growth cartilage persistence in iguanas, agamas, and chameleons." *Scientific Reports* 9.1 (2019): 18913.

Fyhrie, D. P., and D. R. Carter. "A unifying principle relating stress to trabecular bone morphology." *Journal of Orthopaedic Research* 4.3 (1986): 304-317.

Gatesy, Stephen M., et al. "A proposed standard for quantifying 3-D hindlimb joint poses in living and extinct archosaurs." *Journal of Anatomy* 241.1 (2022): 101-118.

Georgiou, Leoni, et al. "Evidence for habitual climbing in a Pleistocene hominin in South Africa." *Proceedings of the National Academy of Sciences* 117.15 (2020): 8416-8423.

Georgiou, Leoni, et al. "Trabecular architecture of the great ape and human femoral head." *Journal of Anatomy* 234.5 (2019): 679-693.

Georgopoulos, Neoklis A., et al. "Height velocity and skeletal maturation in elite female rhythmic gymnasts." *The Journal of Clinical Endocrinology & Metabolism* 86.11 (2001): 5159-5164.

Gibson, Lorna J. "Biomechanics of cellular solids." *Journal of biomechanics* 38.3 (2005): 377-399.

Gillette, Laurence N. "Movement patterns of radio-tagged opossums in Wisconsin." *American Midland Naturalist* (1980): 1-12.

Grau, Gerald A., Glen C. Sanderson, and John P. Rogers. "Age determination of raccoons." *The Journal of Wildlife Management* (1970): 364-372.

Griffin, Nicole L., et al. "Comparative forefoot trabecular bone architecture in extant hominids." *Journal of human evolution* 59.2 (2010): 202-213.

Hanna, Jandy B., et al. "The evolution of vertical climbing in primates: evidence from reaction forces." *Journal of Experimental Biology* 220.17 (2017): 3039-3052.

Harcourt-Smith, William EH, and Leslie C. Aiello. "Fossils, feet and the evolution of human bipedal locomotion." *Journal of anatomy* 204.5 (2004): 403-416.

Harmon, L. "treeplyr:'dplyr'Functionality for Matched Tree and Data Objects. R package version 0.1. 10." 2020,

Hébert, David, Renaud Lebrun, and Laurent Marivaux. "Comparative three-dimensional structure of the trabecular bone in the talus of primates and its relationship to ankle joint loads generated during locomotion." *The Anatomical Record: Advances in Integrative Anatomy and Evolutionary Biology* 295.12 (2012): 2069-2088.

Hijmans, Robert J. "raster: Geographic data analysis and modeling." *R package version* 2 (2018): 8.

Hildebrand, Milton, et al., eds. *Functional vertebrate morphology*. Harvard University Press, 1985.

Hoebeke M., Trubuil A. Quant3D, a Linux/UNIX software. 1999

Houssaye, Alexandra, P. Martin Sander, and Nicole Klein. "Adaptive patterns in aquatic amniote bone microanatomy—more complex than previously thought." *Integrative and Comparative Biology* 56.6 (2016): 1349-1369.

Hutchinson, John R. "The evolution of locomotion in archosaurs." *Comptes Rendus Palevol* 5.3-4 (2006): 519-530.

Hutson, Joel D., and Kelda N. Hutson. "A test of the validity of range of motion studies of fossil archosaur elbow mobility using repeated-measures analysis and the extant phylogenetic bracket." *Journal of Experimental Biology* 215.12 (2012): 2030-2038.

Iijima, Masaya, V. David Munteanu, and Richard W. Blob. "Variations in humeral and femoral strains across body sizes and limb posture in American alligators." *Journal of Experimental Biology* 227.24 (2024): jeb249211.

ImageJ. U.S. National Institutes of Health, 1997, https://imagej.nih.gov/ij/.

International Union for Conservation of Nature. The IUCN Red List of Threatened Species. Version 2024-1, IUCN, 2024, https://www.iucnredlist.org/. Accessed October 23, 2023

Jansa, Sharon A., F. Keith Barker, and Robert S. Voss. "The early diversification history of didelphid marsupials: a window into South America's “Splendid Isolation”." *Evolution* 68.3 (2014): 684-695.

Jenkins Jr, Farish A. "A survey of mammalian origins." *Series in Geology, Notes for Short Course* 8 (1984): 32-47.

Johnson, Albert Sydney. "Biology of the raccoon (*Procyon lotor* varius Nelson and Goldman) in Alabama." (1970): vi+-148.

Judex, Stefan, et al. "Low-magnitude mechanical signals that stimulate bone formation in the ovariectomized rat are dependent on the applied frequency but not on the strain magnitude." *Journal of biomechanics* 40.6 (2007): 1333-1339.

Junge, Randall, and Donald F. Hoffmeister. "Age determination in raccoons from cranial suture obliteration." *The Journal of Wildlife Management* 44.3 (1980): 725-729.

Kammerer, Christian F., et al. "Effects of taphonomic deformation on geometric morphometric analysis of fossils: a study using the dicynodont *Diictodon feliceps* (Therapsida, Anomodontia)." *PeerJ* 8 (2020): e9925.

Kanis, J. A. "Estrogens, the menopause, and osteoporosis." *Bone* 19.5 (1996): 185S-190S.

Keaveny, Tony M., et al. "Biomechanics of trabecular bone." *Annual review of biomedical engineering* 3.1 (2001): 307-333.

Keaveny, Tony M., Edward F. Wachtel, and David L. Kopperdahl. "Mechanical behavior of human trabecular bone after overloading." *Journal of Orthopaedic Research* 17.3 (1999): 346-353.

Keaveny, Tony M., et al. "Differences between the tensile and compressive strengths of bovine tibial trabecular bone depend on modulus." *Journal of biomechanics* 27.9 (1994): 1137-1146.

Kim, Seongho. "ppcor: an R package for a fast calculation to semi-partial correlation coefficients." *Communications for statistical applications and methods* 22.6 (2015): 665.

Kim, Young-Seong, et al. "The correlation between bone mineral density/trabecular bone score and body mass index, height, and weight." *Osteoporosis and Sarcopenia* 3.2 (2017): 98-103.

Kivell, Tracy L. "A review of trabecular bone functional adaptation: what have we learned from trabecular analyses in extant hominoids and what can we apply to fossils?." *Journal of Anatomy* 228.4 (2016): 569-594.

Kivell, Tracy L., et al. "Methodological considerations for analyzing trabecular architecture: an example from the primate hand." *Journal of anatomy* 218.2 (2011): 209-225.

Kley, Nathan J., and Maureen Kearney. "Adaptations for digging and burrowing." *Fins into limbs: evolution, development, and transformation* (2007): 284-309.

Koch, John C. "The laws of bone architecture." *American Journal of Anatomy* 21.2 (1917): 177-298.

Krause, Willliam J., and Winifred A. Krause. *The opossum: its amazing story*. William Krause, 2006.

Kruskal, William H., and W. Allen Wallis. "Use of ranks in one-criterion variance analysis." *Journal of the American statistical Association* 47.260 (1952): 583-621.

Kuhn, Janet L., et al. "Comparison of the trabecular and cortical tissue moduli from human iliac crests." *Journal of orthopaedic research* 7.6 (1989): 876-884.

Lang, Jan J., et al. "Numerical evaluation of internal femur osteosynthesis based on a biomechanical model of the loading in the proximal equine hindlimb." *BMC veterinary research* 20.1 (2024): 188.

Larson, Susan G., et al. "Uniqueness of primate forelimb posture during quadrupedal locomotion." *American Journal of Physical Anthropology: The Official Publication of the American Association of Physical Anthropologists* 112.1 (2000): 87-101.

Lieberman, Daniel E., John D. Polk, and Brigitte Demes. "Predicting long bone loading from cross-sectional geometry." *American Journal of Physical Anthropology: The Official Publication of the American Association of Physical Anthropologists* 123.2 (2004): 156-171.

Linhart, Samuel B., and Frederick F. Knowlton. "Determining age of coyotes by tooth cementum layers." *The Journal of Wildlife Management* (1967): 362-365.

Losos, Jonathan B. "The evolution of form and function: morphology and locomotor performance in West Indian Anolis lizards." *Evolution* 44.5 (1990): 1189-1203.

Lotz, Jeffrey C., Tobin N. Gerhart, and Wilson C. Hayes. "Mechanical properties of trabecular bone from the proximal femur: a quantitative CT study." *Journal of computer assisted tomography* 14.1 (1990): 107-114.

Lovejoy, C. Owen. "Evolution of human walking." *Scientific American* 259.5 (1988): 118-125.

Lukova, Andrea, et al. "Trabecular architecture of the distal femur in extant hominids." *Journal of Anatomy* 245.1 (2024): 156-180.

Lull, Richard Swann. "Adaptations to aquatic, arboreal, fossorial and cursorial habits in mammals. IV. Cursorial adaptations." *The American Naturalist* 38.445 (1904): 1-11.

MacClintock D, and Thomas JS. *Natural History of Raccoons.* Scribner (1981).

Mackie, EJ1, et al. "Endochondral ossification: how cartilage is converted into bone in the developing skeleton." *The international journal of biochemistry & cell biology* 40.1 (2008): 46-62.

MacLatchy, Laura, and Ralph Müller. "A comparison of the femoral head and neck trabecular architecture of Galago and Perodicticus using micro-computed tomography (μCT)." *Journal of Human Evolution* 43.1 (2002): 89-105.

Maga, Murat, et al. "Preliminary observations on the calcaneal trabecular microarchitecture of extant large-bodied hominoids." *American Journal of Physical Anthropology: The Official Publication of the American Association of Physical Anthropologists* 129.3 (2006): 410-417.

Maher, Michelle. "Aging coyotes using dental characteristics." (2002).

Mazzetti, Gillian, et al. "Densitometer-specific differences in the correlation between body mass index and lumbar spine trabecular bone score." *Journal of clinical densitometry* 20.2 (2017): 233-238.

McClearn, Deedra. "Locomotion, posture, and feeding behavior of kinkajous, coatis, and raccoons." *Journal of Mammalogy* 73.2 (1992): 245-261.

Mc Donnell, P., P. E. Mc Hugh, and D. O'mahoney. "Vertebral osteoporosis and trabecular bone quality." *Annals of biomedical engineering* 35 (2007): 170-189.

McKinley, Todd O., and Brian K. Bay. "Trabecular bone strain changes associated with cartilage defects in the proximal and distal tibia." *Journal of Orthopaedic Research* 19.5 (2001): 906-913.

Mescher, Anthony L. *Junqueira's basic histology: text and atlas (--2023)*. McGraw-Hill Education/Medical, 2023.

Metzger, Thomas A., et al. "Pressure and shear stress in trabecular bone marrow during whole bone loading." *Journal of biomechanics* 48.12 (2015): 3035-3043.

Mielke, Maja, et al. "Trabecular architecture in the sciuromorph femoral head: allometry and functional adaptation." *Zoological letters* 4 (2018): 1-11.

Moreno, Rodrigo, Magnus Borga, and Örjan Smedby. "Techniques for computing fabric tensors: a review." *Visualization and processing of tensors and higher order descriptors for multi-valued data* (2014): 271-292.

Morgan, Elise F., and Louis C. Gerstenfeld. "The bone organ system: form and function." *Marcus and Feldman's Osteoporosis*. Academic Press, 2021. 15-35.

Morgan, Elise F., and Tony M. Keaveny. "Dependence of yield strain of human trabecular bone on anatomic site." *Journal of biomechanics* 34.5 (2001): 569-577.

Mori, Toshiharu, et al. "Climbing exercise increases bone mass and trabecular bone turnover through transient regulation of marrow osteogenic and osteoclastogenic potentials in mice." *Journal of bone and mineral research* 18.11 (2003): 2002-2009.

Nadell, Jason A., Sarah Elton, and Kris Kovarovic. "Ontogenetic and morphological variation in primate long bones reflects signals of size and behavior." *American Journal of Physical Anthropology* 174.2 (2021): 327-351.

Nafei, Adel, et al. "Properties of growing trabecular ovine bone: PART II: architectural and mechanical properties." *The Journal of Bone & Joint Surgery British Volume* 82.6 (2000): 921-927.

Nagy, Kenneth A. "Field metabolic rate and body size." *Journal of experimental biology* 208.9 (2005): 1621-1625.

Noble, Brendon S. "The osteocyte lineage." *Archives of biochemistry and biophysics* 473.2 (2008): 106-111.

Nottestad, Sheri Y., et al. "The proportion of trabecular bone in human vertebrae." *Journal of Bone and Mineral Research* 2.3 (1987): 221-229.

Nowak, Ronald M. *Walker's Mammals of the World*. Vol. 1. JHU press, 1999.

Oskyrko, Oleksandra, et al. "ReptTraits: a comprehensive dataset of ecological traits in reptiles." *Scientific Data* 11.1 (2024): 243.

Otsu, Nobuyuki. "A threshold selection method from gray-level histograms." *Automatica* 11.285-296 (1975): 23-27.

Ozcivici, Engin, Russell Garman, and Stefan Judex. "High-frequency oscillatory motions enhance the simulated mechanical properties of non-weight bearing trabecular bone." Journal of biomechanics 40.15 (2007): 3404-3411.

O'Connell, Margaret A. "Marmosa robinsoni." *Mammalian Species* 203 (1983): 1-6.

O'Connor, Anahad. "The Claim: After Being Broken, Bones Can Become Even Stronger." *New York Times* (2010).

Parfitt, A. Michael. "Bone Remodeling." *Henry Ford Hospital Medical Journal*, vol. 36, 1988, pp. 143-44.

Parfitt, A. Michael, et al. "Bone Histomorphometry: Standardization of Nomenclature, Symbols, and Units." *Journal of Bone and Mineral Research*, vol. 2, no. 6, 1987, pp. 595-610.

Parkinson, Ian H., and Nicola L. Fazzalari. "Characterisation of Trabecular Bone Structure." *Skeletal Aging and Osteoporosis: Biomechanics and Mechanobiology*, Springer, 2012, pp. 31-51.

Parrish, J. Michael. "The origin of crocodilian locomotion." *Paleobiology* 13.4 (1987): 396-414.

Pawlina, Wojciech, and Michael H. Ross. *Histology: a text and atlas: with correlated cell and molecular biology*. Lippincott Williams & Wilkins, 2018.

Pianka, Eric P., and Laurie J. Vitt. *Lizards: windows to the evolution of diversity*. Vol. 5. Univ of California Press, 2003.

Pinheiro, Jose. "nlme: Linear and nonlinear mixed effects models." *R package version* 3 (2011): 1.

Plasse, Martial, et al. "Trabecular architecture in the humeral metaphyses of non-avian reptiles (Crocodylia, Squamata and Testudines): Lifestyle, allometry and phylogeny." *Journal of Morphology* 280.7 (2019): 982-998.

Polk, John D., J. Blumenfeld, and D. Ahluwalia. "Knee posture predicted from subchondral apparent density in the distal femur: an experimental validation." *The Anatomical Record: Advances in Integrative Anatomy and Evolutionary Biology: Advances in Integrative Anatomy and Evolutionary Biology* 291.3 (2008): 293-302.

Pollock, Sarah, et al. "A musculoskeletal model of the equine forelimb for determining surface stresses and strains in the humerus—Part I. Mathematical modeling." (2008): 041006.

Pough FH., Andrews RM, Cadle JE. et al. *Herpetology, Third Edition*. New York: Prentice Hall, (2003)

Pyron, R. Alexander, Frank T. Burbrink, and John J. Wiens. "A phylogeny and revised classification of Squamata, including 4161 species of lizards and snakes." *BMC evolutionary biology* 13 (2013): 1-54.

R Core Team. *R: A Language and Environment for Statistical Computing*. R Foundation for Statistical Computing, 2023, https://www.R-project.org/.

Racicot, Rachel. "Fossil secrets revealed: X-ray CT scanning and applications in paleontology." *The Paleontological Society Papers* 22 (2016): 21-38.

Rafferty, K. L. "Structural Design of the Femoral Neck in Primates." *Journal of Human Evolution*, vol. 34, no. 4, 1998, pp. 361-83.

Ragni, Anna J. "Trabecular architecture of the capitate and third metacarpal through ontogeny in chimpanzees (Pan troglodytes) and gorillas (Gorilla gorilla)." *Journal of Human Evolution* 138 (2020): 102702.

Rasband, Wayne S. "ImageJ." (1997).

Ragni, Anna J. "Trabecular architecture of the capitate and third metacarpal through ontogeny in chimpanzees (*Pan troglodytes*) and gorillas (*Gorilla gorilla*)." *Journal of Human Evolution*, vol. 138, 2020, 102702.

Reid, Rebecca A. G., et al. "Trabecular bone ontogeny of the human distal tibia." *American Journal of Biological Anthropology*, vol. 186, no. 1, 2025, e25043.

Reilly, Stephen M., et al. "Hindlimb function in the alligator: integrating movements, motor patterns, ground reaction forces and bone strain of terrestrial locomotion." *Journal of Experimental Biology* 208.6 (2005): 993-1009.

Reilly, Stephen M., and Jason A. Elias. "Locomotion in *Alligator mississippiensis*: kinematic effects of speed and posture and their relevance to the sprawling-to-erect paradigm." *Journal of Experimental Biology* 201.18 (1998): 2559-2574.

Reilly, Stephen M., et al. "Tuataras and salamanders show that walking and running mechanics are ancient features of tetrapod locomotion." *Proceedings of the Royal Society B: Biological Sciences* 273.1593 (2006): 1563-1568.

Reinecke, T., and K. D. Angielczyk. "Raccoons Reveal Hidden Diversity in Trabecular Bone Development." *Integrative Organismal Biology*, vol. 6, no. 1, 2024, obae038.

Reno, Philip L., et al. "Growth plate formation and development in alligator and mouse metapodials: evolutionary and functional implications." *Journal of Experimental Zoology Part B: Molecular and Developmental Evolution* 308.3 (2007): 283-296.

Romer, A. S. "Osteology of the reptiles university of chicago press." *Chicago, Illinois* (1956).

Rubin, Clinton T., and Lance E. Lanyon. "Limb mechanics as a function of speed and gait: A study of functional strains in the radius and tibia of horse and dog." *Journal of Experimental Biology*, vol. 101, no. 1, 1982, pp. 187-211.

Ruff, Christopher B. "Body size, body shape, and long bone strength in modern humans." *Journal of Human Evolution*, vol. 38, no. 2, 2000, pp. 269-90.

Ruff, Christopher, Brigitte Holt, and Erik Trinkaus. "Who's afraid of the big bad Wolff?:"Wolff's law" and bone functional adaptation." *American Journal of Physical Anthropology: The Official Publication of the American Association of Physical Anthropologists* 129.4 (2006): 484-498.

Ruimerman, R., et al. "A theoretical framework for strain-related trabecular bone maintenance and adaptation." *Journal of biomechanics* 38.4 (2005): 931-941.

Ryan, Timothy M., et al. "Human-like hip joint loading in *Australopithecus africanus* and *Paranthropus robustus*." Journal of Human Evolution 121 (2018): 12-24.

Ryan, Timothy M., and Richard A. Ketcham. "Angular orientation of trabecular bone in the femoral head and its relationship to hip joint loads in leaping primates." *Journal of Morphology* 265.3 (2005): 249-263.

Ryan, Timothy M., and Gail E. Krovitz. "Trabecular bone ontogeny in the human proximal femur." *Journal of human evolution* 51.6 (2006): 591-602.

Ryan, Timothy M., and Colin N. Shaw. "Gracility of the modern *Homo sapiens* skeleton is the result of decreased biomechanical loading." *Proceedings of the National Academy of Sciences* 112.2 (2015): 372-377.

Ryan, Timothy M., and Colin N. Shaw. "Trabecular bone microstructure scales allometrically in the primate humerus and femur." *Proceedings of the Royal Society B: Biological Sciences* 280.1758 (2013): 20130172.

Ryan, Timothy M., and Colin N. Shaw. "Unique suites of trabecular bone features characterize locomotor behavior in human and non-human anthropoid primates." *PloS one* 7.7 (2012): e41037.

Ryan, Timothy M., and Alan Walker. "Trabecular bone structure in the humeral and femoral heads of anthropoid primates." *The Anatomical Record*, vol. 293, no. 4, 2010, pp. 719-29.

Ryan, Stephen D., and John L. Williams. "Tensile testing of rodlike trabeculae excised from bovine femoral bone." *Journal of Biomechanics*, vol. 22, no. 4, 1989, pp. 351-55.

Saers, Jaap PP, et al. "Growth and development of trabecular structure in the calcaneus of Japanese macaques (*Macaca fuscata*) reflects locomotor behavior, life history, and neuromuscular development." *Journal of Anatomy* 241.1 (2022): 67-81.

Saers, Jaap P. P. *Ontogeny and Functional Adaptation of Trabecular Bone in the Human Foot*. Dissertation, University of Cambridge, 2017.

Saers, Jaap P. P., et al. "Trabecular bone ontogeny tracks neural development and life history among humans and non-human primates." *Proceedings of the National Academy of Sciences*, vol. 119, no. 49, 2022, e2208772119.

Sapthagirivasan, V., M. Anburajan, and V. Mahadevan. "Bone trabecular analysis of femur radiographs for the assessment of osteoporosis using DWT and DXA." *International journal of computer theory and engineering* 5.4 (2013): 616.

Scherf, Heike, et al. "Patterns of activity adaptation in humeral trabecular bone in Neolithic humans and present-day people." *American Journal of Physical Anthropology*, vol. 159, no. 1, 2016, pp. 106-15.

Scheyer, Torsten M., and Ignacio A. Cerda. "Testudines." *Vertebrate skeletal histology and paleohistology*. CRC Press, 2021. 385-398.

Schmidt, Manuela. "Forelimb proportions and kinematics: how are small primates different from other small mammals?." *Journal of Experimental Biology* 211.24 (2008): 3775-3789.

Schmidt, Manuela. "Quadrupedal locomotion in squirrel monkeys (Cebidae*: Saimiri sciureus*): a cineradiographic study of limb kinematics and related substrate reaction forces." *American Journal of Physical Anthropology: The Official Publication of the American Association of Physical Anthropologists* 128.2 (2005): 359-370.

Schmitt, Daniel, and Jandy B. Hanna. "Substrate alters forelimb to hindlimb peak force ratios in primates." *Journal of Human Evolution* 46.3 (2004): 237-252.

Seeman, Ego. "Pathogenesis of bone fragility in women and men." *The Lancet* 359.9320 (2002): 1841-1850.

Senter, Philip J., and Corwin Sullivan. "Forelimbs of the theropod dinosaur *Dilophosaurus wetherilli*: range of motion, influence of paleopathology and soft tissues, and description of a distal carpal bone." (2019): 1-19.

Shimer, H. W. "Adaptations to aquatic, arboreal, fossorial and cursorial habits in mammals. III. Fossorial adaptations." *The American Naturalist* 37.444 (1903): 819-825.

Shin, Young Ho, et al. "Older age and higher body mass index are associated with a more degraded trabecular bone score compared to bone mineral density." *Journal of Clinical Densitometry* 22.2 (2019): 266-271.

Siddiqui, Laiq Hussain. *Medical Histology*. 6th International Edition, MedTech, 2019.

Skoyles, John R. "Human balance, the evolution of bipedalism and dysequilibrium syndrome." *Medical hypotheses* 66.6 (2006): 1060-1068.

Smith, Heather F., et al. "Adaptations to cursoriality and digit reduction in the forelimb of the African wild dog (*Lycaon pictus*)." *PeerJ* 8 (2020): e9866.

Smith, S. M., L. R. Heaney, and K. D. Angielczyk. "Small skeletons show size-specific scaling: an exploration of allometry in the mammalian lumbar spine." *Proceedings of the Royal Society B* 291.2021 (2024): 20232868.

Smith, Stephanie M., et al. "The roles of phylogeny, body size and substrate use in trabecular bone variation among Philippine 'earthworm mice' (Rodentia: *Chrotomyini*)." *Biological Journal of the Linnean Society*, vol. 140, no. 1, 2023, pp. 1-25.

Smith, Stephanie M., and Kenneth D. Angielczyk. "Deciphering an extreme morphology: Bone microarchitecture of the hero shrew backbone (Soricidae: *Scutisorex*)." *Proceedings of the Royal Society B*, vol. 287, no. 1926, 2020, 20200457.

Smith, S. Y., et al. "Skeletal health: primate model of postmenopausal osteoporosis." *American Journal of Primatology*, vol. 71, no. 9, 2009, pp. 752-65.

Sode, Miki, et al. "Resolution dependence of the non-metric trabecular structure indices." *Bone* 42.4 (2008): 728-736.

Šromová, Veronika, Dinara Sobola, and Pavel Kaspar. "A brief review of bone cell function and importance." *Cells* 12.21 (2023): 2576.

Stein, B. R., and A. Casinos. "What is a cursorial mammal?." *Journal of Zoology* 242.1 (1997): 185-192.

Straehl, Fiona R., et al. "Evolutionary patterns of bone histology and bone compactness in xenarthran mammal long bones." *PLoS One* 8.7 (2013): e69275.

Streeter, GEORGE L. "Developmental horizons in human embryos (fourth issue). A review of the histogenesis of cartilage and bone." *Contrib Embryol* 33 (1949): 149.

Sukhdeo, Simone, et al. "Trabecular bone structure in the distal femur of humans, apes, and baboons." *The Anatomical Record*, vol. 303, no. 1, 2020, pp. 129-49.

Svejme, Ola, et al. "Early menopause and risk of osteoporosis, fracture and mortality: A 34-year prospective observational study in 390 women." *BJOG: An International Journal of Obstetrics & Gynaecology*, vol. 119, no. 7, 2012, pp. 810-16.

Tanck, E., et al. "Increase in bone volume fraction precedes architectural adaptation in growing bone." *Bone*, vol. 28, no. 6, 2001, pp. 650-54.

Taylor, M. E., et al. "Stress and strain distribution within the intact femur: Compression or bending?" *Medical Engineering & Physics*, vol. 18, no. 2, 1996, pp. 122-31.

Taylor, William R., et al. "Tibio-femoral loading during human gait and stair climbing." *Journal of Orthopaedic Research*, vol. 22, no. 3, 2004, pp. 625-32.

Teitelbaum, Steven L. "Bone resorption by osteoclasts." *Science*, vol. 289, no. 5484, 2000, pp. 1504-08.

Thomson, Robert C., Phillip Q. Spinks, and H. Bradley Shaffer. "A global phylogeny of turtles reveals a burst of climate-associated diversification on continental margins." *Proceedings of the National Academy of Sciences* 118.7 (2021): e2012215118.

Tsai, Henry P., and Casey M. Holliday. "Articular soft tissue anatomy of the archosaur hip joint: structural homology and functional implications." *Journal of Morphology* 276.6 (2015): 601-630.

Tsegai, Zewdi J., et al. "Ontogeny and variability of trabecular bone in the chimpanzee humerus, femur and tibia." *American Journal of Physical Anthropology*, vol. 167, no. 4, 2018, pp. 713-36.

Tyrovola, Joanna B. "The 'Mechanostat theory' of Frost and the OPG/RANKL/RANK system." *Journal of Cellular Biochemistry*, vol. 116, no. 12, 2015, pp. 2724-29.

van der Meulen, Marjolein C. H., et al. "Cancellous bone adaptation to in vivo loading in a rabbit model." *Bone*, vol. 38, no. 6, 2006, pp. 871-77.

van der Plaats, Gerardus Jacobus. *Medical X-ray techniques in diagnostic radiology: A textbook for radiographers and radiological technicians*. Springer Science & Business Media, 2012.

van Rietbergen, Bert, et al. "A new method to determine trabecular bone elastic properties and loading using micromechanical finite-element models." *Journal of Biomechanics*, vol. 28, no. 1, 1995, pp. 69-81.

Vander Sloten, Jos, and Georges Van der Perre. "Trabecular structure compared to stress trajectories in the proximal femur and the calcaneus." *Journal of Biomedical Engineering*, vol. 11, no. 3, 1989, pp. 203-08.

von Meyer, G. H. "Die architektur der spongiosa." *Archiv für Anatomie Physiologie und wissenschaftliche Medicin*, vol. 34, 1867, pp. 615-28.

Wang, Haicheng, et al. "Biomechanical properties and clinical significance of cancellous bone in proximal femur: A review." *Injury*, vol. 54, no. 6, 2023, pp. 1432-38.

Wang, Ji, et al. "Trabecular plates and rods determine elastic modulus and yield strength of human trabecular bone." *Bone* 72 (2015): 71-80.

Wawrzyniak, Agata, and Krzysztof Balawender. "Structural and metabolic changes in bone." *Animals* 12.15 (2022): 1946.

Wehrli, Felix W. "Role of cortical and trabecular bone architecture in osteoporosis." *International Society for Magnetic Resonance in Medicine 17th Annual Meeting*, 2009.

White, M. A., et al. "Forearm range of motion in *Australovenator wintonensis* (Theropoda, Megaraptoridae)." *PLoS One*, vol. 10, no. 9, 2015, e0137709.

Williams, J. L., and J. L. Lewis. "Properties and an anisotropic model of cancellous bone from the proximal tibial epiphysis." (1982): 50-56.

Willie, Bettina M., et al. "Bone adaptation: Safety factors and load predictability in shaping skeletal form." *Bone* 131 (2020): 115114.

Williston, Samuel Wendell. *The osteology of the reptiles*. Harvard University Press, 1925.

Wisniewski, Anna L., Jonathan A. Nations, and Graham J. Slater. "Bayesian prediction of multivariate ecology from phenotypic data yields new insights into the diets of extant and extinct taxa." *The American Naturalist* 202.2 (2023): 192-215.

Wolff, Julius. "Das gesetz der transformation der knochen." *DMW-Deutsche Medizinische Wochenschrift*, vol. 19, no. 47, 1892, pp. 1222-24.

"World Health Organization – WHO criteria for diagnosis of osteoporosis." *4BoneHealth*, https://www.4bonehealth.org/who-criteria-for-diagnosis-of-osteoporosis/.

Yamada, Satoshi, et al. "The role of geometrical features of the microarchitecture in the cancellous stiffness of the bovine femoral bone." *Medical Engineering & Physics* 105 (2022): 103823.

Yingling, Vanessa R., et al. "The effect of a short-term delay of puberty on trabecular bone mass and structure in female rats: a texture-based and histomorphometric analysis." *Bone* 40.2 (2007): 419-424.

Young, Jesse W. "Ontogeny of limb force distribution in squirrel monkeys (*Saimiri boliviensis*): insights into the mechanical bases of primate hind limb dominance." *Journal of human evolution* 62.4 (2012): 473-485.

Zack, Ellianna H., Stephanie M. Smith, and Kenneth D. Angielczyk. "Effect of captivity on the vertebral bone microstructure of xenarthran mammals." *The Anatomical Record* 305.7 (2022): 1611-1628.

Zack, E. H., S. M. Smith, and K. D. Angielczyk. "From fairies to giants: untangling the effect of body size, phylogeny, and ecology on vertebral bone microstructure of Xenarthran mammals." *Integrative Organismal Biology* 5.1 (2023): obad002..

Zeininger, Angel, et al. "Trabecular architecture in the StW 352 fossil hominin calcaneus." *Journal of Human Evolution* 97 (2016): 145-158.

Zysset, Philippe K. "A review of morphology–elasticity relationships in human trabecular bone: theories and experiments." *Journal of biomechanics* 36.10 (2003): 1469-1485.